

Statement of Originality

Characterising Organic Thin Films with Photodeflection Spectroscopy:

Measuring the losses in films intended for use as nonlinear optical waveguide devices.

D. J. Fotheringham

David James Fotheringham B.Sc.(Hons)

Acknowledgments

I would like to acknowledge the support of the Laser Physics Centre at ANU, in particular my chief supervisor Betty Lubet-Davies. A special thanks goes to her for her always been great examples of diligent work and good supervision. I also thank Dr. Woodruff who she was with the group.

I am also extremely grateful to the various technical officers who were always very patient with my various requests: Mike Pennington, Craig Marshall, Warren Baker, John Battaglia, Anita Smith, Ian McRae, and Raymond Keller. I am very grateful to Andrew Perry, of the Plasma Research Lab in RSPhysSE, ANU, for the granting of time to work using the PRL's equipment.

My thanks also go to David and to other students and staff (including Wladimir Kucharski) who contributed to this project and enjoyed working in the (her) lab.

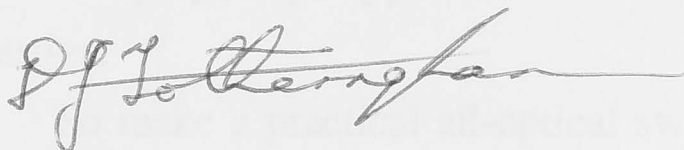
My special thanks to Maria for her support and encouragement during the project. It was a pleasure to work with her and she has been a great friend throughout the project.

February 1998

A thesis submitted for the degree of Master of Science
of the Australian National University.

Statement of Originality

Except as otherwise cited, the work presented in this thesis is by David James Fotheringham. The precursor polymers for poly(p-phenylenevinylene) were prepared by Dr. M. Woodruff, and most of the films were prepared by Dr. A. Samoc, and Mrs. R.M. Krolikowska, all of the Laser Physics Centre at the Australian National University. The measurements of the total losses in the films were made by Dr. A. Samoc.



D. J. Fotheringham

Acknowledgments

I would like to acknowledge the support of the Laser Physics Centre at the A.N.U., in particular my chief supervisor Barry Luther-Davies. Anna and Marek Samoc have always been great examples of diligent work and good science, as was Manee Woodruff while she was with the group.

I am also extremely grateful to the various technical officers who were always very patient with my various requests: Mike Pennington, Craig Macleod, Warren Baker, John Bottega, Anita Smith, Ian McRae, and Raymond Keifer. I am very grateful to Andrew Perry, of the Plasma Research Lab in RSPHysSE, A.N.U. for the grating etching work using the PRL's equipment.

My thanks also to Doug and to other students and staff (including Wieslaw Krolikowski) who contributed to much encouragement and enjoyment during the project.

My special thanks to Maryla Krolikowska, who made working in the ('her') chem lab most enjoyable, and whose cheerfulness and friendship I have valued throughout the project.

Abstract

There is much current interest in developing all-optical switching devices for applications in photonics. One direction of research, being pursued at the Laser Physics Centre at the Australian National University, is the development of organic conjugated polymer waveguides for this application.

Poly(*p*-phenylenevinylene) (PPV) is a conjugated polymer with a high third order nonlinearity, making it a possible candidate for all-optical switching devices, but it also has high optical losses. These losses can be reduced when PPV is combined with a host matrix of poly(vinyl pyrrolidinone) (PVP) which has much better waveguiding properties.

To make a practical all-optical switch, both high nonlinearity and low losses are necessary. The work presented here was motivated by the need to identify the cause of the optical losses in PPV-doped waveguides - whether being due to absorption, an intrinsic characteristic of the material, or due to extrinsic causes such as scattering or waveguide irregularities. Since the polymer films are generally very thin (≈ 1 micron), standard spectrophotometer measurements are not able to resolve the absorption levels which are important even at the level of 0.1cm^{-1} .

This dissertation presents the preparation of a photodeflection spectroscopy system, able to measure the absorption in these films independently of other sources of waveguiding losses like scattering. This technique was used to measure the absorption spectra of thin films of PPV, PVP, and composites of PPV with PVP, determining that the absorption losses in the composite films were much smaller than the total losses which had been measured for waveguided light propagating in the films. Thus, the losses in the material are not limited by absorption, and so further attention to the extrinsic sources of loss may yield material suitable for the production of nonlinear optical devices.

Contents

1. INTRODUCTION.....	11
1.1 Nonlinear Optical Switches.....	11
1.2 Measuring Low Absorption Losses	18
2. THEORY AND EXPERIMENTAL DESIGN.....	21
2.1 Studies of Photodeflection Spectroscopy.....	21
2.1.1 Theoretical Considerations	21
2.1.2 Alternative Designs and Uses.....	23
2.2 Numerical Simulations.....	23
2.2.1 Computational Method.....	24
2.2.2 Parameters	27
2.2.3 Frequency dependence.....	28
2.2.4 Probe beam height dependence	29
2.2.5 Linearity with absorption.....	30
2.3 Pump Beam Optics	32
2.3.1 Bandwidth.....	34
2.4 Probe Beam Optics	35
2.5 Detection System	37
2.5.1 Photodiode.....	37
2.5.2 Circuit	39
2.5.3 Electronic Noise.....	40
2.6 Overall Environment	41
2.6.1 Vibration Isolation	41
2.6.2 Sample Mounting	42
2.6.3 Computer Control.....	43
2.7 Calibration.....	43
2.7.1 Calibration for lamp power	43
2.7.2 Calibration with samples of known absorption	45
2.7.3 Absolute Calibration for each sample.....	46
2.8 Preparation of Materials.....	47
2.8.1 Preparation of Poly(<i>p</i> -phenylenevinylene) (PPV).....	47
2.8.2 Preparation of Poly(vinyl pyrrolidinone) (PVP).....	48
2.8.3 Preparation of Poly(vinyl alcohol) (PVA)	48
2.9 Total Loss Measurements.....	50

3. PDS INVESTIGATIONS OF PPV AND PVP 55

3.1 Introduction.....55

3.2 Spectral Absorption Calibration.....56

3.3 Absorption of PPV films from different precursors61

3.4 Absorption characteristics of PVP64

 3.4.1 Various PVP films subject to different conditions..... 64

 3.4.2 PVP films heated to different temperatures 68

3.5 Measurements of PPV / PVP composites.....70

 3.5.1 Introduction..... 70

 3.5.2 Photodeflection Spectroscopy Results 71

 3.5.3 Comparison with Total Loss Measurements..... 75

4. CONCLUSION 81

APPENDIX A

 Operating and Maintenance Guide for the Photodeflection Spectroscopy Apparatus....**83**

BIBLIOGRAPHY.....89

Table of Figures

Figure 1.1 The Structures of PPV and PVP.....	15
Figure 1.1 Schematic diagram of PDS system.....	19
Figure 2.1 Representation of node structure for finite difference technique.....	24
Figure 2.2 Dependence of the refractive index gradient on the chopping frequency.	28
Figure 2.3 Variation of signal with probe beam height above sample.....	30
Figure 2.4 Simulations of varying absorption and sample thickness.....	31
Figure 2.5 Pump Beam Optical System.....	33
Figure 2.6 Filters used on the pump beam	34
Figure 2.7 Probe Beam Optical System.....	36
Figure 2.8 The knife-edge detector.....	37
Figure 2.9 Linearity of position sensitive photodiode with position	38
Figure 2.10 Circuit used for photodetector.....	40
Figure 2.11 Photodeflection Spectroscopy Apparatus Side View	42
Figure 2.12 Measurements of the power in the pump beam using a black absorber as the sample.	44
Figure 2.13 Absorption signals for PVA slides with various levels of chlorophyllin doping	45
Figure 2.14 Preparation of Poly(<i>p</i> -phenylenevinylene) (PPV)	49
Figure 2.15 Images showing the decay in scattered light intensity with distance from the in-coupling point for waveguiding PPV-PVP films.....	52
Figure 2.16 Schematic diagram of grating writing system	53
Figure 3.1 2.53% PPV in PVP, spectrum obtained by photodeflection spectroscopy...	56
Figure 3.2 2.53% PPV in PVP, as measured by the spectrophotometer and PDS	57
Figure 3.3 Absorption spectrum of PMMA (perspex), showing the C-H stretch overtone.	58
Figure 3.4 Absorption spectrum of water, as measured by the spectrophotometer using a 1mm cuvette, with spectroscopic grade carbon tetrachloride as the reference.....	59
Figure 3.5 Benzene, NMP and VPN, measured against spectroscopic grade CCl ₄ in the spectrophotometer, showing the aromatic and aliphatic C-H stretch overtones at 1140nm and 1180nm	60
Figure 3.6 Absorption spectra of PPV slides prepared from different precursors.....	63
Figure 3.7 Absorption spectra of PVP films	66

Figure 3.8 Linear plot of the PVP absorption spectra, showing an increased absorption floor on some of the samples.....67

Figure 3.9 Absorption spectra from a series of PVP films dried at different temperatures.....69

Figure 3.10 Spectrophotometer measurements of the absorption spectra of PVP films dried at different temperatures.....69

Figure 3.11 PPV in PVP series heated to 130 degrees.....72

Figure 3.12 PPV in PVP series heated to 150 degrees.....73

Figure 3.13 PPV in PVP series heated to 200 degrees.....74

Figure 3.14 Absorption and Total Losses in 130 degree series of PPV/PVP films.....77

Figure 3.15 Absorption and Total Losses in 150 degree series of PPV/PVP films.....78

Figure 3.16 Absorption and Total Losses in 200 degree series of PPV/PVP films.....79

1. Introduction

In this dissertation I describe the development and use of a photodeflection spectrometer (PDS) for measuring the absorption spectra of thin, weakly absorbing films. The system has been used to characterise the absorption of some composite polymer films which are intended for use in all-optical switching. The conjugated polymers, in particular those containing poly(*p*-phenylenevinylene) (PPV), have a high third order optical nonlinearity and thus have potential for photonic switching in structured waveguides. In this application it is essential that the waveguides have low propagation losses. By using photodeflection spectroscopy, the contribution of the material absorption to the total propagation losses can be measured, and this determines whether absorption or other loss mechanisms, such as scattering, are the limiting factors. Whilst excess material absorption could focus our materials research on factors such as the role of doping on optical absorption or towards alteration of the molecular structure of the polymers in an attempt to reduce absorption at the wavelength of interest, other sources of loss such as scattering could imply a different approach since, for example, scattering caused by the presence of impurities or irregularity in composition due to aggregation (crystallization) would direct attention to the chemical processing used in the creation of the polymers.

1.1 Nonlinear Optical Switches

In recent years, optical fibres have become a preferred means of transmitting large amounts of information over long distances, replacing the lower bandwidth electronic copper cables. However, no commercially viable optical equivalent of the transistor has been developed, and so all switching and processing of the information carried by optical fibres has to be performed electronically or opto-electronically.

Electronic switching is limited to about 20Gbit/s by circuit capacitance.^{1,2} In contrast photonic switches, which have potential advantages of a broad bandwidth and potentially dense integration because of the lack of cross-talk, can reach picosecond speeds since there is no electronic drive.³

To make an optical switch requires having a material in which the presence of one stream of photons affects the passage of other photons through the material. This is so for a material in which the polarisation is a nonlinear function of the electric field of the incident light.

In general, the polarisation of a medium in which there is an applied electric field \mathbf{E} due to the incident light, will be

$$\mathbf{P} = \epsilon_0 (\chi^{(1)}\mathbf{E} + \chi^{(2)}\mathbf{E}^2 + \chi^{(3)}\mathbf{E}^3 + \dots) \quad (1.1)$$

where the higher order terms represent the nonlinear effects; $\chi^{(1)}$ is the linear susceptibility, $\chi^{(2)}$ is the second-order susceptibility, and so on. In centrosymmetric materials, $\chi^{(2)} = 0$ and hence the lowest order nonlinear term which can be used for all-optical switching is that proportional to $\chi^{(3)}$. Materials research has therefore been focussed on optimising this third order nonlinearity. Recently it has been recognised that $\chi^{(2)}$ can also be used for all-optical switching using the so called "cascading" process and hence there has been a renewed interest in non-centrosymmetric materials.⁴ In this work we concentrate on $\chi^{(3)}$ materials based on conjugated polymers.

For centrosymmetric materials, the nonlinear refractive index n_2 is related to the optical Kerr susceptibility $\chi^{(3)} = \chi^{(3)}(-\omega; \omega, -\omega, \omega)$ by⁵

$$n_2 = \frac{3\chi^{(3)}}{4c\epsilon_0 n_0^2} \quad (1.2)$$

and the total refractive index n can be described by

$$n = n_0 + n_2 I \quad (1.3)$$

where c is the speed of light in a vacuum; ϵ_0 is the vacuum permittivity; n_0 is the linear (low-power) refractive index; and I is the intensity of the light.

Physically, optical nonlinearities can originate from the distortion of the electron distribution around molecules in the material (electronic nonlinearities); from the creation of excited states (e.g. optical pumping); due to thermal effects; or due to more complex processes such as the photorefractive effect. However, long-lived excited states, slow thermal effects, and the photorefractive effect (which depends on movements of charges within the material) will not provide the switching rates around 100Gbit/s rates that are required.

All-optical switching devices ideally should be compact, and operate at low average powers. Thus for 100Gbit/s switching rates, using 5ps duration pulses, and an average optical power of 100mW it would be necessary to switch with around 1pJ of pulse energy. This will only be achieved using any conceivable third order nonlinearity

when the pulse energy is concentrated into a channel waveguide with a small cross-sectional area. Ideally the dimensions of these waveguide should also compatible with the optical fibres by which the switching device is linked into the transmission network (cross sectional area 10^{-6} - 10^{-7} cm²).

Several different configurations of photonic switch using structured channel waveguides have been proposed including nonlinear directional couplers;⁶ nonlinear grating devices;⁷ switches based on a Mach-Zehnder interferometer design;⁸ and soliton based switches.^{9,10,11,12}

Nonlinear directional couplers consist of two optical waveguides in close proximity, with the same propagation constants, so that at low power in a length known as the half-beat length, the power couples across from the first waveguide into the other. If the waveguides continue in proximity the light will periodically couple across and back, as described by coupled mode theory. At high intensities though, if the material has an optical nonlinearity, the propagation constant of the first waveguide will be altered by the high intensity, and the coupling between the two waveguides will be detuned, and the amount of light coupled across into the second waveguide in the original interaction length will be reduced. This detuning may be caused by the intensity of the signal pulse or as a result of a co-propagating probe pulse.⁶

Nonlinear effects relying on grating coupling have also been observed in polymeric waveguides, for example the study of Crook et al. into the nonlinear optical behaviour of a grating coupled poly[5,7-dodecadiyn-1,12-diol-bis(n-butoxycarbonyl-methyl-urethane)] (P4BCMU) waveguide. P4BCMU has a $\chi^{(3)}$ nonlinearity; Crook et al. obtained a shift in coupling angle of 0.10° when changing from $1\mu\text{J}$ to $10\mu\text{J}$ pulses from a Nd³⁺:YAG laser, with a concurrent change in coupling efficiency from 95% to 76%.⁷

A "push-pull" switch has been proposed by Ironside et al, based on a Mach-Zehnder interferometer and using a cascaded second-order.⁸ It involves using gratings of different periods in each arm of the interferometer, to give nonlinear phase shifts with different signs to the parts of the beam travelling down the two arms. The phase-shifts are dependent on the beam intensity.

Solitons also have potential application in all-optical signal processing. Temporal solitons in fibres are pulses of light in which the nonlinear effect balances the temporal dispersion to create pulses which propagate without changing shape. They exhibit particle-like behaviour, and can interact with each other elastically.⁹ They have been applied to optical switching using mechanisms such as the soliton dragging gate.^{10,11} In the spatial domain, solitons form paths of light in which the nonlinear (self-focussing) effects exactly balance diffraction. Since the nonlinear effect changes the refractive index

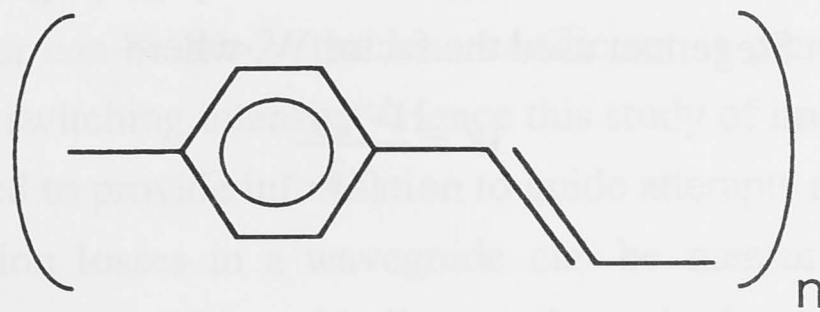
of the medium near the soliton, it can be thought of as creating a waveguide in the medium, which can be used to steer or guide other signal carrying beams.¹² These soliton induced waveguides can be switched on or off, or steered in various ways as the basis of an all-optical switch. The same principle can be applied to soliton induced waveguides created in self-defocussing nonlinear optical materials.¹²

Polymer waveguides are a possible building block for such switches. Polymers are generally inexpensive to produce, and can be subjected to a certain amount of "molecular engineering"—the lengths of conjugated chains, and the atoms and functional groups attached to the chains can be varied, thus altering the polarisability and nonlinear optical properties. Whilst polymers can be susceptible to degradation by heat or abrasion, they do offer a great deal of processing flexibility. Some polymers may be spin-coated into place (by solvent evaporation); other polymers may be injection moulded or set in place by thermal or photochemical curing.¹³

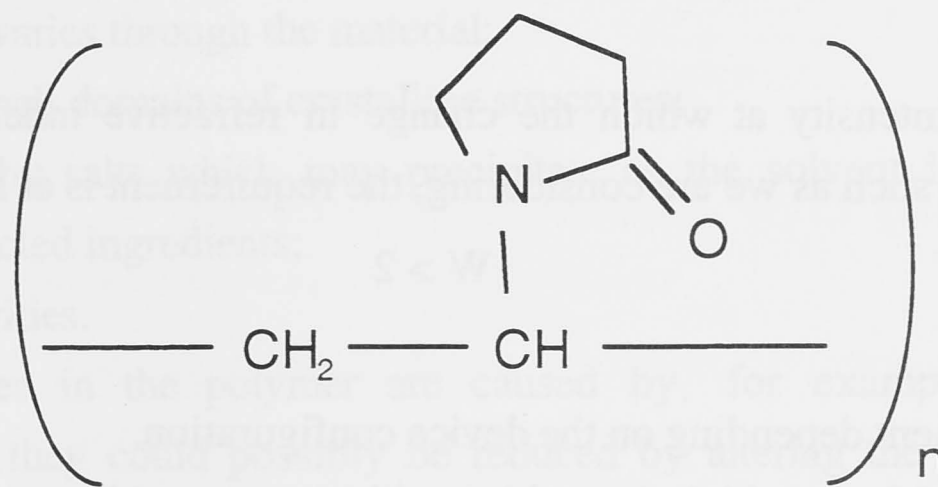
Polymers with aromatic rings, double or triple bonds alternated with single bonds between neighbouring carbon atoms are referred to as conjugated polymers: poly(*p*-phenylenevinylene) (PPV) is an example of such a conjugated polymer (see Figure 1.1).¹⁴ These polymers have a hyperpolarisability which is dependent on the length of the conjugated system,¹⁵ and the π -bonded electron system can be distorted strongly by the presence of an optical field.

Poly(*p*-phenylenevinylene), which is the main material being investigated here, has a non-linear refractive index which can be described by equation (1.3). It has been the subject of considerable investigation as a potential organic polymer for active optical devices.^{16,17} It has been shown to have a high nonlinearity ($n_2 > 10^{-11}$ cm²/W at 800nm), and a two photon figure of merit (see below) $T < 0.6$.¹⁶

However, pure PPV has been found to be extremely lossy, and furthermore, it is highly anisotropic (due to preferential alignment of the rod-like PPV molecules in the plane of the films) leading to a large TE-TM mode birefringence and high TE-mode refractive index.¹⁸ The need to lower the TE-index to bring it closer to that of silica glass fibre, and reduce the birefringence motivates the development of composite materials where PPV is used as a dopant in a lower index host material. As an example PPV can be incorporated in a matrix with poly(vinyl pyrrolidinone) (PVP), which has high transparency and a small nonlinearity, and then spun into waveguiding films with relatively low losses. The structure of PVP is also shown in Figure 1.1. By making composite PPV/PVP films, it is hoped to make films with high nonlinearity and low losses with optical properties closer to those required for a practical planar waveguide. Whilst preparing composites might be thought to simply "dilute" the nonlinearity due to



Poly (*p*-phenylenevinylene)
(PPV)



Poly (vinyl pyrrolidinone)
(PVP)

Figure 1.1 The Structures of PPV and PVP.

the PPV at the same time as lowering the losses, control of the matrix and conversion procedures may result in an improvement of the figures of merit.¹⁸

Various merit factors have been used to rate materials for all-optical switching based on their nonlinearity, time response and losses. The nonlinear response must obviously be large enough for the device to “switch” and this in general means that a sufficiently large nonlinear phase change must accumulate on the beam as it propagates through the switch. However, both linear and nonlinear propagation losses cause the beam intensity to decay and this can limit the total phase change integrated along the beam path that may be achieved, preventing complete switching. Thus two figures of merit prove to be the most useful and these parameterize the nonlinear phase change achievable over a distance equal to a single or two-photon absorption length.

Regarding the linear absorption losses, Wong et al. used the ratio of the nonlinear refractive index n_2 to the linear absorption coefficient α as a figure of merit, when

comparing the third-order nonlinearities in various conjugated polymers (α is defined as per equation (1.7)).¹⁹ Stegeman used the factor W , where

$$W = \frac{\Delta n_{\max}}{\alpha \lambda} \quad (1.4)$$

where Δn_{\max} is the maximum change in refractive index, and λ is the wavelength, so

$$W = \frac{n_2 I_{\text{sat}}}{\alpha \lambda} \quad (1.5)$$

where I_{sat} is the intensity at which the change in refractive index saturates.²⁰ For a waveguide device such as we are considering, the requirement is at least

$$W > 2 \quad (1.6)$$

the exact requirement depending on the device configuration.

When working at high intensities within waveguides two photon absorption (TPA) can also be important. This absorption can be described by

$$\frac{\partial I}{\partial z} = -\alpha I - \beta I^2 \quad (1.7)$$

where I is the effective laser beam intensity as a function of distance traversed in the medium z , α is the linear absorption coefficient and β is the TPA coefficient. Mizrahi et al. have made a study of the limitation that TPA places on optical switching devices.²¹ They show that for an operable switching device the criterion to be satisfied is

$$2T = \frac{2\beta\lambda}{n_2} < a \quad (1.8)$$

where a is of the order unity, and depends on the specific device design.

The third order nonlinearity of the polymer samples can be measured by techniques such as time-resolved degenerate four-wave mixing (DFWM),^{16,19,22,23} Kerr ellipsometry,²⁴ the Z-scan technique,²⁵ etc, and from the data both real and imaginary components must be obtained allowing evaluation of the "T" merit factor. From work on PPV our own group has established that PPV has $T < 1$ at 800nm which indicates the

material has nonlinear properties which satisfy this merit factor for all optical switching. Although the W factor can be $W > 2$, the loss coefficient is generally unacceptably high implying a very high switching intensity. Hence this study of linear losses in PPV doped waveguides is required to provide information to guide attempts at loss reduction.

The propagation losses in a waveguide can be measured by the decay in the scattered light, or propagating light, with distance from the in-coupling point. However, the total losses in a waveguide are due to more than just absorption. Losses can also be caused by scattering due to²⁶

- Inhomogeneities - which can be present in amorphous polymers, wherein the refractive index varies through the material;
- Crystallinity - small domains of crystalline structures;
- Contamination, by salts which may precipitate as the solvent is evaporated, dust, bubbles or unreacted ingredients;
- Surface irregularities.

If the losses in the polymer are caused by, for example, scattering from contaminants, then they could possibly be reduced by altering the polymer processing conditions and purification methods. However if the losses are due to absorption of the material, they may be more difficult to combat; changes to the chemical composition or conjugation length may shift the position of absorption bands but may have only limited effect on lowering the absorption floor.

Thus it is necessary to distinguish the source of the losses in the PVP/PPV films under investigation. Further, the losses must be measured for the films in a waveguide configuration, since the losses in a bulk sample are likely to be different to the losses *in situ* in a thin film; spin-coating the thin film can have an effect on the orientation of molecules in the film and may affect their agglomeration, and waveguide losses from surface irregularities are relevant to the investigation.

The total losses for the polymers have been measured by using a CCD camera to photograph the scattering of light out of the waveguide as a function of distance from the point at which light is in-coupled (usually here by prism coupling). Assuming that the scattering is uniform and not too large (or dominated by isolated scratches or waveguide nonuniformities), the local intensity of the scattered light can be assumed to be proportional to the intensity of the light in the guide, and thus the decay in the intensity of the light with propagation distance can be measured. A modification of this method involved doping the polymer with a dye such as phloxine-B which can be optically pumped by a propagating beam with wavelength lying in a transmission band of the PPV. Up-conversion fluorescence from the phloxine-B can be distinguished from

scattered light at the pump wavelength and the decay in the fluorescent light measured as a function of distance.

An investigation was made into the use of grating in-coupling for these measurements. This involved etching gratings into the substrates before spinning on the polymeric waveguides, with the specific advantage over prism coupling that coupling could still be achieved when a cladding layer was added over the top of the polymeric waveguide. Brief results of the grating coupling method are presented in section 2.9, however prism in-coupling was finally used for all of the samples presented here, which were unclad.

1.2 Measuring Low Absorption Losses

Standard spectrophotometers,²⁷ which measure the drop in transmission due to reflection and absorption, are able to measure optical densities up to $\alpha l \approx 5.0$, with a best absorbance resolution of 0.002. For a 1 micron film, this represents absorptions up to $5 \times 10^4 \text{cm}^{-1}$ measured through the plane, with an absorption coefficient resolution of 20cm^{-1} at best. The absorption coefficient of poly(*p*-phenylenevinylene) ranges from $>10^5 \text{cm}^{-1}$ at $\lambda_{\text{max}} \approx 430 \text{nm}$, to $<1 \text{cm}^{-1}$ at $\lambda > 900 \text{nm}$. The low absorption range is particularly critical for waveguiding applications, and poses difficulties for the spectrophotometer which registers small losses against a bright transmitted beam. Spectrophotometers are also sensitive to losses from both reflection and scattering, and can have further problems with interference fringes developing with high index thin films (see for example Figure 3.10).

Hence a technique is needed which can measure the absorption of a thin film of material over a large wavelength range, and be only weakly affected by scattering, reflection or interference. Photodeflection spectroscopy, as first developed by Boccara, Fournier and Badoz²⁸ and used for thin film purposes by others [references 29,30,31,32,33] is well suited to this purpose. A photodeflection spectroscopy system has been constructed to determine the contribution of absorption to the losses in the polymeric films under investigation.

Photodeflection spectroscopy (PDS) involves irradiating a sample with chopped, monochromatic pump light. As the sample absorbs the light, in the absence of significant fluorescence, the sample exhibits periodic heating in proportion to the absorption of the sample at the wavelength of the pump. As the sample is periodically heated, the medium immediately above the sample also develops a periodically varying temperature gradient.

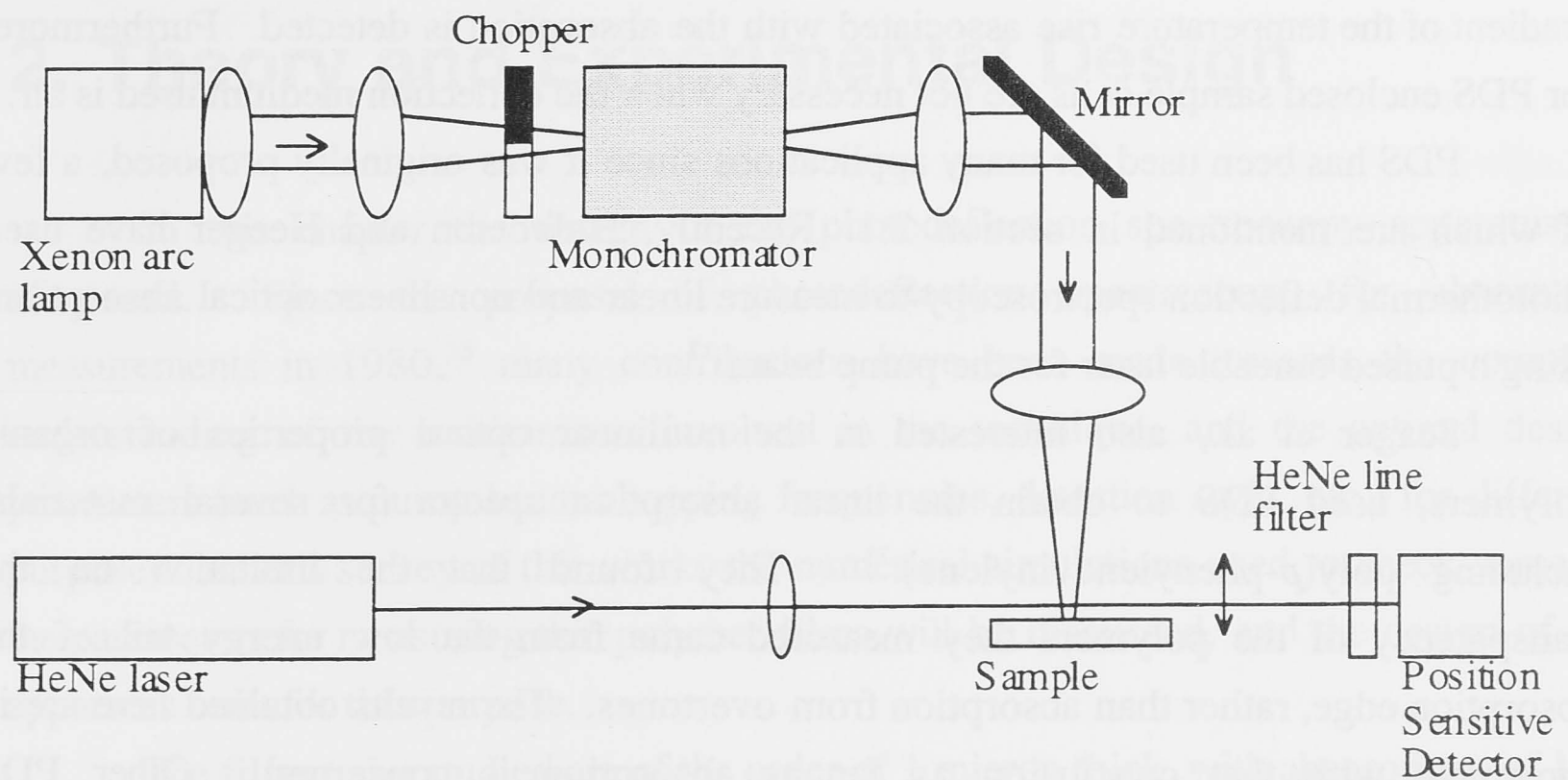


Figure 1.1 Schematic diagram of PDS system

The medium above the sample may be air, or another fluid with a strongly temperature dependent refractive index, such as carbon tetrachloride. The periodically varying temperature gradient causes a varying refractive index profile in this medium, and a probe laser beam propagating just above the sample surface will be deflected in a manner analogous to that which occurs with a mirage. The magnitude of the periodic deflection of the beam thus gives a measure of the absorption of the sample. A schematic diagram of a typical PDS apparatus is shown in Figure 1.1.

The primary advantage of PDS over spectrophotometers is that it is not a transmission technique; zero absorption should give a zero signal (in the absence of noise), rather than 100% as for a spectrophotometer. Furthermore, since the probe beam does not pass through the sample, the PDS results are independent of scattering, unlike the transmission measurements and measurements which involve propagation of light through the waveguide. Questions of the linearity, dynamic range and the absolute calibration of the absorption data obtained using a PDS are important and are treated in chapter 2 (especially section 2.7).

One of the serious alternatives to PDS is photoacoustic spectroscopy.^{34,35} As pointed out by Murphy and Aamodt,³⁶ PDS has a significant advantage over photoacoustic spectroscopy in that rather than detecting only the small fraction of the total thermal energy which is converted into a propagating acoustic wave, here the spatial

gradient of the temperature rise associated with the absorption is detected. Furthermore, for PDS enclosed sample cells are not necessary when the deflection medium used is air.

PDS has been used for many applications since it was originally proposed, a few of which are mentioned in section 2.1. Recently, Halvorson and Heeger have used Photothermal deflection spectroscopy to measure linear and non-linear optical absorption, using a pulsed tuneable laser for the pump beam.³⁷

Seager et al., also interested in the nonlinear optical properties of organic polymers, used PDS to obtain the linear absorption spectra for several materials, including poly(*p*-phenylenevinylene).³¹ They found that the limitation on the transparency of the polymers they measured came from the low energy tail of the absorption edge, rather than absorption from overtones. The results obtained here are in agreement with that conclusion as far as absorption is concerned. Other PDS measurements of polymer films have been reported by So et al.,³³ although their films were free-standing and between 40-120 microns thick – far thicker than is appropriate for the waveguide configuration.

My intention in this work has been to develop and use a photodeflection spectroscopy system to measure the absorption in thin films of PPV and PPV/PVP composites, comparing the losses in polymers prepared under different processing conditions, and to determine whether the losses in such waveguides are dominated by absorption or other processes.

Some of the theoretical modelling on which the photodeflection spectroscopy system is based is presented in Chapter 2, with numerical simulations which were used to determine the best set of parameters for working with thin polymeric films on glass substrates. The experimental design and construction of the system is then discussed.

Chapter 3 presents the results of measurements of slides of PPV and PVP, from which the most suitable samples and preparation conditions were chosen for use in the composite PPV/PVP films. The studies of the composite films show that the linear absorption of the films is not the dominant factor in the propagation losses recorded in the films as waveguides. Rather, the losses are most likely dominated by scattering from impurities present in the PPV after conversion or from crystalline domains. As these may be reduced by altering the polymer processing, PPV in composite films has been shown to be worth continued study as a material for all-optical switching devices.

2. Theory and Experimental Design

In this chapter the design of the photodeflection spectroscopy apparatus is discussed. Since the proposal of photodeflection spectroscopy for absorption measurements in 1980,²⁸ many contributions have been made towards the complete understanding of the mechanisms involved in the technique, and the optimal design parameters (such as pump beam chopping frequencies, detection style, etc.) for different purposes. After a survey of this work, the numerical simulations used to check some of the parameters for measuring thin polymer films will be discussed, and the design of the apparatus built for this purpose.

The films to be studied are of the order of 1 micron thick, with absorptions of less than 1cm^{-1} at wavelengths between 600nm and $1.5\mu\text{m}$. The photodeflection spectroscopy system was constructed so as to be sensitive enough to be able to measure this. The various elements of the system are discussed in the second half of this chapter, and the approach to calibration is discussed in section 2.7. The preparation of the polymers for the waveguiding films is discussed in section 2.8, and in section 2.9 the technique for obtaining the total propagation losses for light in the waveguiding films is presented.

2.1 Studies of Photodeflection Spectroscopy

2.1.1 Theoretical Considerations

Jackson, Amer, Boccara, and Fournier presented the first detailed description of the theory of photodeflection spectroscopy.³⁸ They considered both collinear and transverse photodeflection spectroscopy arrangements; in the collinear arrangement, the probe beam must also pass through the sample, rather than passing parallel to the medium adjacent to the sample as used in the transverse arrangement shown in Figure 1.1. They derived formulae for the temperature distribution and its effect on the propagation of a Gaussian probe beam, including the influence of the angle between the pump and the probe beam. In an analysis of the detector responses, they concluded that whilst the signal given by lateral position sensors depends on the distance between the sample and the detector, for their approximately 1cm length detectors both these and quadrant position

sensors gave results with similar sensitivity. They reported experimental verification of the signal falling exponentially with increasing chopping frequency, the signal being inversely proportional to the pump beam radius, and the dependence of the signal on pump and probe beam offsets and angles. The experiments here were performed using a zero tilt angle for the probe beam (parallel to the sample surface) for the best results. The other parameters will be commented on in the discussion which follows.

Jackson et al. also compared photothermal deflection spectroscopy (PDS) with thermal lensing (TL), which probes the curvature rather than the gradient of the temperature field. They concluded that PDS and TL have almost the same sensitivity, but PDS is far less sensitive to probe laser intensity fluctuations (although pointing noise still contributes to both systems), as well as being easily applicable to opaque or scattering samples.³⁹

Murphy and Aamodt, like Jackson et al., showed that the acoustic wave gives a signal which is very much smaller than the thermal effect, and so can be neglected.⁴⁰ Rousset, Charbonnier and Lepoutre showed that convective and radiative effects can still dominate the deflection of the probe beam, but only with a high pump power ($10\text{W}/\text{cm}^2$) and sample temperatures reaching 400-500K - higher for the radiative effects.⁴¹ For the pump powers used in the experiments here (the order of 3mW at the sample), the thermal effect dominates.

Unlike Jackson et al., Murphy and Aamodt were interested in considering other forms of sample heating such as resistance heating, and not just an impinging modulated light beam such as is necessary for this purpose. Murphy and Aamodt further discussed how both the phase and amplitude of the optical beam deflection vary with offset, incident angle and frequency, the best response corresponding to zero beam offset and tilt angle, as used here. They also compared the beam deflection technique with photoacoustic spectroscopy (PAS), finding that PDS is less frequency dependent than is PAS, and has advantages for making *in situ* measurements without necessarily requiring elaborate sample cells.

Other authors have considered the effects of DC heating, interferometry and wave optics, and the relative positions of the pump and probe beams.^{42,43,44,45}

Photodeflection spectroscopy is thus now a well known technique, having been explored and used in many different ways.

2.1.2 Alternative Designs and Uses

Various proposals have been made for the use of the principles of photodeflection spectroscopy in novel designs; for the measurement of the absorption spectra of thin films, solids, liquids or gases, in situ; for measuring other thermal parameters; or for imaging.³⁸ PDS has also been used for detecting trace gases,⁴⁶ monitoring laser heating of surfaces,⁴⁷ and for measuring optical and transport properties and Silicon and solid state materials.^{48,49} Thin films of carbon 60 have been studied using this technique.⁵⁰

Techniques which involved the probe beam being almost collinear with the pump beam were suggested early.⁵¹ Chen and Zhang have suggested using interferometry, in particular for use with strongly light-scattering samples such as powders (see also ref. 43);⁵² and Charbonnier and Fournier developed a compact modular structure less than 20cm in length, which can be used both for spectroscopy and for imaging, wherein the sample can be scanned beneath the pump and probe beam.⁵³ Manning et al. considered a reverse geometry, where the probe beam is on the opposite side of the sample to the illuminating pump light.⁵⁴ Horita et al. suggested a double pass method, which increases the sensitivity for films of absorbance much less than 1;⁵⁵ this is not necessary in the current situation.

For the purpose considered here, with a thin polymer film on a fused silica substrate, a transverse probe beam which can sample the temperature gradient above a small region of the film is preferred to a probe beam collinear with the pump beam and having to pass through the sample, being affected by surface irregularities and scattering. Having the probe beam incident on the other side of the sample to the pump beam would be unhelpful, only serving to reduce the pump intensity on passing through the substrate. A reasonably compact structure with readily interchangeable samples and automatic operation is required.

2.2 Numerical Simulations

A one-dimensional numerical simulation of the periodically varying thermal gradient (and hence refractive index profile) in the fluid above the periodically heated sample surface was constructed in order to help to choose the deflecting medium (air or a higher thermal conductivity solvent); to confirm that the deflection would increase linearly

with the absorption in the sample; and to determine what range of absorptions would be measurable for a given set of experimental parameters.

A one-dimensional model was sufficient because for the experimental conditions, the pump beam spot size on the sample is larger than the distance of the probe beam above the surface of the sample, and so heat flow parallel to the sample surface could be neglected in the region of the probe beam. A finite difference approach was taken,⁵⁶ and the program written in FORTRAN.

2.2.1 Computational Method

In the one-dimensional version of the program, two arrays of temperatures were constructed. Each array was divided into three, representing the layers of air, polymer and substrate; additional divisions could be added as necessary. Each number in the array represented the temperature at that point in the system. This scheme can be depicted as in Figure 2.1.

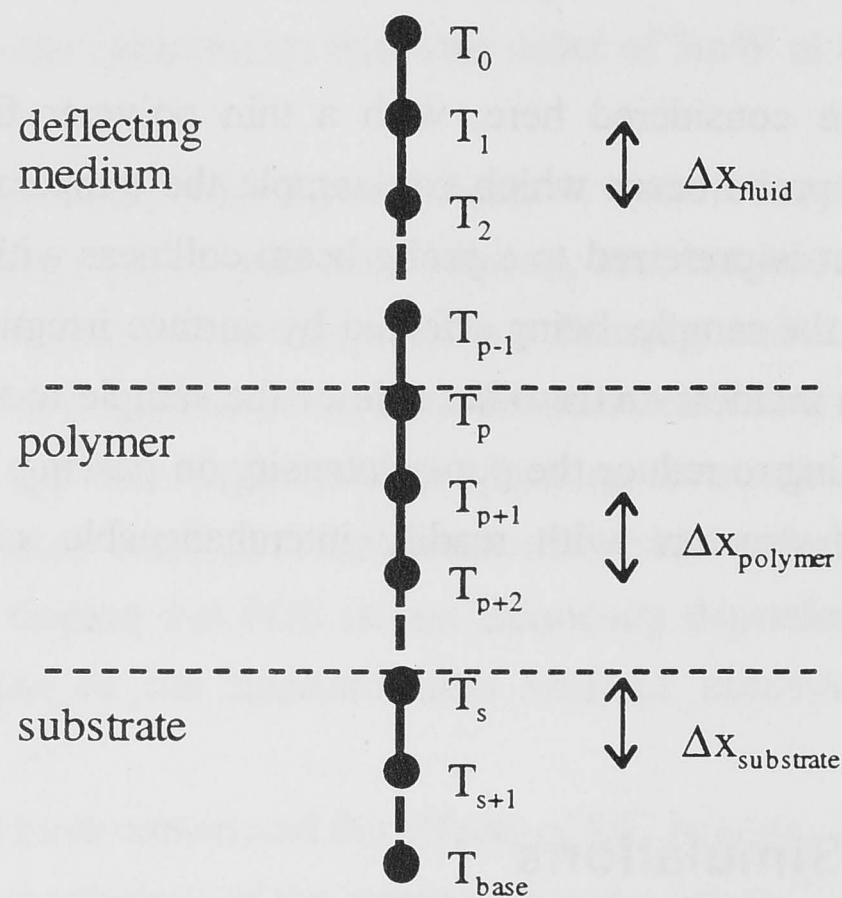


Figure 2.1 Representation of node structure for finite difference technique.

The simulation proceeded according to the time dependent heat conduction equation

$$\rho c \frac{\partial T(x,t)}{\partial t} = \frac{\partial}{\partial x} \left(k \frac{\partial T(x,t)}{\partial x} \right) + g(x,t) \quad (2.1)$$

where $T(x,t)$ was the temperature at position x and time t , k was the thermal conductivity, ρ was the density and c was the specific heat of the material at constant pressure. $g(x,t)$ was the rate of energy generation per unit volume, from the absorption of light in the material.

The heat conduction equation was discretised (see Figure 2.1), so that position $x = m\Delta x$ and time $t = i\Delta t$, where $m = 0,1,2,\dots,M$; $i = 0,1,2,\dots$. With $T_m^i = T(x,t)$, and the thermal diffusivity α given by

$$\alpha = \frac{k}{\rho c} \quad (2.2)$$

the heat conduction equation (away from boundaries) became

$$\frac{T_m^{i+1} - T_m^i}{\Delta t} = \alpha \frac{T_{m-1}^i + T_{m+1}^i - 2T_m^i}{(\Delta x)^2} + \frac{g_m^i}{\rho c} \quad (2.3)$$

or

$$T_m^{i+1} = r(T_{m-1}^i + T_{m+1}^i) + (1 - 2r)T_m^i + \frac{g_m^i \Delta t}{\rho c} \quad (2.4)$$

with

$$r = \frac{\alpha \Delta t}{(\Delta x)^2} \quad (2.5)$$

At nodes on the boundary between different materials equation (2.4) becomes

$$T_b^{i+1} = T_b^i + \left[\frac{k_-}{\Delta x_-} (T_{b-1}^i - T_b^i) + \frac{k_+}{\Delta x_+} (T_{b+1}^i - T_b^i) \right] \frac{2\Delta t}{(\rho_- c_- \Delta x_- + \rho_+ c_+ \Delta x_+)} + \frac{g_b \Delta t}{\rho_+ c_+} \quad (2.6)$$

where one medium is represented with the subscript (+), the adjacent medium with the subscript (-), and assuming that absorption occurs only in the former medium.

It was assumed that the pump light, with incident intensity I_0 is absorbed only in the polymer layer. If α is the absorption coefficient, then the heating term for equation (2.4), in Wm^{-2} , is

$$g_m = I \exp(-\alpha m \Delta x) [\exp(\alpha \Delta x / 2) - \exp(-\alpha \Delta x / 2)] \quad (2.7)$$

At the upper and lower boundaries of the array a constant temperature was assumed. The distances to these points were very large in comparison to the thermal diffusion length in the materials.

It was assumed that because the pump beam is broad compared with the width of the probe beam and with the thermal diffusion length, the heat flow horizontally (if the array is considered vertical) was negligible, as the same heating was occurring throughout a region wider than the thermal diffusion length.

The program stepped the temperature arrays forward in time. The size of the time steps were limited by numerical stability criteria, the basic criterion being that the parameter r (equation (2.5)), had to satisfy⁵⁷

$$0 < r \leq \frac{1}{2} \quad (2.8)$$

The time steps were thus limited according to the spatial step size.

In the program, both heating and cooling cycles were simulated, and the temperature gradient in the deflecting medium at a particular height above the polymer was sampled. This was multiplied by a sine wave at the same phase as the simulated chopped light, simulating the phase-locked loop of the lockin amplifier. A similar result was obtained using a cosine, with the two results added in quadrature to obtain the total signal, which was then averaged over time.

The program thus gave the time variance of the temperature gradient at a point above the sample surface for each given set of program parameters.

2.2.2 Parameters

The values of the thermal conductivity k , the density ρ , and the specific heat at constant pressure c of the main materials used in the numerical simulations are given in Table 2.1.

The values of k , ρ , and c used in the simulations for the polymer layer were based on general values for plastics, and may not exactly match the poly(*p*-phenylenevinylene) used in the experiments. Other values were trialed in the simulations, making little difference to the overall results. The value of the thermal conductivity shown in the table is high for plastics, representing the “worst case” in which the most heat could flow away from the deflecting medium.

The values for quartz shown in the table were used for the substrate, to reflect the fused silica slides used for the majority of the samples. Polyethersulphone⁶¹ was also used as a substrate for the experiments in which air was used as a deflecting medium. This was because using a substrate of low thermal conductivity caused more of the heat from the absorbed light to flow in the direction of the deflecting medium (the air) where the probe laser was propagating, rather than being lost through the substrate.

Carbon tetrachloride was investigated as a deflection medium because of the strong temperature dependence of its refractive index ($dn/dT = -0.271$).⁵⁹ Importantly though, it does not have any major absorption in the wavelength region of interest (near UV to near IR), unlike chloroform for example which has a higher dn/dT (-0.598) but also a stretch absorption feature in the near IR. Importantly also, carbon tetrachloride did not chemically damage the polymers being studied here.

Typical computational runs used step sizes of 50nm in the polymer, 25 μ m in the other media, and 5ns time steps; when very strong absorptions were investigated smaller step sizes down to 5nm were used in the polymer, requiring time steps of 0.05ns.

	k (Wm ⁻¹ K ⁻¹)	ρ (kg m ⁻¹)	c (J kg ⁻¹ K ⁻¹)	dn/dT (K ⁻¹)
Air ⁵⁸	0.023	1.204	1005.7	-0.95x10 ⁻⁶
Carbon Tetrachloride ⁵⁹	0.099	1.5833x10 ³	850	-6.118x10 ⁻⁴
Polymer	0.35	1.0x10 ³	1.5x10 ³	
Glass (quartz) ⁶⁰	1.381	2.2x10 ³	754	
Polyethersulphone ⁶¹	0.15	1.37x10 ³	1.5x10 ³	

Table 2.1 Values used in numerical simulations

Chopping frequencies of 14 and 30 Hz were used for most simulations in carbon tetrachloride and air respectively, but could be varied.

2.2.3 Frequency dependence

As the chopping frequency increases, the thermal diffusion length μ decreases as

$$\mu = \frac{1}{a} = \sqrt{\frac{2k}{\rho c \omega}}$$

where a is the thermal diffusion coefficient, k , ρ and c are as defined above, and ω is the frequency.

At high frequencies, the diffusion length is smaller than the separation between the sample and the probe beam, and the modulations in the temperature do not travel to the probed region. Low frequencies are therefore the most desirable. For experiments performed under air, the lower limits on the frequency are given by the system reaching

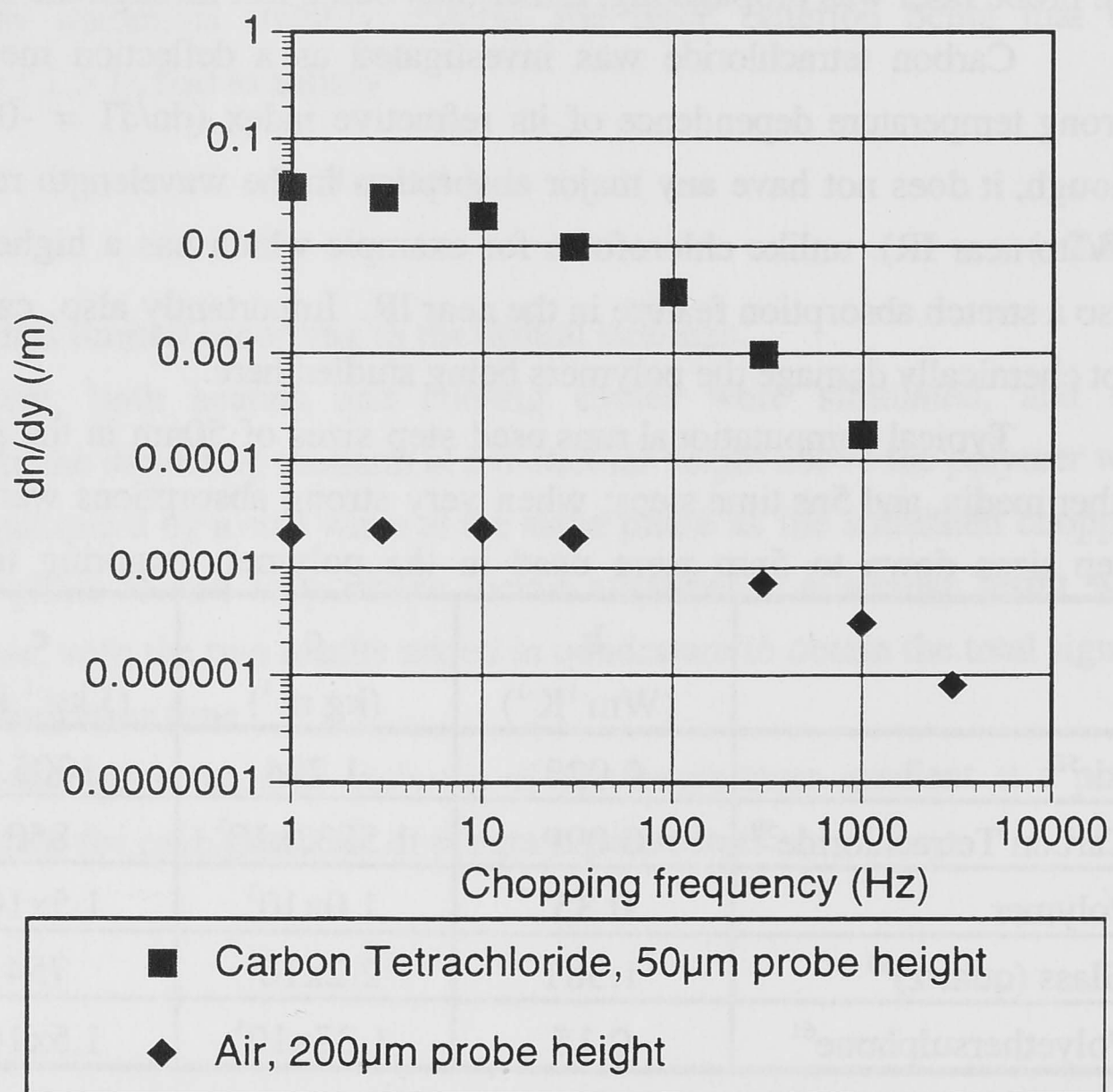


Figure 2.2 Dependence of the refractive index gradient on the chopping frequency, for air and CCl_4 as deflection media.

steady state after the peak in the temperature gradient when the sample is first irradiated; further limitations on the frequency are due to the low-frequency cut off in the electronics and the increasing $1/f$ noise, and the long integration times which become necessary for the lock-in amplifier.

The results of numerical simulations are shown in Figure 2.2. The thermal gradient obtained from the simulations has been multiplied by dn/dT (the change of refractive index with temperature) to give the gradient of the refractive index (dn/dy , y being vertical distance). Since dn/dT for carbon tetrachloride is approximately 640 times greater than that for air, carbon tetrachloride is the preferred medium. At the low frequencies in air, where dn/dy is seen to be depressed in Figure 2.2, the results have been affected by the size of the computational array which has limited the flow of heat from the system.

A chopping frequency of 30 Hz was chosen for these experiments. This frequency is sufficiently low to take advantage of the improvement in signal with reduced frequency, but sufficiently high to be able to obtain good noise rejection with a lockin time constant of 3 seconds, without $1/f$ noise being a limitation.

2.2.4 Probe beam height dependence

Numerical simulations using air as a deflection medium, and in this case a chopping frequency of 50Hz, showed an exponentially decreasing signal with increasing probe beam height above the sample. This is plotted in Figure 2.3.

To experimentally verify this relationship, a film of poly(vinyl alcohol) doped with chlorophyllin was placed in the sample holder. Chlorophyllin has a strong absorption peak at 630nm, which was measured with the photodeflection spectroscopy system. The sample holder, being on an adjustable height platform, could be adjusted for height using a micrometer screw. The sample was lowered away from the probe beam height, and the signal strength measured for steps of 0.5mm. Though the exact distance between the probe beam and the sample was not measured, the signal decreased as expected and the points have been plotted on Figure 2.3 to show a fit with the points from the numerical simulation.

The best results are obtained for the closest possible approach of the probe beam to the sample surface. The samples were prepared on substrates with the width of a microscope slide (25mm), and so the closeness of approach of the probe beam was

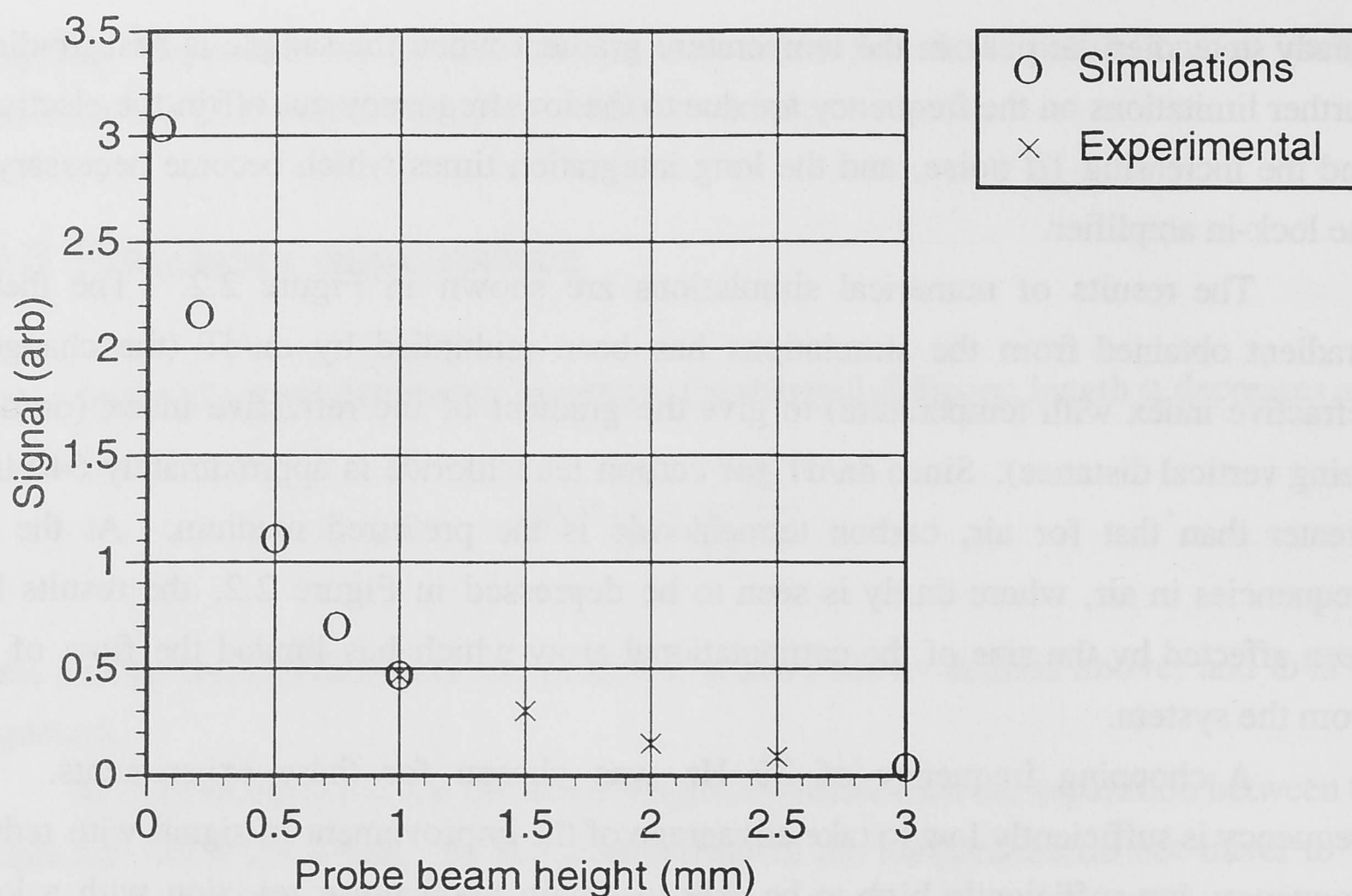


Figure 2.3 Variation of signal with probe beam height above sample. The simulations were for air as the deflecting medium. The experimental points are from chlorophyllin doped poly(vinyl alcohol) slides in air, measured at the 630nm peak, with accurate spacing between probe beam heights but not absolute calibration.

limited by its confocal parameter. The implications for the focussing of the probe beam are discussed further in section 2.4 below.

2.2.5 Linearity with absorption

The strength of the signal (the amount by which the probe beam is deflected due to the temperature and refractive index gradient) increases when the amount of energy deposited by the pump beam in the absorbing sample within a thickness of the order of the thermal diffusion length is increased. However, it is possible for the PDS signal to saturate once all the light is absorbed within this region.

Figure 2.4 shows the results of simulations in which the thickness and absorption of the polymer layer of the sample were varied. The plot shows the magnitude of the time-varying temperature gradient for a series of samples of different thicknesses, for different magnitudes of the absorption coefficient. All other parameters are as indicated in Table 2.1, with air as the deflection medium in this case.

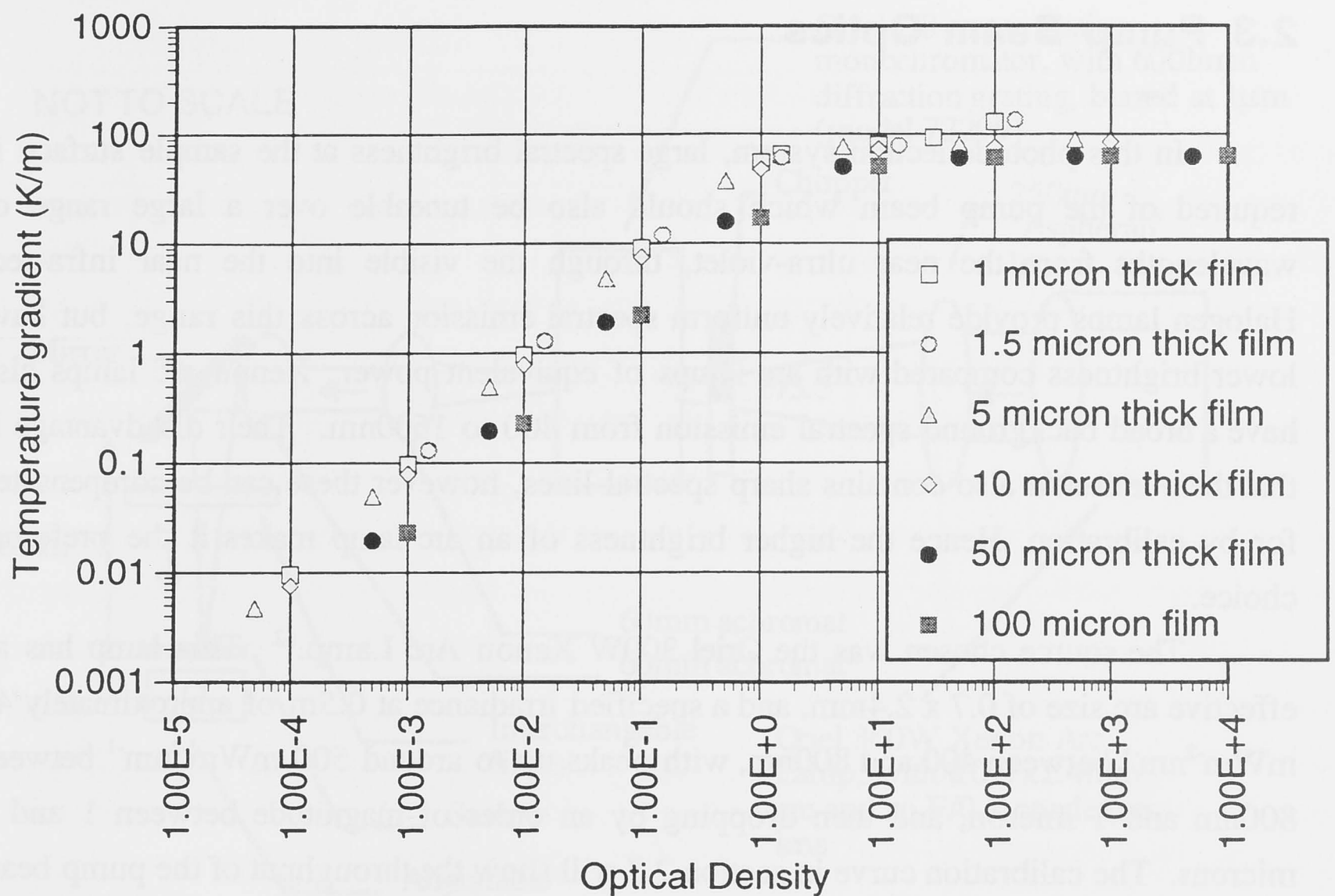


Figure 2.4 Simulations of varying absorption and sample thickness. The deflection medium is air, the probe height 0.2mm.

It can be seen that the plots for the 1 to 10 micron thick films fall on the same line, showing that the signal is proportional to αl (where α is the absorption coefficient and l is the film thickness). For films greater than 10 microns thick, the absorption of the pump beam occurring deeper into the (thick) film does not equally affect the strength of the signal. For films up to 10 microns thick, the signal strength is directly proportional to the thickness of the film (below saturation).

The plot has been drawn as a function of optical density αl to show the effect of saturation which occurs at an optical density of approximately 0.5. The signal varies linearly below that level and is hence directly proportional to the absorption of the film.

Similar curves plotted for different probe beam heights indicate that saturation occurs at the same value of αl , but at different absolute signal strengths (see section 2.2.4).

2.3 Pump Beam Optics

In this photodeflection system, large spectral brightness at the sample surface is required of the pump beam which should also be tuneable over a large range of wavelengths from the near ultra-violet, through the visible into the near infra-red. Halogen lamps provide relatively uniform spectral emission across this range, but have lower brightness compared with arc lamps of equivalent power. Xenon arc lamps also have a broad background spectral emission from 400 to 1500nm. Their disadvantage is that their emission also contains sharp spectral lines, however these can be compensated for by calibration. Hence the higher brightness of an arc lamp makes it the preferred choice.

The source chosen was the Oriel 300W Xenon Arc Lamp.⁶² This lamp has an effective arc size of 0.7 x 2.4mm, and a specified irradiance at 0.5m of approximately 40 $\text{mWm}^{-2}\text{nm}^{-1}$ between 400 and 800nm, with peaks up to around 500 $\text{mWm}^{-2}\text{nm}^{-1}$ between 800nm and 1 micron, and then dropping by an order of magnitude between 1 and 2 microns. The calibration curve in section 2.7 will show the throughput of the pump beam system. Higher powered Xenon lamps had larger arc sizes which gave them lower brightness, and hence were less suitable.

The entire pump beam system is shown in Figure 2.5.

The monochromator chosen was an Oriel 1/8m grating monochromator. This compact monochromator has a variety of gratings available, and was stepper motor driven for automatic operation.

The grating for the monochromator had to be chosen for the best throughput over the whole spectrum being measured (300 or 400nm-1500nm). The grating chosen was Oriel catalogue number 77299, a 600 lines/mm ruled grating blazed at $1\mu\text{m}$. The grating is specified as useable between 400 and 2000nm, so the lower end of the spectrum is limited; however the major spectral features being studied were within the grating's operating range.

The pump light had to be focused into the monochromator, matching its F-number (F/3.5) as closely as possible. The wide output of the arc lamp required a 69mm aperture condenser lens for collimation. An Oriel F/0.7 four element silica-borosilicate crown 'Aspherab' lens was used to collimate the light from the arc source, and then an $f=250\text{mm}$ lens selected to focus the light into the monochromator. This gave a magnification of $3.5/0.7 = 5$, so that the approximately 0.7 x 2.4mm arc was imaged at approximately 3.5 x 12mm at the entrance slit of the monochromator. The monochromator had slits 12mm high, with variable widths. The entrance slit was generally kept slightly wide (4.3mm),

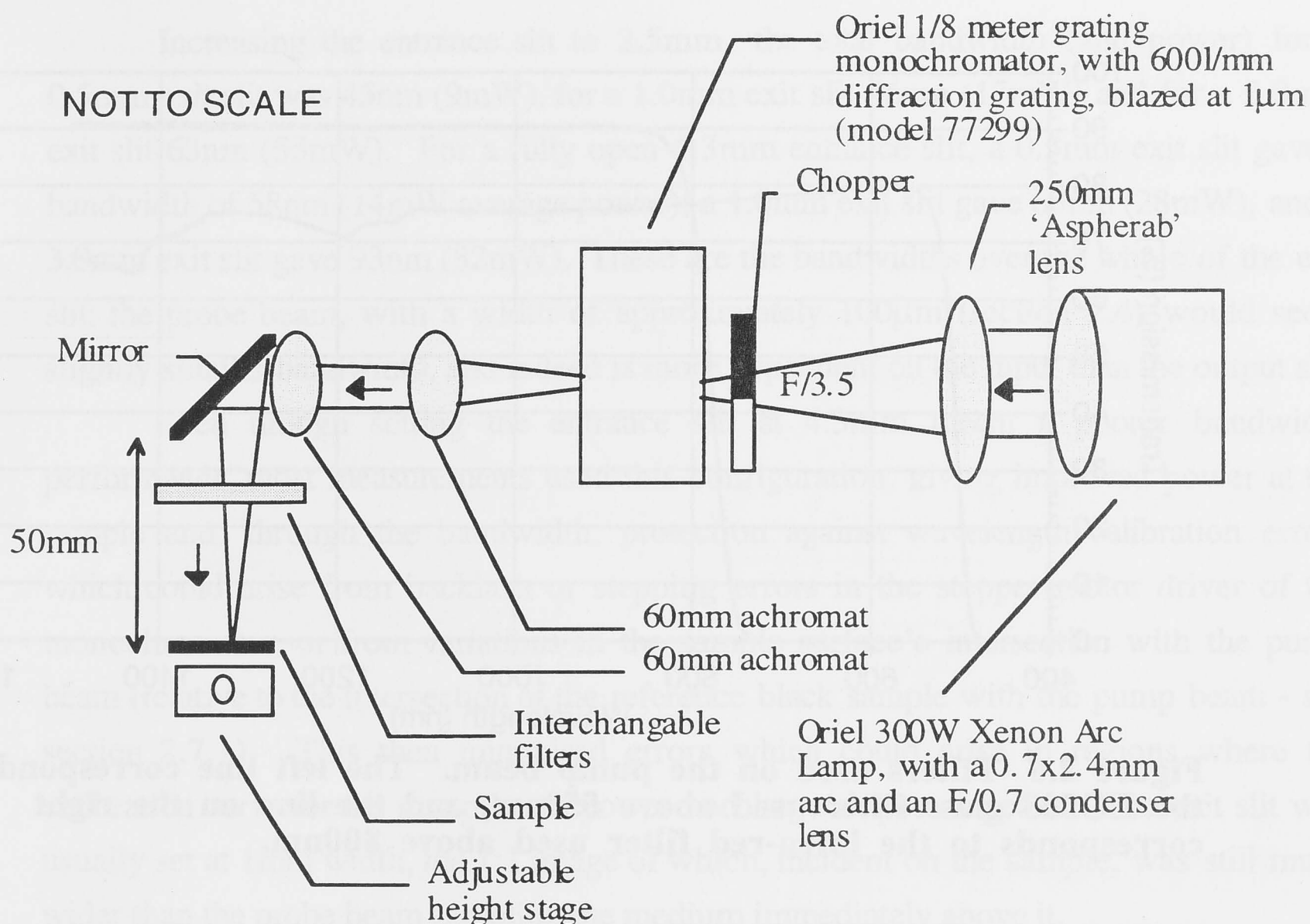


Figure 2.5 Pump Beam Optical System

to allow as much light as possible through, at some expense to bandwidth, which is discussed below.

The light is chopped before entry into the monochromator, typically at 30Hz (see section 2.2.3).

A telescope and mirror arrangement was constructed to 1:1 image the vertical monochromator slit onto the horizontal sample surface, with the probe beam propagation in the directions of the longer dimension of the image. Two 60mm achromats were used for this purpose. The length of the stripe, approximately 10mm, was appropriate for working with samples of microscope-slide dimensions.

Prior to striking the sample the pump beam is also passed through an interchangeable high-pass filter, to block the higher orders of diffraction from the grating monochromator. The filters are changed by a computer-controlled stepper motor. Below 550nm, no filters are used, since the drop in ultra-violet transmission through the lenses is sufficient to prevent stray orders below that. The transmission spectra of the filters used between 550nm and 800nm, and above 800nm, are shown in Figure 2.6.

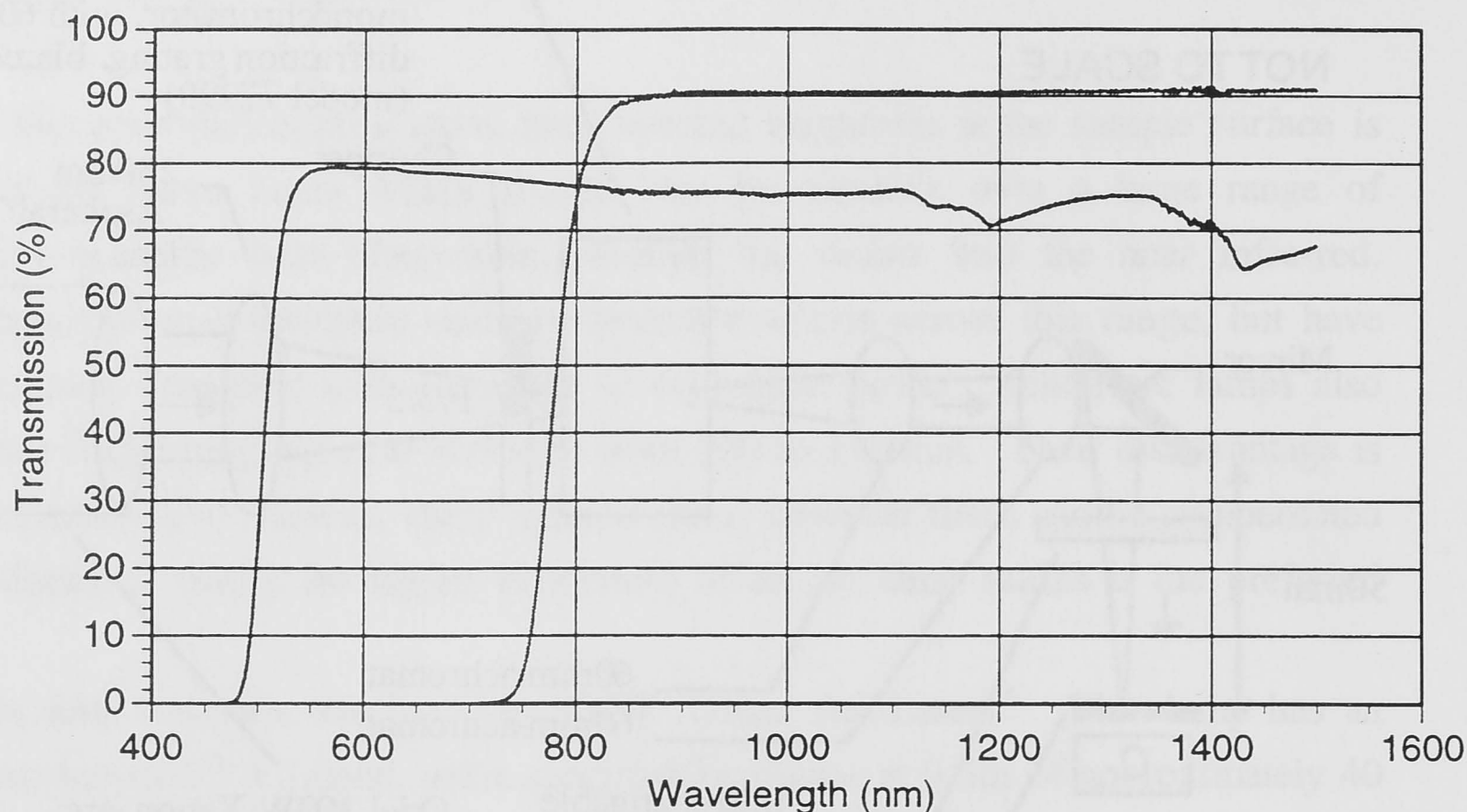


Figure 2.6 Filters used on the pump beam. The left line corresponds to the LG505 glass filter used above 550nm, and the line on the right corresponds to the infra-red filter used above 800nm.

2.3.1 Bandwidth

The bandwidth through the system is a function of the slit width, and is limited by the size of the lamp arc and its image at the entrance aperture of the monochromator. The dispersion of the grating was 13.0nm/mm. Reducing the size of the slits also reduces the pump power incident at the sample, which is undesirable for samples less than a micron thick with absorptions of the order of 0.1cm^{-1} . Since the shape of the lamp arc means that its image imperfectly fits the entrance aperture of the monochromator, narrowing the entrance slit has a large effect on the power throughput.

The actual bandwidth of the pump light at the sample has been measured using an optical fibre to gather light from the location of the sample, to take it to another monochromator attached to a spectral imaging system. The power in the pump beam was measured using a Newport power meter, averaged over the chopped pump beam at 900nm.

For 1.0mm entrance and exit slits, the fibre at any one location in the pump beam measured the full-width half-maximum bandwidth of 14nm, but over the whole of the exit slit image a total bandwidth of 32nm. The measured power at the sample was 7mW. For 0.5mm slits, the power was 2mW.

Increasing the entrance slit to 2.5mm, the total bandwidth (and power) for a 0.5mm exit slit was 45nm (9mW), for a 1.0mm exit slit 46nm (17mW) and for a 3.0mm exit slit 63nm (53mW). For a fully open 4.3mm entrance slit, a 0.5mm exit slit gave a bandwidth of 58nm (14mW average power); a 1.0mm exit slit gave 63nm (28mW), and a 3.0mm exit slit gave 93nm (82mW). These are the bandwidths over the whole of the exit slit; the probe beam, with a width of approximately 100 μ m (section 2.4) would see a slightly smaller bandwidth, and indeed is more dependent on the input than the output slit.

Even though setting the entrance slit at 4.3mm meant a poorer bandwidth performance, most measurements used this configuration, giving improved power at the sample and, through the bandwidth, protection against wavelength calibration errors which could arise from backlash or stepping errors in the stepper motor driver of the monochromator, or from variations in the sample surface's intersection with the pump beam (relative to the intersection of the reference black sample with the pump beam - see section 2.7.1). This then minimised errors which could arise in regions where the calibration curve for the pump beam power had large slopes or peaks. The exit slit was usually set at 1mm width, the 1:1 image of which, incident on the sample, was still much wider than the probe beam sampling the medium immediately above it.

2.4 Probe Beam Optics

The probe beam system, which has to satisfy requirements of stability, sensitivity and a close approach between the probe beam and the sample, is shown in Figure 2.7.

The probe beam was required to make a close approach to the sample surface, and not be broadened too much by diffraction upon reaching the detector. It could not be refocussed after the sample since that would also reduce the absolute deflection of the probe beam at the detector. The probe beam also had to be stable from power fluctuations, and needed good pointing stability. For this reason diode lasers were rejected, and a polarised laser chosen. A Helium:Neon 632.8nm laser was chosen as satisfying these requirements, as well as having a wavelength suitable for detection. The laser was a 10mW Melles Griot laser, from which the beam emerged from with a $1/e^2$ diameter of 0.68 μ m, and a divergence of 1.18mrad.⁶³ Those figures were the given specifications, and were consistent with measurements by a Spiricon beam analysis system.

TOP VIEW
NOT TO SCALE

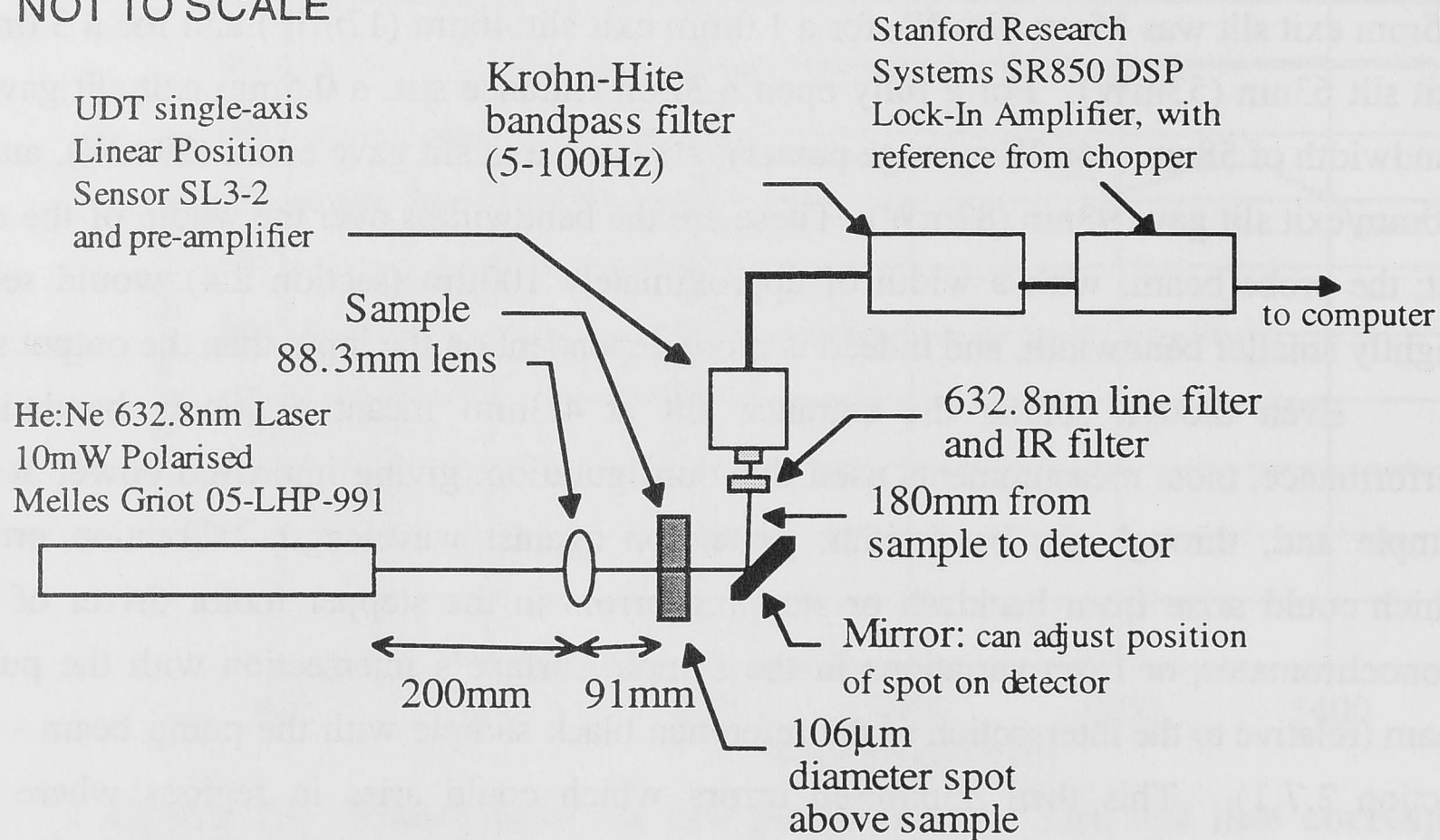


Figure 2.7 Probe Beam Optical System

The beam had to be focused to a small diameter waist over the sample surface, but in order to obtain a close approach to the surface, a sufficiently large confocal-parameter was required. For convenience the samples were based on the width of a microscope slide - 25mm. By using an 88.3mm lens situated 200mm from the laser's exit aperture, a waist of 102µm diameter was obtained 91mm from the lens, with a confocal parameter $2b = 26\text{mm}$. Measured with the Spiricon beam analysis system, the waist was found to be 106µm in diameter, at a distance of $92 \pm 4\text{mm}$.

When Carbon Tetrachloride was used as the deflection medium, it was kept within a sealed stainless-steel cell with glass windows on every side. The cell was placed on a special mount on the adjustable-height stage, which ensured that the position and angle of the cell was repeatable (see section 2.6.2). The cell was at a slight angle to the probe beam, so that the reflections from the glass faces did not enter the detection system, or were backreflected into the laser, causing interference. The length of the beam path through the cell was 50mm. With a refractive index of 1.459,⁶⁴ the probe laser system had to be adjusted by 7mm to account for the shift in the beam focus.

The probe beam was set at a fixed height, but the sample platform could be raised to obtain the closest possible approach to the beam without causing significant diffraction. After passing over the sample, the beam was reflected by an adjustable mirror onto the

detector. This mirror also turned the beam away from the monochromator stand, as shown in the diagram of the complete setup, Figure 2.11.

The detector was 180mm from the sample, struck by a 1.4 mm spot.

A 633nm line filter and an infra-red blocking filter were used to prevent any stray light from the arc lamp from striking the detector. All of the optical elements were slightly mis-aligned, to prevent back-reflections and interference, and thus preventing spurious noise from stray reflections back into the laser destabilising it.

2.5 Detection System

2.5.1 Photodiode

The deflection of the beam by the thermal gradient above the sample surface had to be measured. The distance of the detector from the sample was kept small so as to reduce the diffraction broadening of the beam and minimise the possibility of drafts or air-borne dust from disturbing the beam path.

A bi-cell detector could be used to measure the deflection, the deflection being determined by the variation in the relative power striking the different halves of the detector. Simple knife-edge schemes, wherein a single photodetector measures the variation of the power in the beam which passes by a knife edge, have also been proposed.^{28,38} Various groups have used knife edges,⁶⁵ bi-cells,^{50,66} quadrant detectors³³ and continuous detectors.⁴⁷

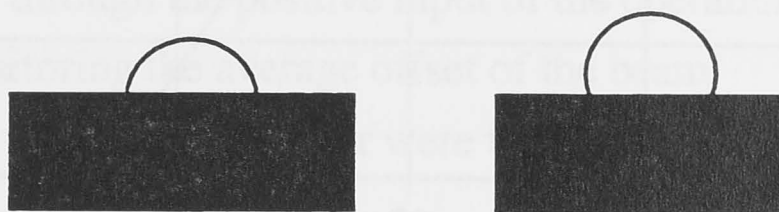


Figure 2.8 The knife-edge detector measures the deflection of the beam by how much of the beam gets past the knife edge just in front of the detector.

Using a linear position sensor has the advantage that the reading is a direct linear measurement of the position of the centre of the spot on the detector; this linearity is typically correct to 0.5% over the central 25% of the active area of the detector.⁶⁷ There is

no gap in the centre of the detecting area, as with bi-cells. The resolution of bi-cells may be better, but linear position sensors have a high signal-to-noise ratio.⁶⁷

The photodiode chosen for use here was the UDT Super Linear Position Sensor SL3-2, which is a single axis position sensor. It acts like two photodiodes with a common cathode. Current flows down the arms of the photodiode in proportion to the position of the centre of the laser spot along the axis. The photodiode has a typical inter-electrode resistance of 40k Ω , and a responsivity at 632.8nm of about 0.44 A/W.

The linearity of the photodiode was experimentally verified. Figure 2.9 shows a plot of the signals from the two anodes of the photodiode versus the position of the beam. The drop of the signals at large distances from the centre of the photodiode is a result of the beam extending beyond the end of the photodiode. Within the central region, over a distance of 4mm, the signal from one anode increases and from the other decreases as the beam moves along the detector. The difference between the signals has also been plotted on Figure 2.9, and within that central region can be fitted to a straight line with

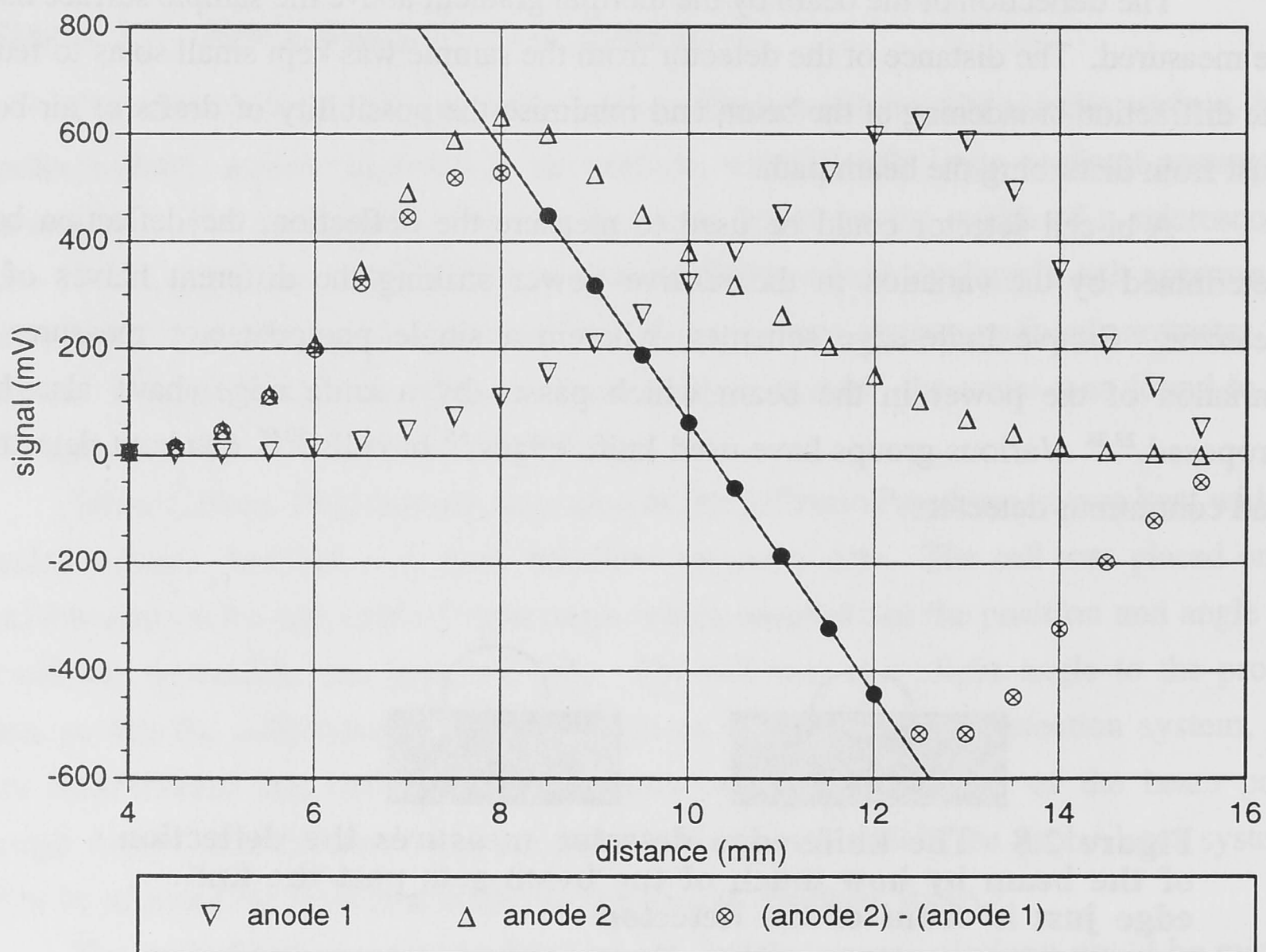


Figure 2.9 Linearity of position sensitive photodiode with position. The circles show the difference between the signals measured on the two anodes (Δ and ∇), with the filled circles fitted to a straight line with $r^2 = 0.9999$.

correlation coefficient r such that $r^2 = 0.9999$.

Because of the relatively high internal impedance of this detector it was necessary to reduce the laser power using a neutral density filter to 0.56mW at the detector. This resulted in a 0.25mA current flowing through the internal resistance and the external 20k Ω load resistors. Voltages of the order of 5V were thus developed at the inputs to the first operational amplifier (AD549JK), well within its range and within the rails (see circuit description below).

2.5.2 Circuit

Figure 2.10 shows the circuit used for the photodetector. Two 4.7 μ F capacitors back-to-back form provided the (bipolar) AC coupling into the amplification stage, with the 10k Ω resistor, giving a knee in the frequency filtering below 10Hz.

Since the AC signals from the photodiode were significantly less than a millivolt and were shot noise limited (see below), the signal had to be preamplified to prevent noise pick-up in the cables. This signals also had to be brought into a suitable range for the lockin amplifier, which could take signals up to 1V.⁶⁸

An AC gain of approximately 1000 was obtained from the amplification stage. The signal was then carried in a shielded coaxial cable to a Krohn-Hite band-pass filter, with a pass band between 5 and 100Hz, to remove the DC component prior to the lockin detector. It was then passed into the lockin amplifier, which was referenced to the chopping frequency. With a time constant of 3 seconds, the bandwidth of the lockin was $\Delta f = 26$ mHz.

Any DC component of the signal from the photodiode, which could be caused by a probe beam offset from the centre of the photodetector, was passed from the second arm of the photodiode through the positive input of the operational amplifier. This allowed the possibility of monitoring the average offset of the beam.

Signals at the lockin amplifier were then in the range of 100 μ V to 1V.

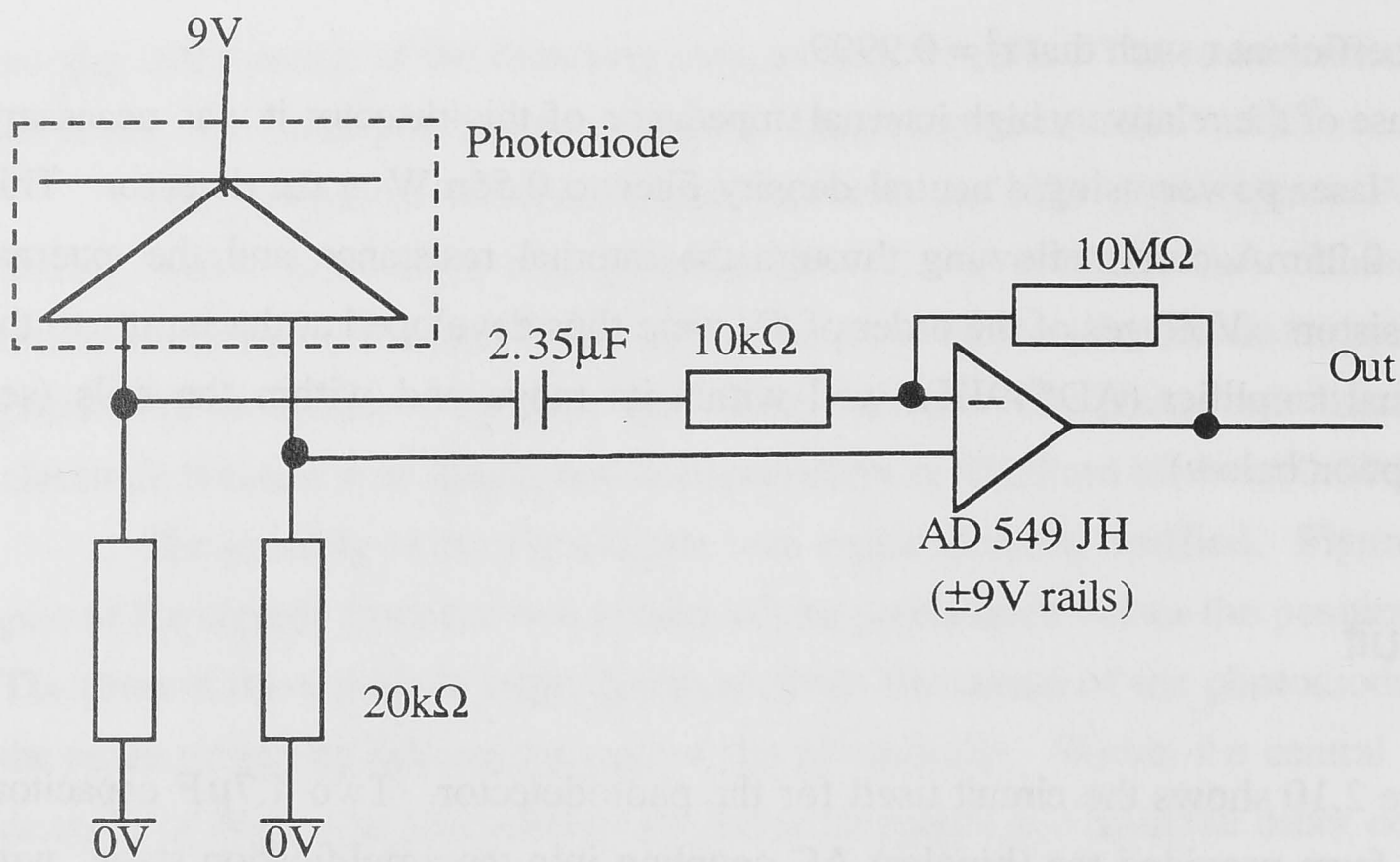


Figure 2.10 Circuit used for photodetector

2.5.3 Electronic Noise

The components of the noise generated in the detection circuit at the chopping frequency limit the small-signal resolution of the system. Shot noise and Johnson (thermal) noise are analysed below.

Shot noise results from the statistics of photons striking the photodiode to produce the photo-electrons which make up the current. It can be calculated from the relation

$$I_{sn} = \sqrt{2qI} \quad (/ \sqrt{\text{Hz}})$$

where I is the photocurrent and q is the charge of an electron.

A photocurrent of $I = 0.25\text{mA}$ is generated by 0.56mW of laser power incident on the photodiode, operating at an efficiency of 0.44A/W . This gives a shot noise of $I_{sn} = 8.9\text{pA}/\sqrt{\text{Hz}}$.

The Johnson (or thermal) noise through the load resistors on the anodes of the photodiode is given by

$$I_{th} = \sqrt{\frac{4kT}{R}} \quad (/ \sqrt{\text{Hz}})$$

where T is the temperature, k is Boltzmann's constant and R is the resistance. With a minimum load resistance of $20\text{k}\Omega$, this gives $I_{\text{th}} = 0.90\text{pA}/\sqrt{\text{Hz}}$ which is much smaller than the shot noise. Jackson et al. also found shot noise to be the dominant noise source.³⁸

The shot noise current of $8.9\text{pA}/\sqrt{\text{Hz}}$ develops a voltage of $0.18\mu\text{V}$ over the $20\text{k}\Omega$ anode resistor, which through the 1000 times gain of the pre-amplification circuit gives $180\mu\text{V}/\sqrt{\text{Hz}}$. With the lock-in operating at a bandwidth of 26mHz , this is around $30\mu\text{V}$ of noise.

The dark current from the photodiode was, according to the specifications of the device, typically 5nA but up to a maximum of 50nA . 5nA represents 0.002% of the photocurrent generated by the laser.

Other sources of noise could include pick-up in the cables, and pointing noise from the laser. The peak to peak noise level seen on the lock-in amplifier was approximately $50\mu\text{V}$, consistent with close to shot-noise limited behaviour.

2.6 Overall Environment

2.6.1 Vibration Isolation

The PDS had to be protected from air-drafts and vibration, which would introduce spurious movements of the laser beam on the detector. In order to do this, the optical system was built on an optical vibration-isolated table. Furthermore, since the arc lamp has a cooling fan, and the monochromator a stepper motor driver, the laser, sample and detector were mounted on a second optical table top supported by vibration isolators on the first table. The second table top was completely enclosed in a wooden box to prevent drafts, with a opening for the pump beam from the monochromator to enter, and a hatch through which samples could be exchanged. These are shown in Figure 2.11.

NOT TO SCALE

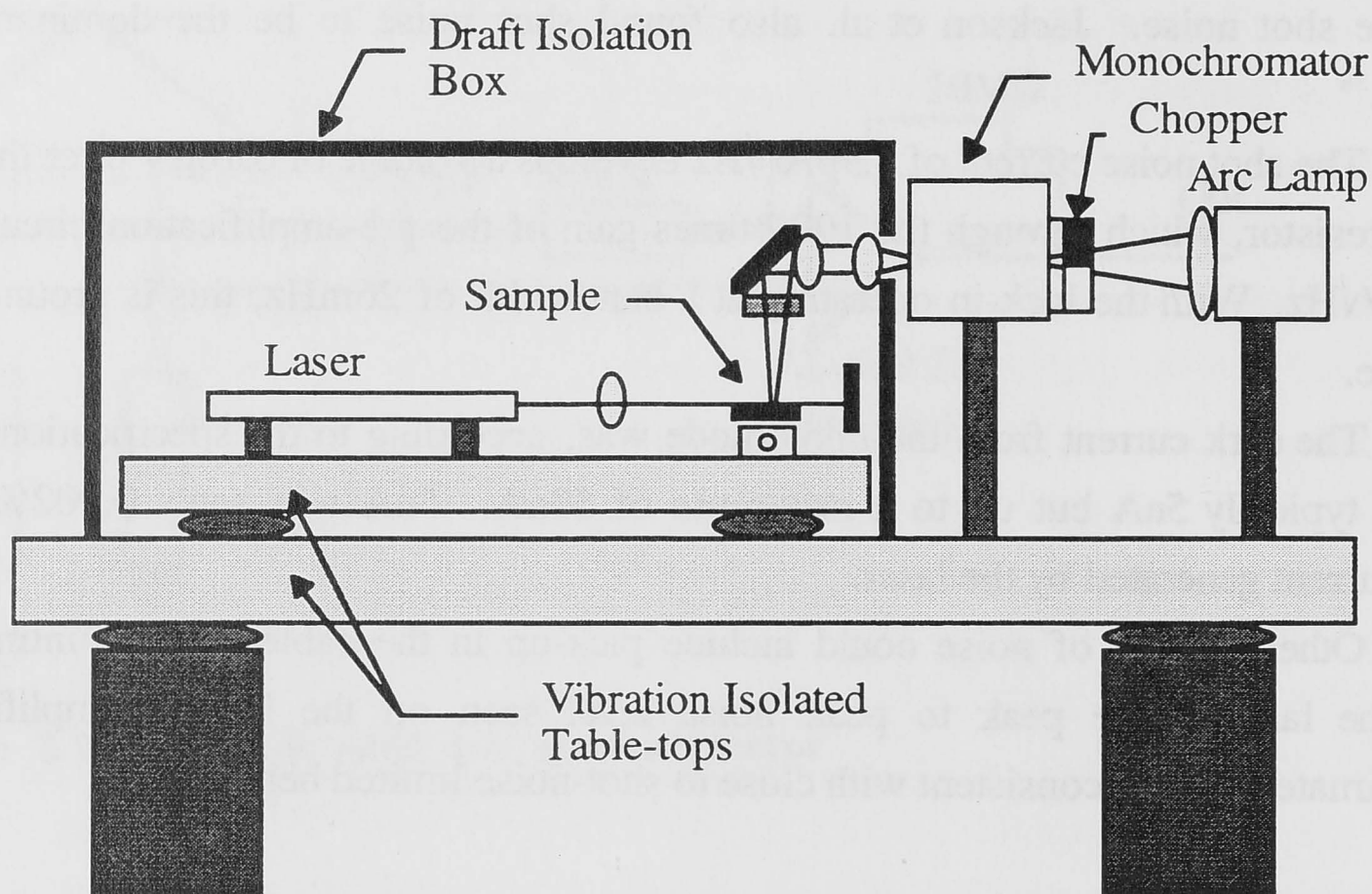


Figure 2.11 Photodeflection Spectroscopy Apparatus Side View

2.6.2 Sample Mounting

For operation under air, the samples were mounted in a spring-clip arrangement, such that the top of the sample was always held by springs against two clips at the same height. The whole stage could however be adjusted for height so as to obtain a close approach to the probe laser beam.

For operation under CCl_4 , a glass-sided stainless steel cell was used, in which the samples could be held in place with springs. The cell was filled completely with CCl_4 and sealed, so that there were no bubbles at the top of the cell which might introduce extra reflections of the pump beam and increase sensitivity to vibration. The cell fitted onto the adjustable height stage, in such a way that the position and angle to the probe beam was repeatable; the probe beam was incident at just off 90° to the window of the cell, so that reflections from the glass did not interfere with the light striking the detector and did not reflect back into the laser.

2.6.3 Computer Control

The control software was written in Visual Basic.

The lockin amplifier was under computer control via a GPIB interface, allowing the time constants and filtering options to be set from the computer.

There are two stepper motors, one for changing the wavelength of the monochromator, and the other to switch between the filters on the pump beam. A PCL-838 Stepper Motor Control Card⁶⁹ was used for the computer interface. The calls from the Visual Basic program (titled 'PDS.EXE') to change the wavelengths and filters involved shelling to executable files written for those purposes; those files were written using Turbo Pascal.

The system was built to collect raw data automatically. The parameters could be changed by the user (eg. wavelength range and step size, integration and pause times, etc). When the system is run, it steps through the wavelengths, at each point waiting for the lockin to settle and then recording the lockin output. Filters are changed automatically when necessary. At the end of a run, the data is saved to a file. It can be calibrated for the power of the pump beam by dividing by a power spectrum obtained by running the system on a black absorber (see section 2.7.1 below).

A practical description of how to use the apparatus is included in the Appendix.

2.7 Calibration

2.7.1 Calibration for lamp power

The strength of the deflection signal depends not only on the level of absorption in the sample, but also the amount of power in the pump beam incident on the sample. The pump beam power varies over the spectrum, due to the variation in the power output from the arc lamp, the diffraction efficiency of the grating in the monochromator, and the throughput of the optical system. Thus the variations in the pump beam power incident at the sample must be measured, and used to calibrate the data.

The variation in the power of the pump beam with respect to wavelength can be obtained by making a photodeflection measurement of a black absorber; that is, an absorber for which there is total absorption over the entire wavelength range. Some black

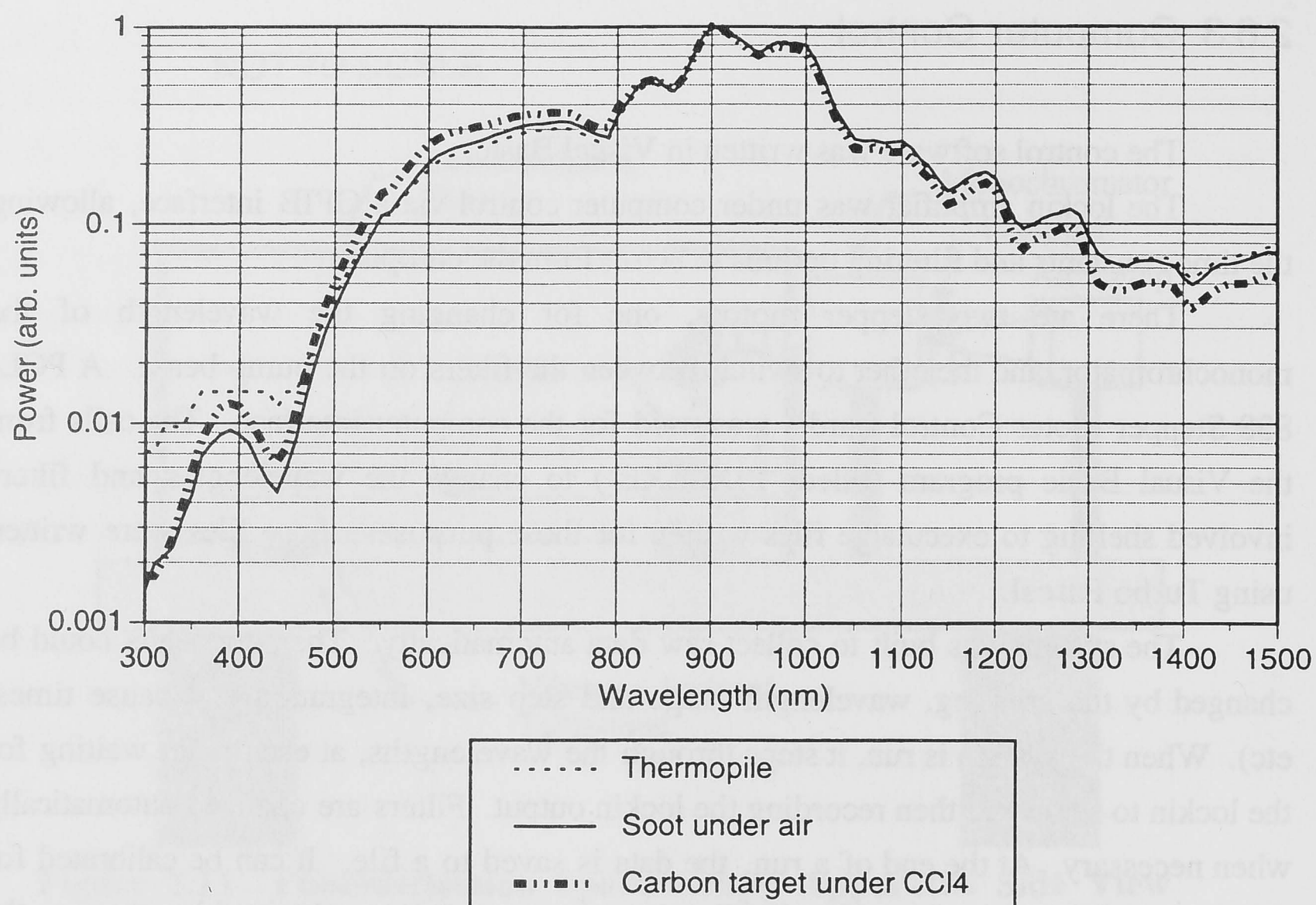


Figure 2.12 Measurements of the power in the pump beam using a black absorber as the sample.

paints are suitable; soot-covered microscope slides have proven to be the best for measurements under air, though it is necessary to lower the pump power, the stage, or the detector amplification since the signal is so large. Different black objects have been used to ensure true “blackness” over the spectrum. In the carbon tetrachloride cell carbon pellets were found to be suitable for making calibrations.

Figure 2.12 shows the results so obtained from a soot slide with air as the deflection medium. On the same graph a measurement of the power made with a thermopile is shown. The two spectra are consistent except for wavelengths below 400nm where there was insufficient power for the thermopile. The actual power at the peak of the spectrum (900nm), under a chopped pump beam, was 28mW.

The spectrum is dominated by the peaks around 900nm, from the Xenon arc lamp. Below 650nm the grating efficiency drops below 50%, and the power from the arc lamp also drops. Beyond 1 micron, the lamp power drops away slowly but the grating efficiency drops away more quickly.

Also on Figure 2.12 is a measurement of the spectrum made under carbon tetrachloride using a carbon pellet. It is easily re-measured, and it was re-measured if the conditions of the pump beam were ever altered (eg. the monochromator slit widths). The

bandwidth of the monochromator system for the spectra shown here was approximately 50nm (see section 2.3.1).

2.7.2 Calibration with samples of known absorption

To check that the photodeflection spectroscopy system was accurately measuring the absorption over a reasonable range, samples of poly(vinyl alcohol) (PVA) doped with different levels of chlorophyllin were prepared. Chlorophyllin has two absorption peaks, at 410 and 630nm, with maximum absorptivities α of 39200cm^{-1} and 4980cm^{-1} respectively. Thus, as well as ensuring that the signal varied linearly as a function of chlorophyllin concentration in the different films, the internal consistency of the spectra could be checked - that the two chlorophyllin peaks were in the correct ratio after lamp power calibration.

Heavily doped PVA samples were very viscous whilst being prepared at 20% concentration in water (see polymer preparation section 2.8.3), so a series of thick films were prepared. The concentration of chlorophyllin ranged from 0.0009% to 21% in PVA.⁷⁰ The films were all approximately $400\mu\text{m}$ thick, and the sample stage was kept at

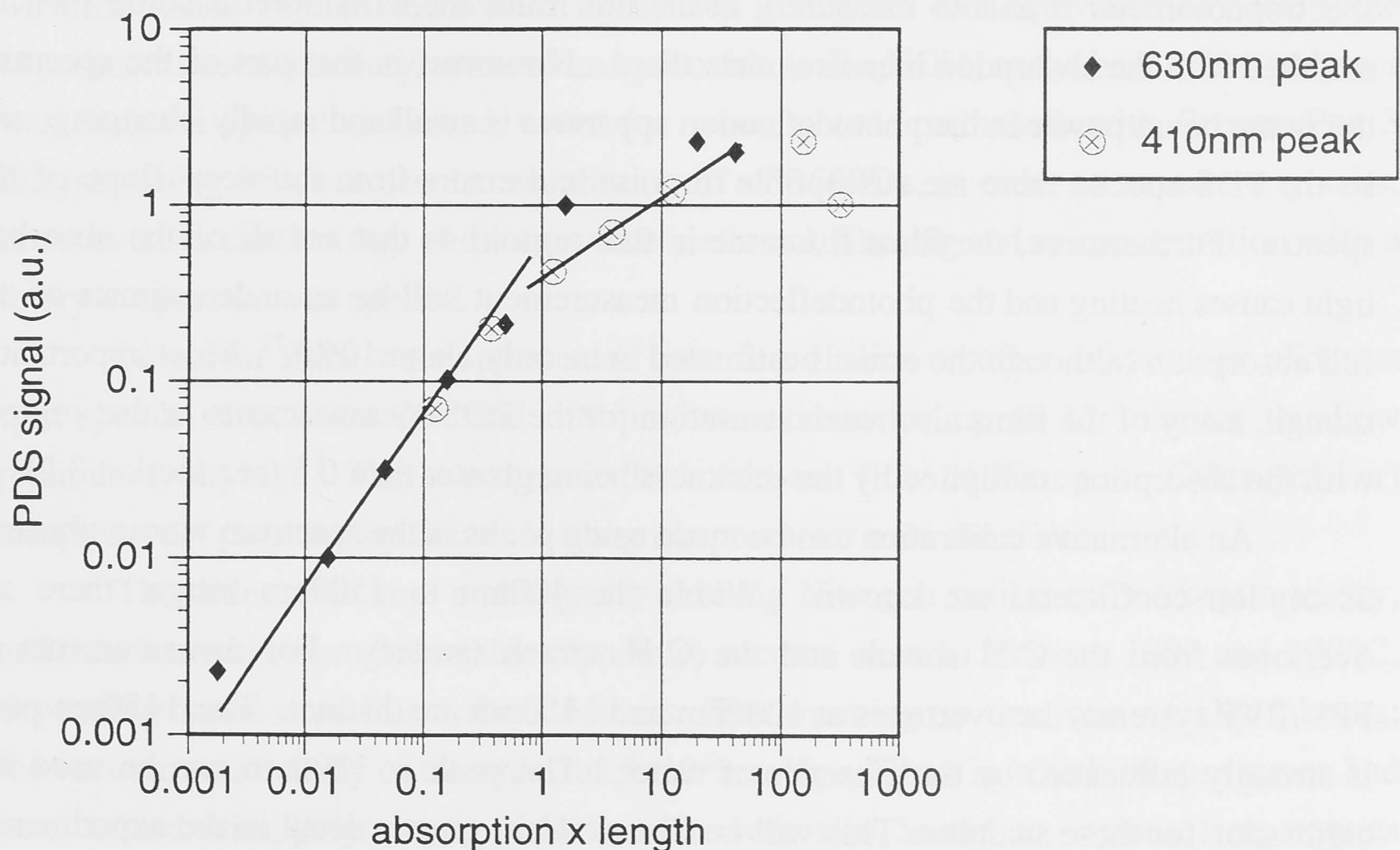


Figure 2.13 Absorption signals for PVA slides with various levels of chlorophyllin doping. Note the saturation above $\alpha l \approx 0.5$ (see section 2.2.5).

the same position for the measurements; air was used as the deflection medium. The signals measured by photodeflection spectroscopy are shown in Figure 2.13 as a function of the absorbance as obtained from measurements using the spectrophotometer.

2.7.3 Absolute Calibration for each sample

Each sample may have a different thickness and surface profile, affecting the separation between the probe beam and the sample surface. The sample stage height is adjusted to bring each sample close to the beam, but it is difficult to guarantee the same sample - probe beam separation each time. Also, the total absorbance of the film depends on the film thickness. For these reasons it is not possible to give a general calibration of the PDS signal to give the absolute absorption for all samples. Each sample has to be calibrated for absolute absorption using known features in the spectra.

There are two possible techniques for this, for the PPV and PVP films being studied here.

The first possibility is that the calibration could be performed at the short wavelength end of the spectrum, where the absorption is sufficiently strong that the spectrophotometer is able to measure it in the thin film; the PDS spectra could then be matched with the absorption measurements there. However, in that part of the spectrum the pump beam power in the photodeflection apparatus is small and rapidly changing, and so the PDS spectra there are susceptible to noise and errors from the steep slope of the spectra. Furthermore, the films fluoresce in that region, so that not all of the absorbed light causes heating and the photodeflection measurement will be an underestimate of the full absorption (although the error is estimated to be only about 10%).⁷¹ Most importantly though, many of the films also reach saturation for the PDS measurements in that region, with the absorption multiplied by the thickness being greater than 0.5 (see section 3.2).

An alternative calibration can be made using peaks in the spectrum whose absolute absorption coefficients are known. Within the 400nm to 1500nm range, there are overtones from the C-H stretch and the O-H stretch (water). For measurements of PPV/PVP systems, the overtones at 1200nm and 1450nm are distinct. The 1450nm peak is strongly influenced by the presence of water. The peak at 1200nm can be used for calibration for these samples. This will be discussed in greater detail in the experimental results section 3.2.

A possible future modification of the system would be to extend the range to cover the stronger overtone peaks above 1500nm.

2.8 Preparation of Materials

2.8.1 Preparation of Poly(*p*-phenylenevinylene) (PPV)

Poly(*p*-phenylenevinylene) films were prepared by first making a precursor polymer, which could be spun or doctor-bladed onto a substrate and subsequently converted into PPV by heating. This is a necessary route because the PPV cannot be readily dissolved and spun itself. PPV precursor polymers used for preparation of the films studied here were synthesised by Dr. M. Woodruff, and most of the chemical processing of the precursor films was carried out by Dr. A. Samoc and Mrs. R.M. Krolikowska in the Laser Physics Centre at the Australian National University.

The preparation procedure was based on references 72,73,74,75 and 76, and the chemical route is shown in Figure 2.14. Wherever possible the preparations were carried out in an inert (Nitrogen) atmosphere. The *bis*-sulfonium salt monomer was prepared from α,α -dichloro-*p*-xylene and tetrahydrothiophene, kept at 50° to 55°C for 24 hours. The monomer was polymerised in basic conditions, in a water:methanol solution. In different experiments the details were varied, but a representative procedure used a 50:50 water:methanol solution and sodium hydroxide giving 0.9 mol equivalent of base; some experiments used tetrabutylammonium hydroxide (n-Bu₄NOH) as the base. The polymer was dialysed against deionised water (or when noted, methanol) with Spectra/Por 3 dialysis tubing with a molecular weight cut off of 3500Da, in order to remove any salts. In some cases another step of dilution with methanol, filtering and re-concentration with a rotary evaporator was applied.

Precursor films were spin-coated onto fused silica or other microscope slides at spin speeds of between 200 and 500rpm, sometimes for up to 15 minutes to allow preliminary drying.⁷⁷ This was done under a constant flow of Nitrogen. Other (thicker) samples were prepared by doctor-blading the precursor onto the slides.

The slides were kept under gently flowing Nitrogen until they had begun to dry, and then heated in a programmable (dynamic) vacuum oven to between 130° and 200°C, depending on the experiment, for 3-5 hours. The warming up time was usually 2 hours; the vacuum was usually of the order of 5×10^{-3} mmHg. Films in which the precursor had been mixed with poly(vinyl pyrrolidinone) were also heated to various temperatures between 130° and 200°C.¹⁸ The heating enabled the conversion of the non-conjugated precursor into the rigid-rod, π -electron conjugated polymer PPV. Composite films were

prepared in such a way as to achieve PPV concentrations after conversion of close to 2.5%, 5%, 10%, 20%, 50% and 100%.¹⁸

The conversion conditions have been found to be critical for the length of conjugation in PPV obtainable during the conversion reaction, the degree of crystallinity in the samples, and the degree of "incipient" doping and absorption induced by the products of the conversion reaction - see reference 78 for a review, and the literature cited there.

Experiments in which different preparation procedures were used are noted in the text where relevant (see especially section 3.3).

2.8.2 Preparation of Poly(vinyl pyrrolidinone) (PVP)

Poly(*N*-vinyl-2-pyrrolidinone) films were usually prepared from Sigma 40,000 molecular weight PVP, dissolved to 30% in 1-methyl-2-pyrrolidinone (NMP). Variations are noted in section 3.4. Films were spin coated onto slides at between 500 and 5000rpm, and then placed in a (dynamic) vacuum oven and heated to 120° for 24 hours to dry. For certain experiments the PVP was be doped with phloxine-B and other dyes.

PVP films tend to be of good optical quality, in comparison to pure PPV films, in which it can be difficult to achieve waveguiding.

2.8.3 Preparation of Poly(vinyl alcohol) (PVA)

Poly(vinyl alcohol) films were made from Sigma 9,000-10,000 molecular weight, 80% hydrolysed PVA, dissolved in water at around 20% concentration. Different concentrations of dopants such as chlorophyllin were used as for the linearity checks for the photodeflection apparatus (section 2.7.2). The slides were warmed at 45°C for 45 hours to allow them to dry.

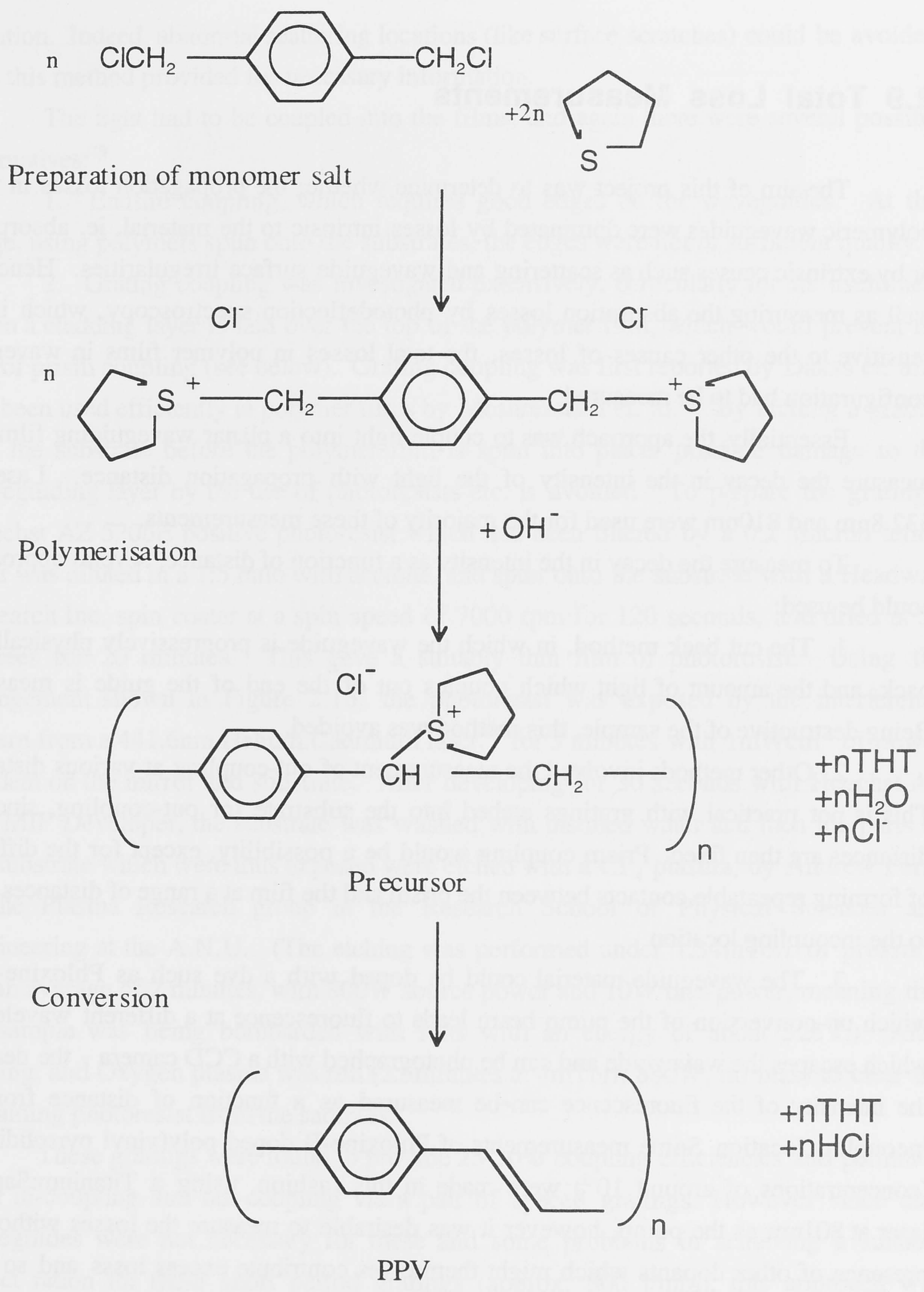


Figure 2.14 Preparation of Poly(*p*-phenylenevinylene) (PPV)

2.9 Total Loss Measurements

The aim of this project was to determine whether the propagation losses in these polymeric waveguides were dominated by losses intrinsic to the material, ie. absorption, or by extrinsic causes such as scattering and waveguide surface irregularities. Hence, as well as measuring the absorption losses by photodeflection spectroscopy, which is not sensitive to the other causes of losses, the total losses in polymer films in waveguide configuration had to be measured.

Essentially, the approach was to couple light into a planar waveguiding film, and measure the decay in the intensity of the light with propagation distance. Lasers at 632.8nm and 810nm were used for the majority of these measurements.

To measure the decay in the intensity as a function of distance, several approaches could be used:

1. The cut back method, in which the waveguide is progressively physically cut back, and the amount of light which couples out of the end of the guide is measured. Being destructive of the sample, this method was avoided.

2. Other methods involved the measurement of out-coupling at various distances: This is not practical with gratings etched into the substrate for out-coupling, since the distances are then fixed. Prism coupling would be a possibility, except for the difficulty of forming repeatable contacts between the prism and the film at a range of distances close to the incoupling location.

3. The waveguide material could be doped with a dye such as Phloxine-B, in which up-conversion of the pump beam leads to fluorescence at a different wavelength, which escapes the waveguide and can be photographed with a CCD camera - the decay in the intensity of the fluorescence can be measured as a function of distance from the incoupling location. Some measurements of Phloxine-B doped poly(vinyl pyrrolidinone) (concentrations of around 10^{-3}) were made in this fashion, using a Titanium:Sapphire laser at 801nm as the pump, however it was desirable to measure the losses without the presence of other dopants which might themselves contribute excess loss and so these measurements were not pursued for the results discussed here.

4. Working on the assumption that the light which was scattering from the waveguides was scattering from small, uniformly placed scattering centres, the decay in the scattered light could be measured as a function of distance from the in-coupling

location. Indeed, abnormal scattering locations (like surface scratches) could be avoided, and this method provided the necessary information.

The light had to be coupled into the films, and again there were several possible alternatives:⁷⁹

1. Endfire coupling, which requires good edges on the waveguides. At this stage, using polymers spun onto the substrates, the edges were not of sufficient quality.

2. Grating coupling was investigated extensively, particularly for its usefulness when a cladding layer is laid over the top of the polymer film, which would prevent the use of prism coupling (see below). Grating coupling was first reported by Dakss et. al.⁸⁰ has been used efficiently in polymer films by Moshrezadeh et. al.⁸¹ By etching a grating into the substrate before the polymer film is spun into place, possible damage to the waveguiding layer by the use of photoresists etc. is avoided. To prepare the gratings, Hoechst AZ 5206E positive photoresist which had been filtered by a 0.2 micron teflon filter was diluted in a 1:5 ratio with acetone, and spun onto the substrate with a Headway Research Inc. spin coater at a spin speed of 7000 rpm for 120 seconds, and dried at 50 degrees for 20 minutes. This gave a suitably thin film of photoresist. Using the arrangement shown in Figure 2.16, the photoresist was exposed by the interference pattern from a 441.6nm Helium:Cadmium laser,⁸² for 3 minutes with 1mWcm^{-2} of power incident on the mirror and substrate. After developing for 30 seconds with Hoechst AZ 524 MIF Developer, the substrate was washed with distilled water and then the parts of the substrate which were thus exposed were etched with a CF_4 plasma, by Andrew Perry in the Plasma Research group in the Research School of Physical Sciences and Engineering at the A.N.U. (The etching was performed under 1.34mTorr of pressure, for an average of 2 minutes, with 800W source power and 10W bias power, meaning that the sample was being bombarded with ions with an energy of about 32eV.) After etching, and Oxygen plasma was run (2.5minutes at 4mTorr, 800W, no bias) to clear the remaining photoresist from the samples.

These gratings were found to provide 25-30% coupling efficiencies and permitted both in-coupling and out-coupling via a pair of spaced gratings. However since clad waveguides were not necessary for these and some problems in achieving a suitable aspect ratio for these short period gratings (approx. 800 1/mm), this approach was abandoned in favour of the simpler Prism Coupling method.

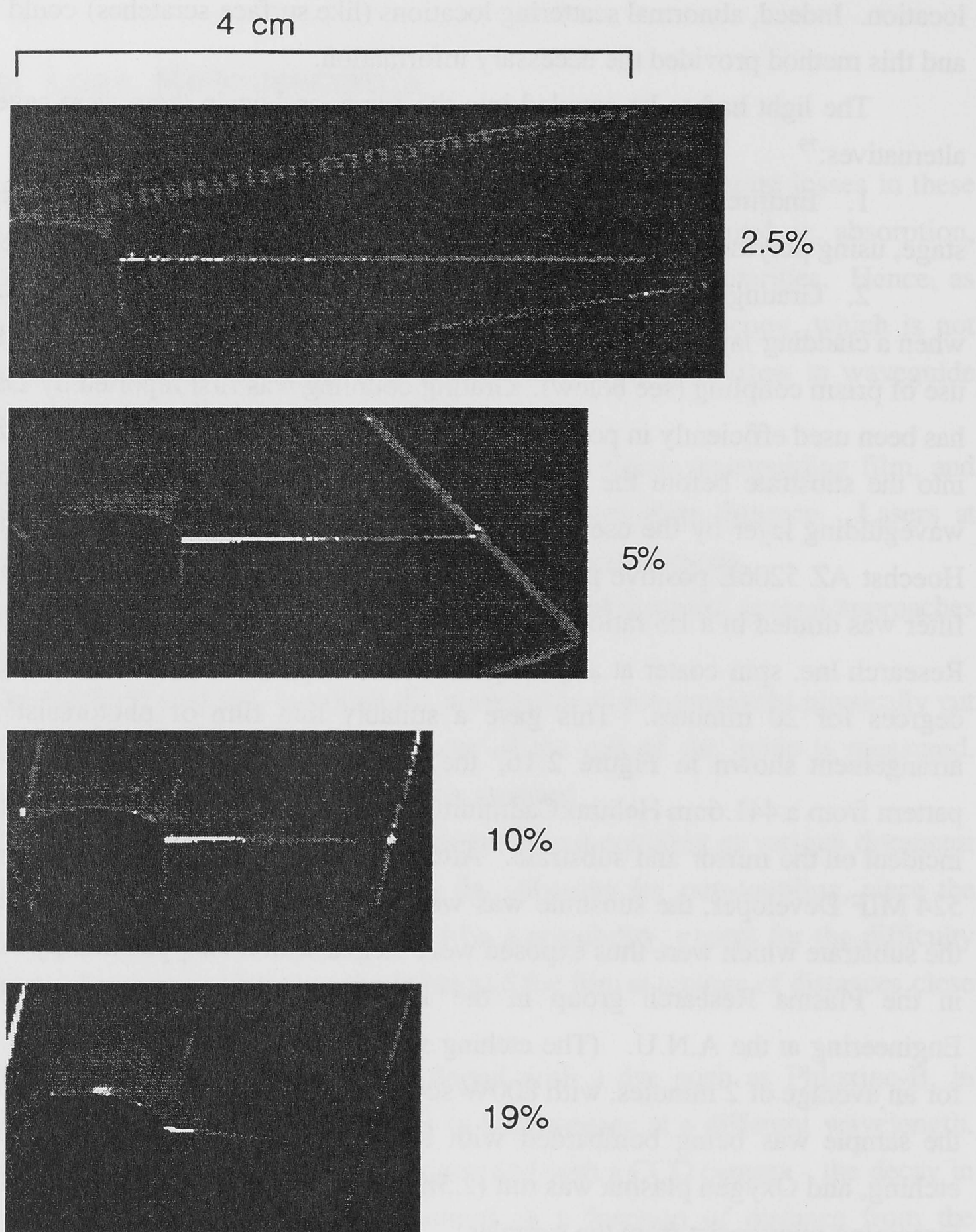


Figure 2.15 Images showing the decay in scattered light intensity with distance from the in-coupling point for waveguiding PPV-PVP films. The images were captured with a CCD camera, at 800nm. The concentrations of PPV in the films are indicated.

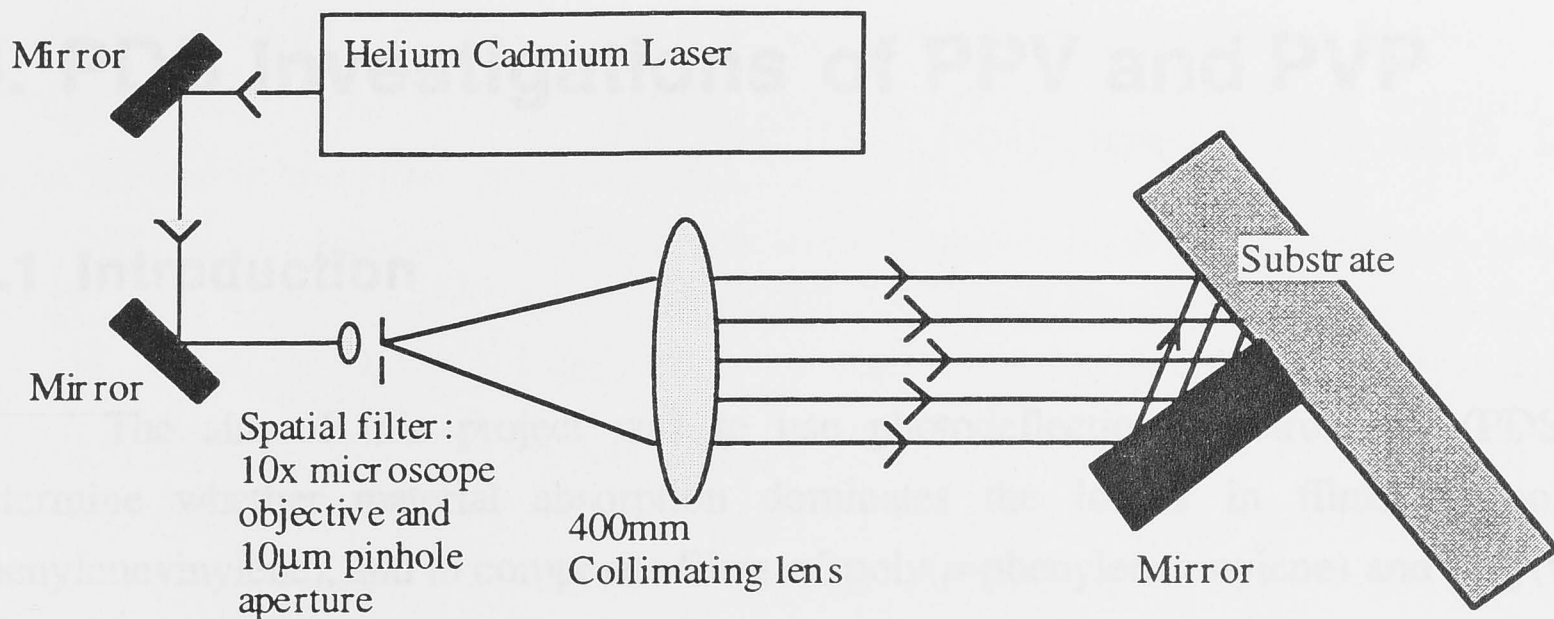


Figure 2.16 Schematic diagram of grating writing system. A 10° angle between the incident beam and the mirror gave a grating period of $1.27\mu\text{m}$.

3. Prism Coupling. By placing a high index prism in direct contact with the waveguiding film, the propagation vector of a beam from a laser striking the prism-film interface at an appropriate angle of incidence can be matched to the propagation vector of the waveguide modes allowing power to flow from the beam into the excited mode. A Metricon Prism Coupler⁸³ makes this a very straightforward procedure, and this was used for all of the measurements reported here.

Figure 2.15 shows some examples of CCD camera photographs of light scattering from polymer waveguides. A wide range of samples were characterized using this technique although the images shown here which are the most relevant to the PDS data presented later were actually recorded by a colleague in the Laser Physics Centre, Dr. A. Samoc, and published in ref. 18. These images were analysed using National Institute of Health (USA) Image software to measure the decay of the intensity of the scattered light. The results are cited in section 3.5.3.

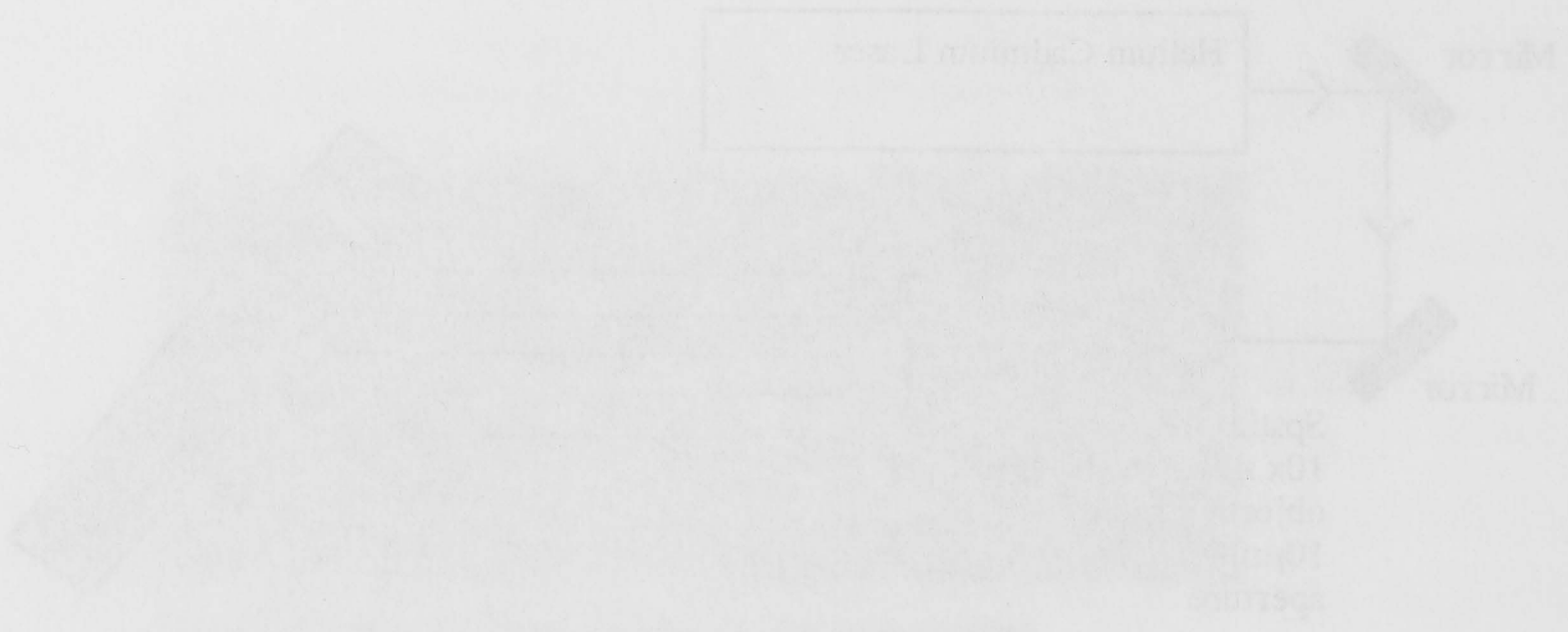


Figure 118 Schematic of the experimental setup. The angle between the incident and reflected beams is 1.17 rad .

3. From Chapter 118, we know that the propagation vector of a beam of light is perpendicular to the wavefronts. At an interface, the angle of incidence is defined as the angle between the incident wavevector and the normal to the interface. A similar definition applies to the angle of reflection. In this experiment, the angle between the incident and reflected beams is 1.17 rad . This angle is related to the angle of incidence θ_i and the angle of reflection θ_r by the equation $\theta_i + \theta_r = 1.17 \text{ rad}$. Since the angle of reflection is equal to the angle of incidence, we have $2\theta_i = 1.17 \text{ rad}$, which gives $\theta_i = 0.585 \text{ rad}$.

Figure 119 shows some data points for the angle of reflection as a function of the angle of incidence. A wide range of angles was used, and the data points are shown with error bars. The data points are fitted with a straight line, and the slope of the line is found to be 1.00 ± 0.02 . This result is consistent with the law of reflection, which states that the angle of reflection is equal to the angle of incidence.

The results are also shown in Figure 119. The data points are shown with error bars, and the straight line fit is shown. The slope of the line is 1.00 ± 0.02 , which is consistent with the law of reflection.

3. PDS Investigations of PPV and PVP

3.1 Introduction

The aim of this project was to use photodeflection spectroscopy (PDS) to determine whether material absorption dominates the losses in films of poly(*p*-phenylenevinylene), and in composite films of poly(*p*-phenylenevinylene) and poly(vinyl pyrrolidinone), by comparison of the absorption measurements with measurements of the total propagation losses in the waveguiding films.

In the previous chapter, the design and construction of the photodeflection spectroscopy system was discussed, as well as the preparation of the materials and the experimental techniques used for obtaining these measurements. In this chapter the measurements obtained by photodeflection spectroscopy on these polymeric films are presented.

As discussed in section 2.7.3, each film must be calibrated individually to obtain absolute absorption values, since all of the films have different thicknesses, thermal conductivities, and surface qualities. The chapter starts with a discussion of how the spectral overtones in the 400nm to 1500nm wavelength region were used for calibrating the absorption of individual films (section 3.2).

Section 3.3 presents a comparison of spectra obtained from PPV films prepared under different processing conditions. From this, the precursor to be used for the composite PPV/PVP films was chosen.

PVP, the non-conjugated polymer which was to form a matrix for the PPV, is the subject of study in section 3.4, with particular attention to the drying temperatures for the films. It is apparent that some form of impurity introduced during the preparation of the PVP affected the absorption characteristics of a number of the films.

The investigation of the complete PPV/PVP composite films are reported in section 3.5. Three series of films are reported, each of which involved a series of different concentrations of PPV in PVP, with each series having been dried (with the conversion of the precursor into PPV) at different temperatures. Their different characteristics are presented, with the comparison of the absorption measurements with the measurements of the total propagation losses in the films for light at 633nm and 810nm. This leads to the conclusion that the absorption losses are well below the level of the total losses; losses extrinsic to the material itself dominate.

3.2 Spectral Absorption Calibration

Figure 3.1 shows an absorption spectrum from a film of 2.53% PPV in PVP, which was spun onto a fused silica slide and then placed in a vacuum oven. The oven was brought up to 150°C over two hours and held there for three hours, to allow the PPV to be converted from the precursor and dried. The resulting film was 5.2μm thick. The spectrum was obtained in a cell filled with carbon tetrachloride as the deflection medium.

In that spectrum, several features can be seen. There is an absorption edge at around 515nm, typical for PPV films, and with a shoulder in the spectrum extending to wavelengths beyond 550nm. This shoulder cannot be seen on measurements made by the spectrophotometer for this thin a film because the spectrophotometer's absorbance resolution is limited to $\alpha l = 0.001$, which for a 5.2 micron film represents an absorption limit of 1.9 cm⁻¹. Figure 3.2 shows how the photodeflection system is able to distinguish absorption features more than an order of magnitude lower than the spectrophotometer, for this sample.

At the short wavelength end of the spectrum, the system is saturated and hence gives a low reading. The saturation has occurred because the film has a maximum

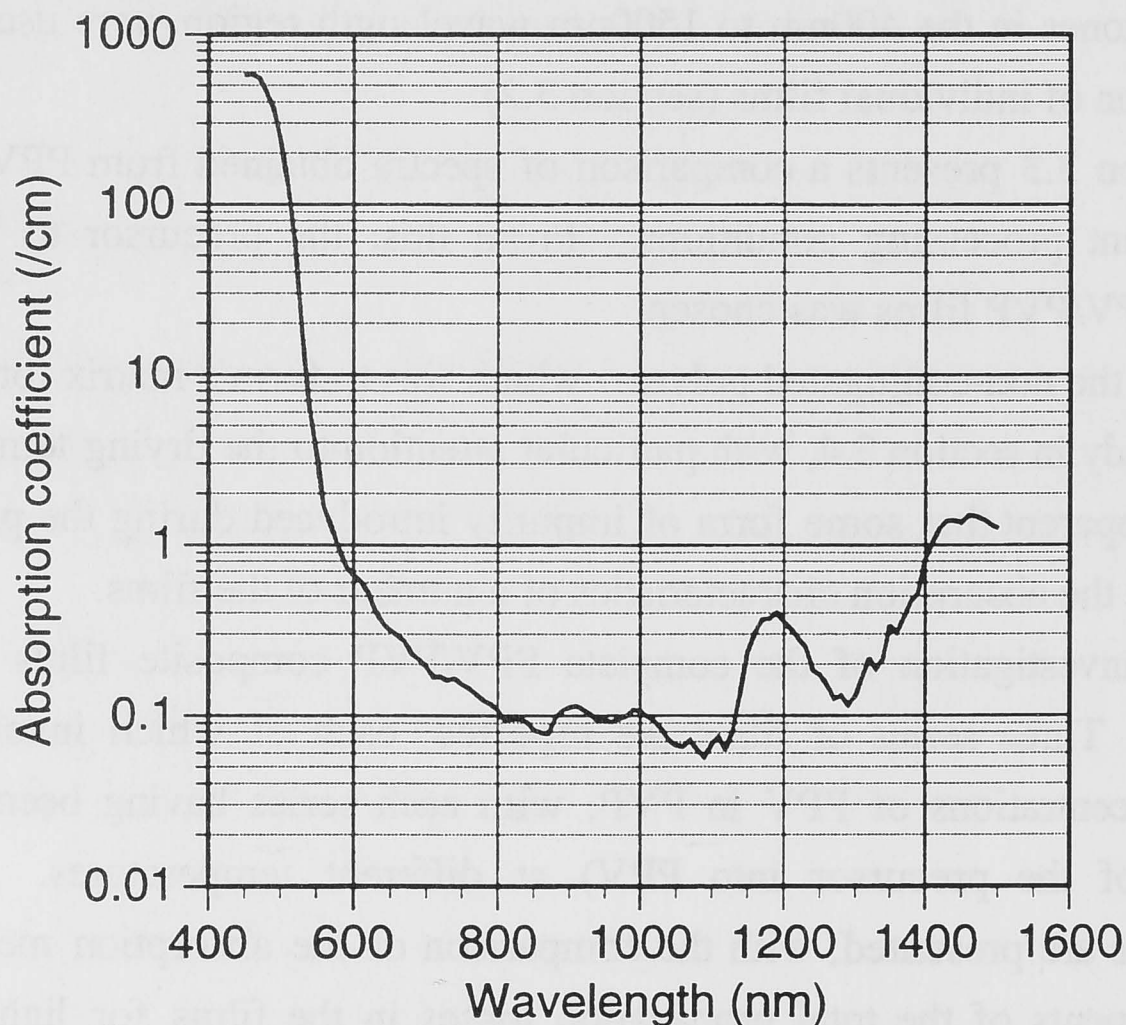


Figure 3.1 2.53% PPV in PVP, spectrum obtained by photodeflection spectroscopy.

absorption of 7000 cm^{-1} seen in the spectrophotometer measurement. This absorption multiplied by the thickness of the film ($5.2\mu\text{m} = 5.2 \times 10^{-4}\text{cm}$) is 3.6, which is greater than the saturation level (≈ 0.5 ; see sections 2.2.5, 2.7.2).

In this part of the spectrum, the films also show some fluorescence, so some of the absorbed energy goes into fluorescence rather than heating the film, and is not measured by the photodeflection system. Köpping-Grem et al. measure a 5% photoluminescence quantum efficiency in PPV prepared by a sulphonium salt precursor route, for 400nm excitation, and believe that efficiencies greater than 10% could be found at other wavelengths.⁸⁴ A third effect in this region is that the energy in the pump beam drops sharply (see section 2.7.1). The steepness of the power spectrum combined with the absorption edge of the film in the same region, convoluted with the large bandwidth of the system, contribute to the error here. Thus, it is very difficult to calibrate the absorption spectrum accurately against the spectrophotometer data in this region; rather, the other absorption peaks in the spectrum have to be used for the calibration.

Four peaks are visible in the PDS spectrum (Figure 3.1): at 910nm, $1.0\mu\text{m}$, $1.19\mu\text{m}$ and $1.46\mu\text{m}$. These are close to overtone peaks in the spectrum of poly(methyl methacrylate) (PMMA), and are due to contributions from overtones of the C-H stretch, as seen in PMMA, and the O-H stretch from the presence of water.

Figure 3.3 shows the absorption spectrum of PMMA, measured in a thick (16mm) piece of perspex using the spectrophotometer. It is consistent with results reported in the literature results, including spectra obtained by measuring the transmission

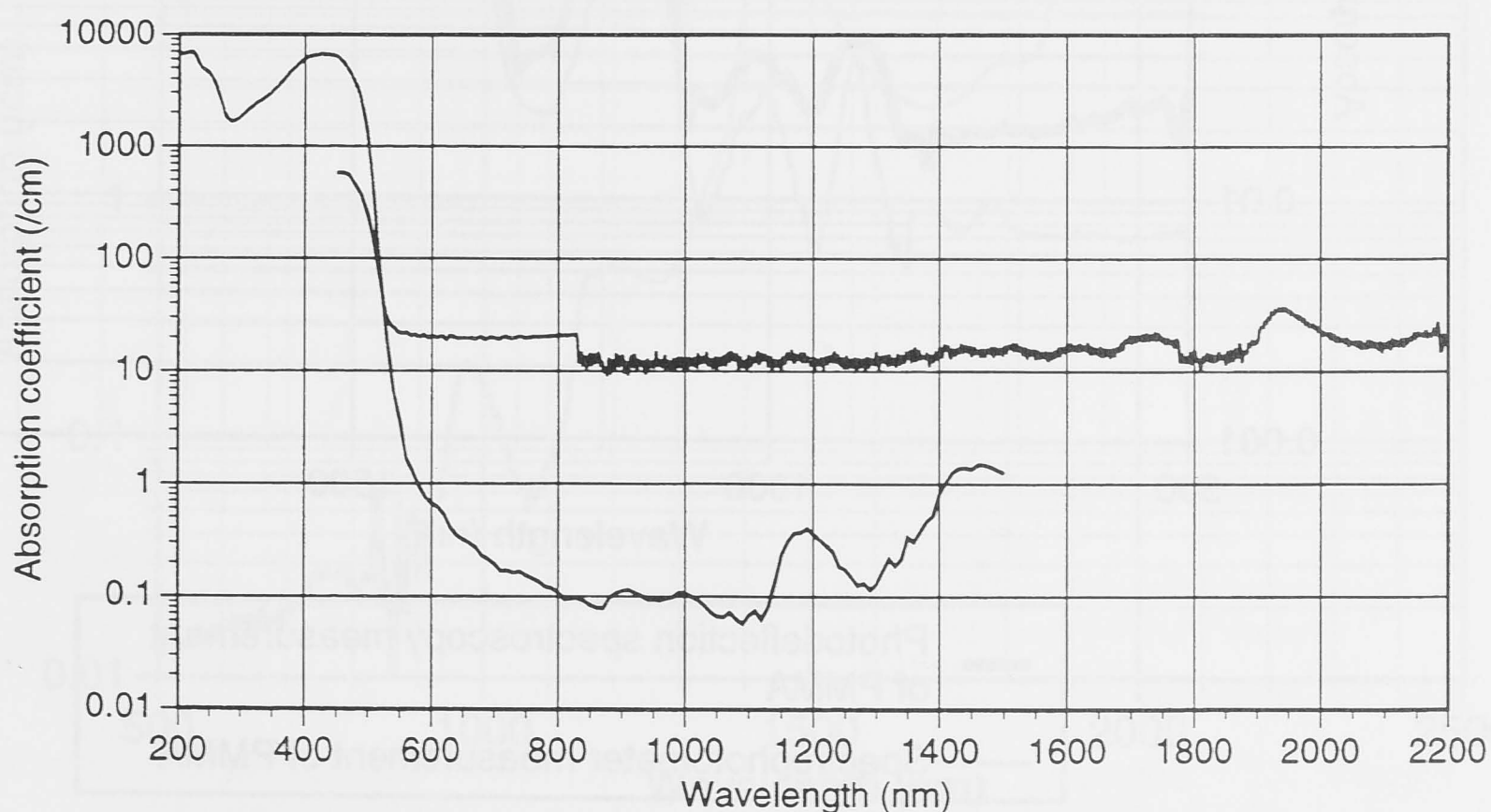


Figure 3.2 2.53% PPV in PVP, as measured by the spectrophotometer (upper line) and PDS (lower line).

loss over a long length of PMMA fibre.⁸⁵ Others have also used photodeflection spectroscopy in combination with UV-VIS spectrophotometer data to measure the C-H stretching overtone in this part of the spectrum.^{31,86} Skumanich et al. identify the 1.2 μm peak as being the second ($n=3$) overtone of the C-H vibration; the 0.9 μm peak as the third ($n=4$) overtone, and the 1.4 μm and 1.0 μm peaks as the 2+1 and 3+1 combination bands respectively.⁸⁵

The spectrum obtained by the photodeflection spectroscopy system for a PMMA film is also shown in figure 3.3. The noise floor at an absorption of 0.02 cm^{-1} influences the lower peaks, but the position and relative intensities agree within experimental error. Thus in principle the PDS can be calibrated against the known absorption strength of the various overtone peaks provided these are clearly identifiable above any background absorption in the film being studied.

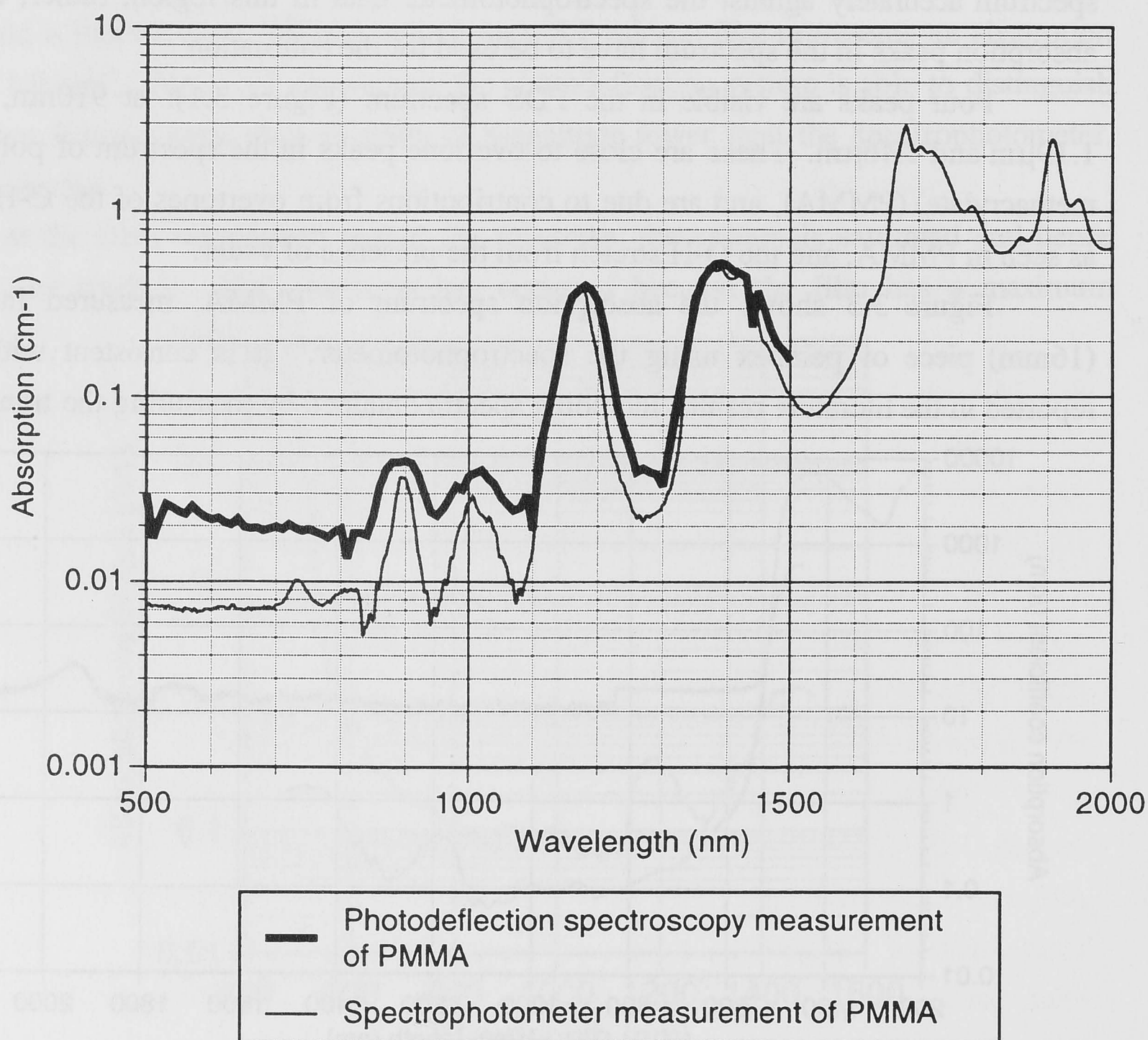


Figure 3.3 Absorption spectrum of PMMA (perspex), showing the C-H stretch overtones.

The relative strength of the O-H overtones were assessed from the absorption spectrum of water as shown in Figure 3.4, measured using a 1mm cuvette in the spectrophotometer against a reference of spectroscopic grade carbon tetrachloride. The measurement saturates at $\alpha l = 5.0$, seen in the peaks at wavelengths longer than $1.9\mu\text{m}$; below $\alpha l = 0.01$ (absorption coefficient 0.1cm^{-1}) the resolution is limited. Significant peaks can be seen at 975, 1198 and 1456nm , with absorption coefficients of 0.21, 0.56 and 13.7cm^{-1} respectively. These overtones could influence the peaks measured in the PPV/PVP spectra. However, it can be seen that the $1.45\mu\text{m}$ "water peak" is a factor of 23 higher than the $1.20\mu\text{m}$ peak, whereas the corresponding peaks in the PPV/PVP spectrum have a ratio of only 3:1 (Figure 3.1). Thus even if the longer wavelength peak is strongly affected by water, the contribution to the $1.2\mu\text{m}$ peak in PPV/PVP must be less than 13% of the observed level, or at most 0.05cm^{-1} in Figure 3.1.

The peak just below $1\mu\text{m}$ is a factor of 12 smaller than the $1.45\mu\text{m}$ peak in PPV/PVP, and a factor of 45 smaller for the corresponding peaks in water. Thus, if water dominated the $1.45\mu\text{m}$ peak in the PPV/PVP, it could contribute up to 27% to the lower peak. The $1.19\mu\text{m}$ peak in the PPV/PVP spectrum is therefore the least influenced

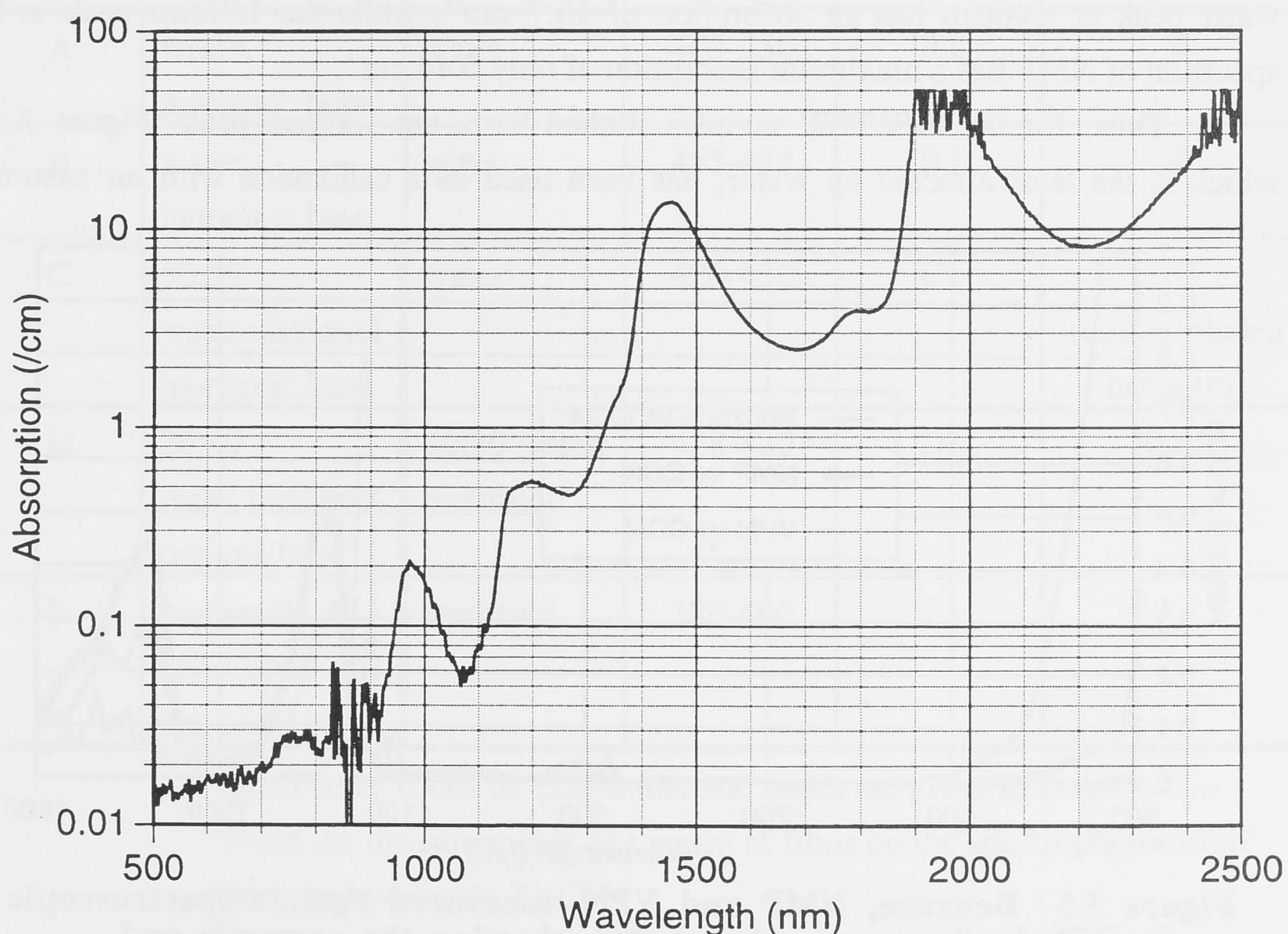


Figure 3.4 Absorption spectrum of water, as measured by the spectrophotometer using a 1mm cuvette, with spectroscopic grade carbon tetrachloride as the reference.

by water.

The $1.17\mu\text{m}$ overtone in PMMA can be identified with the C-H stretch,^{86,86,31} and has an absorption of 0.4 cm^{-1} . It is assumed that the overtone in PPV/PVP has a similar origin.³²

1-methyl-2-pyrrolidinone (NMP) is similar in structure to PVP, and can be used in fluid form in the spectrophotometer. Figure 3.5 shows the absorption spectra of NMP, as well as benzene and 1-vinyl-2-pyrrolidinone (VPN), which has both aromatic and olefinic C-H stretch overtones. Benzene shows a sharp aromatic peak at $1.14\mu\text{m}$ for which there would be a corresponding peak in PPV, and the NMP shows the aliphatic stretch overtones, with a broad aliphatic peak centred at $1.18\mu\text{m}$. Given the large bandwidth being used with the photodeflection apparatus (section 2.3.1) the differences between these spectral structures would not be apparent (apart from a significant wavelength shift) and each would contribute to an absorption band with a strength of $0.4 \pm 0.1\text{ cm}^{-1}$ near $1.18\mu\text{m}$. Even the presence of up to 10% water (which has an absorption peak at $1.2\mu\text{m}$ of 0.6 cm^{-1}) does not significantly change this peak in NMP (as anticipated from arguments above) although at longer wavelengths water has a greater effect: the pure water peak at $1.46\mu\text{m}$ has an absorption of 13.7 cm^{-1} , while the $1.38\mu\text{m}$ peak in the spectrum of NMP has a maximum absorption of only 0.44 cm^{-1} .

Thus, for the PPV/PVP samples studied here, the $1.19\mu\text{m}$ peak (Figure 3.2), which is the least affected by water, has been used as a calibration with an assumed

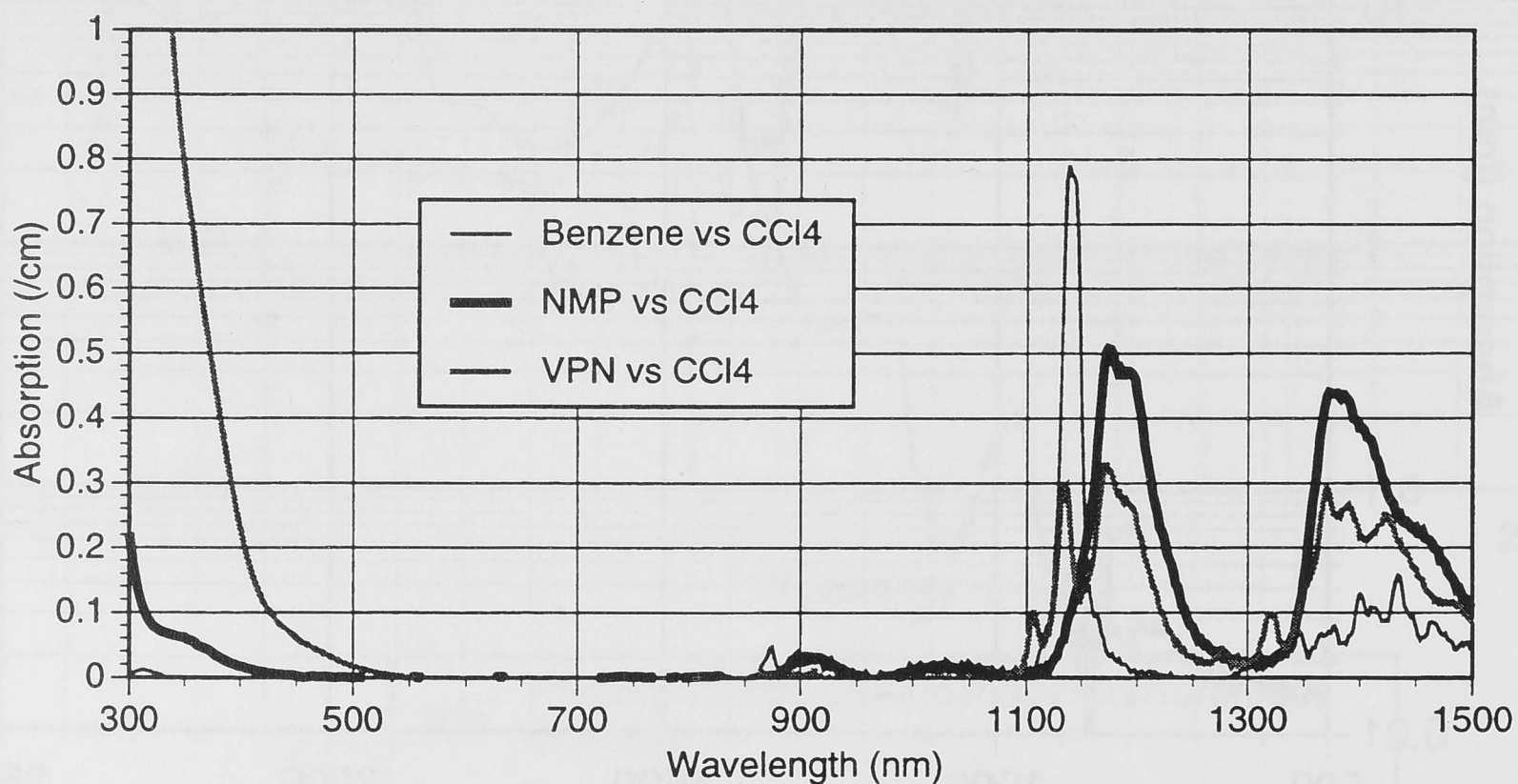


Figure 3.5 Benzene, NMP and VPN, measured against spectroscopic grade CCl_4 in the spectrophotometer, showing the aromatic and aliphatic C-H stretch overtones at 1140nm and 1180nm . Note that the peaks appear sharper here than in the previous figures, which were plotted against a logarithmic scale.

absorption of 0.4 cm^{-1} .

3.3 Absorption of PPV films from different precursors

The exact characteristics of films of poly(*p*-phenylenevinylene) depend on the preparation conditions, which can affect the length of the conjugated chains and the presence of salts and impurities. Before proceeding to an analysis of composite films of PPV and poly(vinyl pyrrolidinone), a number of different films of pure PPV prepared under slightly different conditions were compared in an effort to find the conditions for the lowest possible absorption and highest possible nonlinearity.

The general precursor route used for the preparation of PPV was presented in section 2.8.1, though here a variety of solvent and base conditions were examined.

Pre-cursor ^a	Polymerisation	Dialysis	λ_{max} range ^b (nm)	Slide number	Thickness (μm)
A	water, inorganic base ^c	water	453-458	A1	4
B	water, inorganic base	water	453-458	B1	4
C	50:50 water:methanol inorganic base	water	420-430	C1	3.1 (doctor-bladed not spun)
D	20:80 water:methanol organic base ^d	20:80 water: methanol	428-430	D1	0.85
E	methanol, anhydrous inorganic base	methanol	380-400	E1	4.1

^aLaboratory codes for precursors and slides are given in endnote ⁸⁷.

^bFrom the measurements of a series of films on the spectrophotometer.

^cSodium hydroxide, NaOH

^dTetrabutylammonium hydroxide, n-Bu₄NOH

Table 3.2 Summary of different preparation conditions for PPV films.

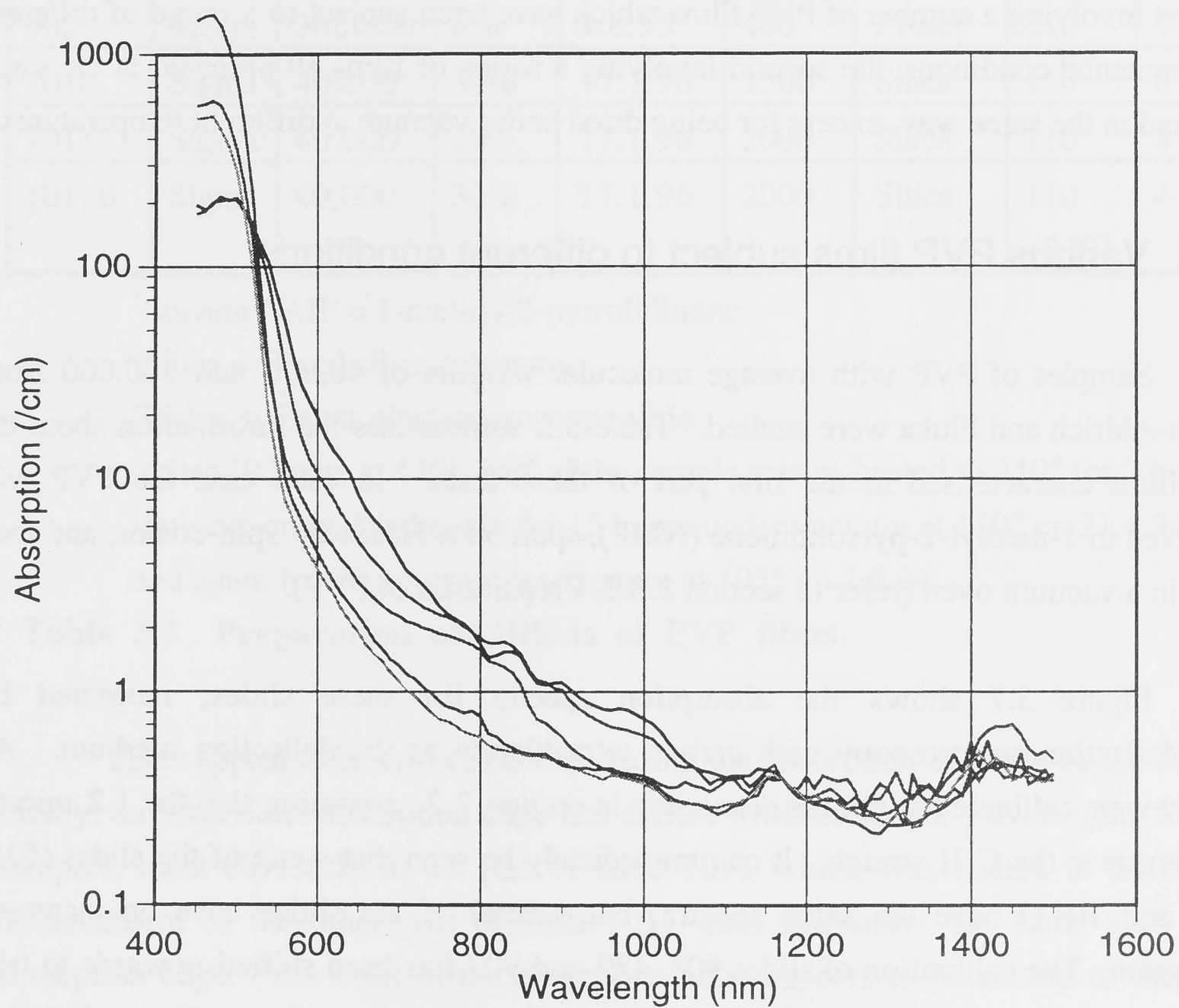
These are shown in Table 3.1, with the range for the absorption peak wavelengths of PPV films which were made from each precursor. On that table specific films which appear on Figure 3.6 and their thicknesses are also listed.⁸⁸

Figure 3.6 shows the PDS absorption spectra of PPV slides made from the different precursors listed in Table 3.1. A feature of the spectra is the change in the slope of the absorption edge at about 540nm, as observed by Seager et al,³² although this is less distinct in the polymers prepared with the water solvent. Precursors prepared with water as a solvent also tend to give rise to PPV with a longer wavelength UV absorption peak (see Table 3.1). The PPV prepared using methanol alone as a solvent had the shortest wavelength λ_{\max} . It has been shown that the nonlinearity of the polymer measured at 800nm decreases as the λ_{\max} decreases.^{16,89}

The spectra shown in Figure 3.6 were calibrated for the absolute absorption coefficient using the 0.4cm^{-1} 1190nm peak. With the pure PPV slides, this peak is not always distinct, as the background absorption is at least equal to that peak height, so the calibrations of some of the films in Figure 3.6 in which the peak is not extremely distinct may be low (but see the more distinct results in section 3.5). The 1190nm peak is most distinct in the films for which the precursor was prepared using methanol, in particular films C1 and E1. Seager et al. claimed a much higher absorption value at this peak - 7cm^{-1} , at least 1cm^{-1} above the background absorption - and reported a minimum absorption value of 6cm^{-1} .³² However, they did not discuss how their data was calibrated, and it appears that the data in question may have been calibrated using the short wavelength end of the spectrum (see discussion in section 3.2), even though for other of their measurements (figure 2 in their paper) overtones were used for the calibration.

The lowest absorption is seen in the slide of PPV from precursor E, which was prepared with methanol. It was also found that the in preparing PPV with a combination of methanol and water as the solvent, solutions prepared using the inorganic base gave rise to films with specks of salts in them, and those from an organic base did not.

However, although the PPV prepared with methanol showed lower absorption, and also appeared to contain fewer scattering centres possibly because fewer salts recrystallise, with the much shorter λ_{\max} it also has a lower non-linearity. The precursor used to make composites with PVP for the analysis that follows in section 3.5 was a compromise: precursor D was used, with a 20:80 water:methanol ratio.



- | | |
|---|--|
| — | A1 - 4 μm , water |
| — | B1 - 4 μm , water |
| — | C1 - 3.1 μm , 50:50 water:methanol |
| — | D1 - 0.85 μm , 20:80 water:methanol |
| — | E1 - 4.1 μm , methanol |

The legend is in the order in which the lines appear on the graph at 700nm.

Figure 3.6 Absorption spectra of PPV slides prepared from different precursors.

3.4 Absorption characteristics of PVP

Composites of poly(vinyl pyrrolidinone) with poly(*p*-phenylenevinylene) yield films which are thicker and have better optical clarity than films of pure PPV. Such films, with different concentrations of PPV, are the subject of the measurements in the next section. In this section the characteristics of the films of pure poly(vinyl pyrrolidinone) (PVP) are reported, with particular attention being paid to material with different average molecular weights and different preparation conditions. Two studies are presented here: the first involving a number of PVP films which have been subject to a range of different environmental conditions; the second involving a series of films all prepared at the same time and in the same way, except for being dried under vacuum at different temperatures.

3.4.1 Various PVP films subject to different conditions

Samples of PVP with average molecular weights of 40,000 and 360,000 from Sigma-Aldrich and Fluka were studied. Table 3.2 summarises the information about the PVP films characterised in the first part of these tests. In each case the PVP was dissolved in 1-methyl-2-pyrrolidinone (NMP), spun on a Headway spin-coater, and then dried in a vacuum oven (refer to section 2.8.2, Preparation of PVP).

Figure 3.7 shows the absorption spectra for these slides, measured by photodeflection spectroscopy with carbon tetrachloride as the deflection medium. All spectra were calibrated as per the discussion in section 3.2, assuming that the 1.2 micron peak is due to the C-H stretch. It can immediately be seen that some of the slides (519, 1010 and 1011) have the same spectra, but several of the slides have an increased absorption. The calibration of slides 908, 479 and 907 has been shifted upwards to take into account the additional contribution of the background absorption to the peak at 1.2 microns (the additional background being approximately 0.3cm^{-1} for slide 908 and 0.1cm^{-1} for slides 479 and 907).

Figure 3.8 shows the same absorption spectra plotted against a linear scale, which makes some of the features discussed below easier to discern.

slide number	PVP source	Ave. Mol. weight	Conc in NMP ¹	Date of preparation	Spin speed (rpm)	Substrate	Temp (°C)	Thickness (μm)
434 ⁵	Sigma	360,000	18%	2.11.93	1500	Silica ²	100	1.91
479	Sigma	40,000	30%	9.12.93	2000	Silica	100	5.3
519	Sigma	40,000	30%	18.1.94	2000	Silica	100	8
907	Fluka	40,000	30%	9.6.95	400	Fisher ³	210	16.5
908	Sigma	360,000	8%	9.6.95	400	Fisher	210	1.3
1010	Sigma	40,000	30%	17.1.96	1500	Silica	110	6
1011	Sigma	40,000	30%	17.1.96	2000	Silica	110	4
1011B	Sigma	40,000	30%	17.1.96	2000	Silica	110 +210 ⁴	4

¹Solvent NMP = 1-methyl-2-pyrrolidinone

²Silica = Fused silica substrate

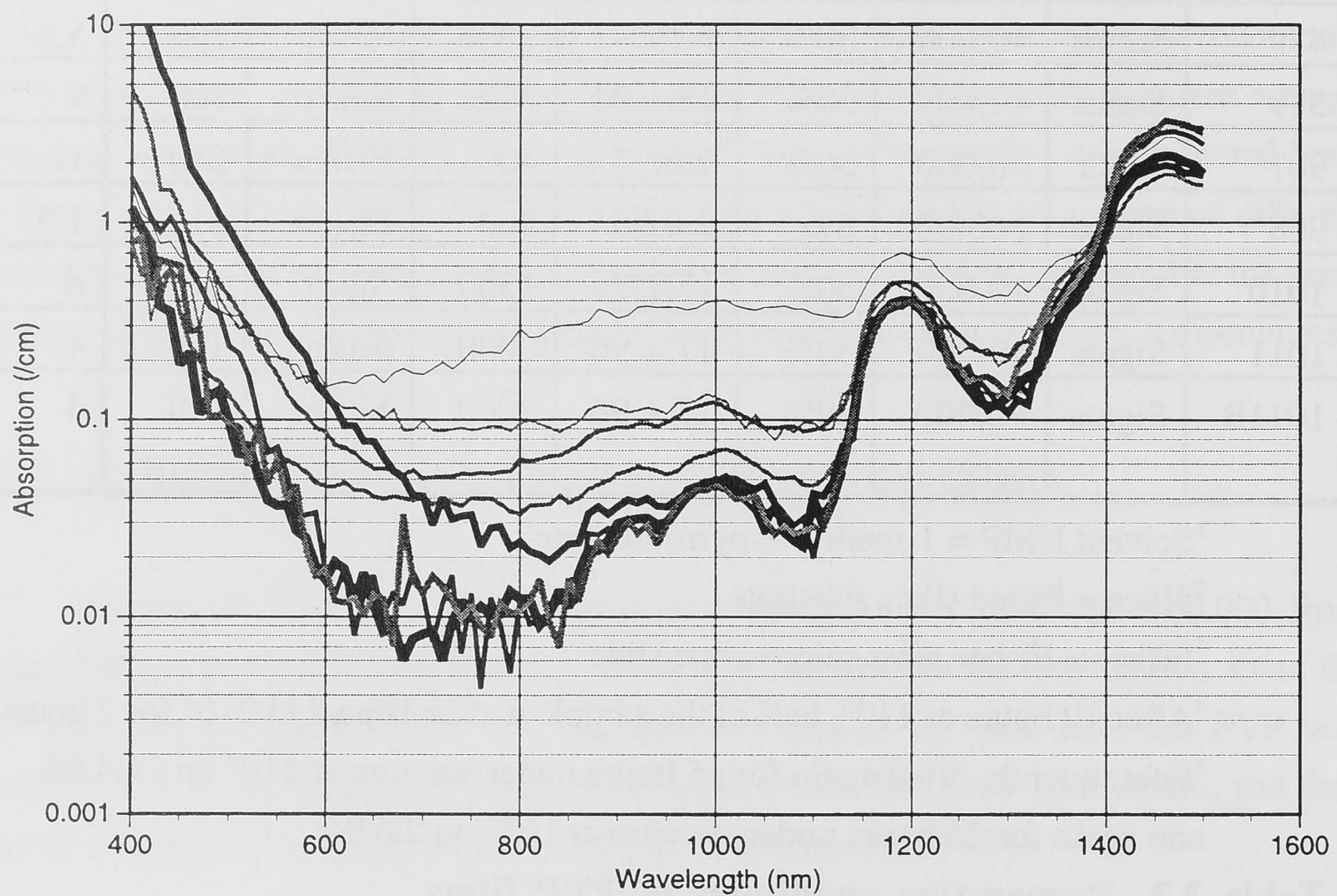
³Fisher = Fisher glass microscope slide

⁴After 10 hours at 110°, half of the sample was re-heated to 210° for 2 hours

⁵Subsequently dried again for 15 hours under vacuum at 110° on 21.4.94, and again for 26 hours under vacuum at 105° on 2.6.94.

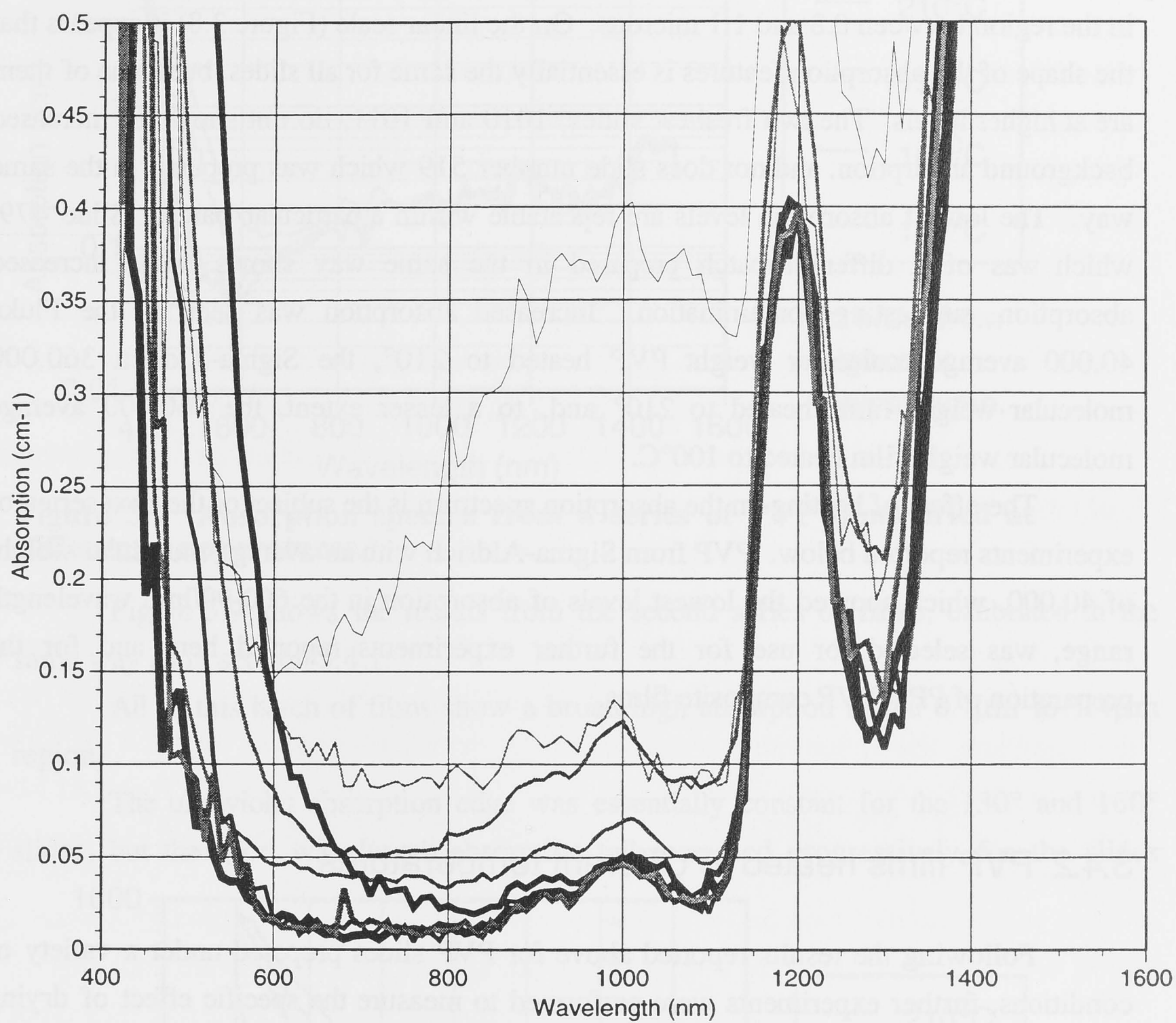
Table 3.2 Preparation conditions of PVP films.

There appear to be two effects increasing the absorption of some of the samples. Firstly, the ultraviolet absorption edge has shifted towards longer wavelengths for some samples, most obviously in the part of slide 1011 which was heated to 210°. The measurement of the other part of slide 1011 does not show the same shift in the absorption edge. The shift in the absorption edge appears to be related to the drying temperature, as will be confirmed below.



- Slide 908 - M.W. 360000, 210⁰ (1.3μm)
- Slide 479 - 100⁰ (5.3μm)
- Slide 907 - Fluka PVP, 210⁰ (16.5μm)
- Slide 434 - M.W. 360000, 100⁰ (2μm)
- Slide 1011 - 110⁰, then additional 210⁰ heating (4μm)
- Slide 519 - 100⁰ (8μm)
- Slide 1010 - 110⁰ (6μm)
- Slide 1011 - 110⁰ (4μm)

Figure 3.7 Absorption spectra of the PVP films listed in the table above, calibrated for the 0.4 cm⁻¹ absorption peak at 1190nm.



- Slide 908 - M.W. 360000, 210⁰ (1.3 μ m)
- Slide 479 - 100⁰ (5.3 μ m)
- Slide 907 - Fluka PVP, 210⁰ (16.5 μ m)
- Slide 434 - M.W. 360000, 100⁰ (2 μ m)
- Slide 1011 - 110⁰, then additional 210⁰ heating (4 μ m)
- Slide 519 - 100⁰ (8 μ m)
- Slide 1010 - 110⁰ (6 μ m)
- Slide 1011 - 110⁰ (4 μ m)

Figure 3.8 Linear plot of the PVP absorption spectra, showing an increased absorption floor on some of the samples.

Secondly, there is an background absorption level which is seen to rise in some samples, in the region between 0.8 and 1.1 microns. On the linear scale (Figure 3.8) it appears that the shape of the absorption features is essentially the same for all slides, but some of them are at higher levels. The two freshest slides, 1010 and 1011, do not show the increased background absorption, and nor does slide number 519 which was prepared in the same way. The lowest absorption levels are repeatable within a particular batch. Slide 479, which was of a different batch prepared in the same way shows some increased absorption, suggesting contamination. Increased absorption was seen in the Fluka 40,000 average molecular weight PVP heated to 210°, the Sigma-Aldrich 360,000 molecular weight films heated to 210° and, to a lesser extent, the 360,000 average molecular weight film heated to 100°C.

The effect of heating on the absorption spectrum is the subject of the next series of experiments reported below. PVP from Sigma-Aldrich with an average molecular weight of 40,000, which showed the lowest levels of absorption in the 600-900nm wavelength range, was selected for use for the further experiments reported here and for the preparation of PPV/PVP composite films.

3.4.2 PVP films heated to different temperatures

Following the results reported above for PVP slides prepared under a variety of conditions, further experiments were performed to measure the specific effect of drying temperature on PVP films. The glass transition temperature for anhydrous PVP is reported in the literature as being 175°C, and decreasing with water content (at 10% water by weight, $T_g \approx 80^\circ\text{C}$).⁹⁰

The films for this series of experiments were prepared from Sigma-Aldrich PVP with an average molecular weight of 40,000. The polymer was dissolved in NMP to a 30% concentration by weight, filtered with a 0.2 μm PTFE (teflon) filter,⁹¹ and spun onto Fisher glass microscope slides on the Headway Spin Coater at 2000rpm for 40 seconds in air. All were dried in the oven under vacuum at 100°, and then one film was removed.⁹² The remainder were heated for a further 2 hours at 130° under vacuum, and then another film was removed. A third was removed after heating to 160° for 2 hours; a fourth after heating to 190°, and a fifth after heating to 210°. Using the Metricon Prism Coupler, these films were all found to be approximately $3.1 \pm 0.1 \mu\text{m}$ thick.⁹³

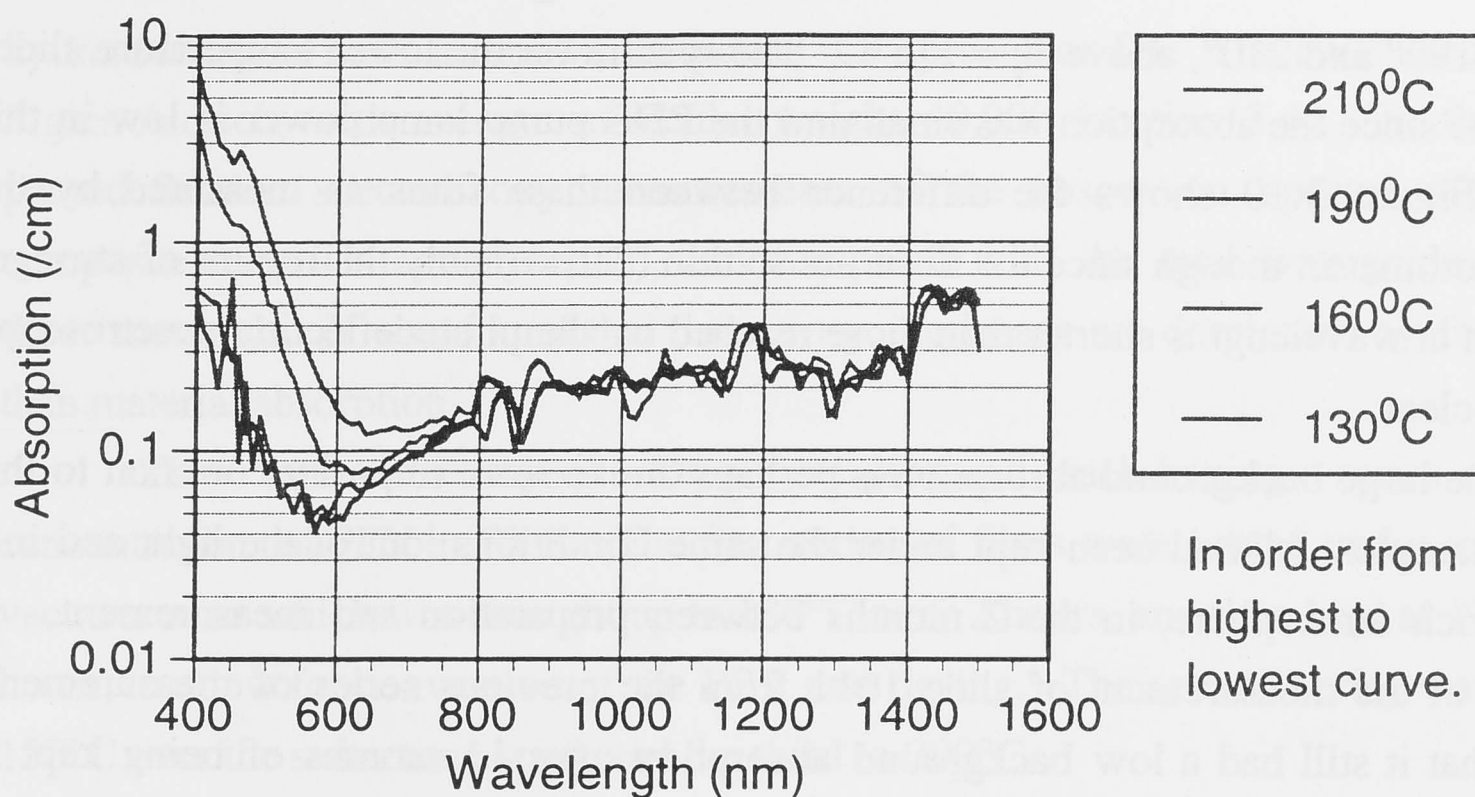


Figure 3.9 Absorption spectra from a series of PVP films dried at different temperatures.

Figure 3.9 shows the results from the second series of films, calibrated in the same way as in section 3.4.1.

All of this batch of films show a broad high absorption in the $0.7\mu\text{m}$ to $1.4\mu\text{m}$ region.

The ultraviolet absorption edge was essentially constant for the 130° and 160° slides, but the short wavelength absorption tail increased progressively for the slides

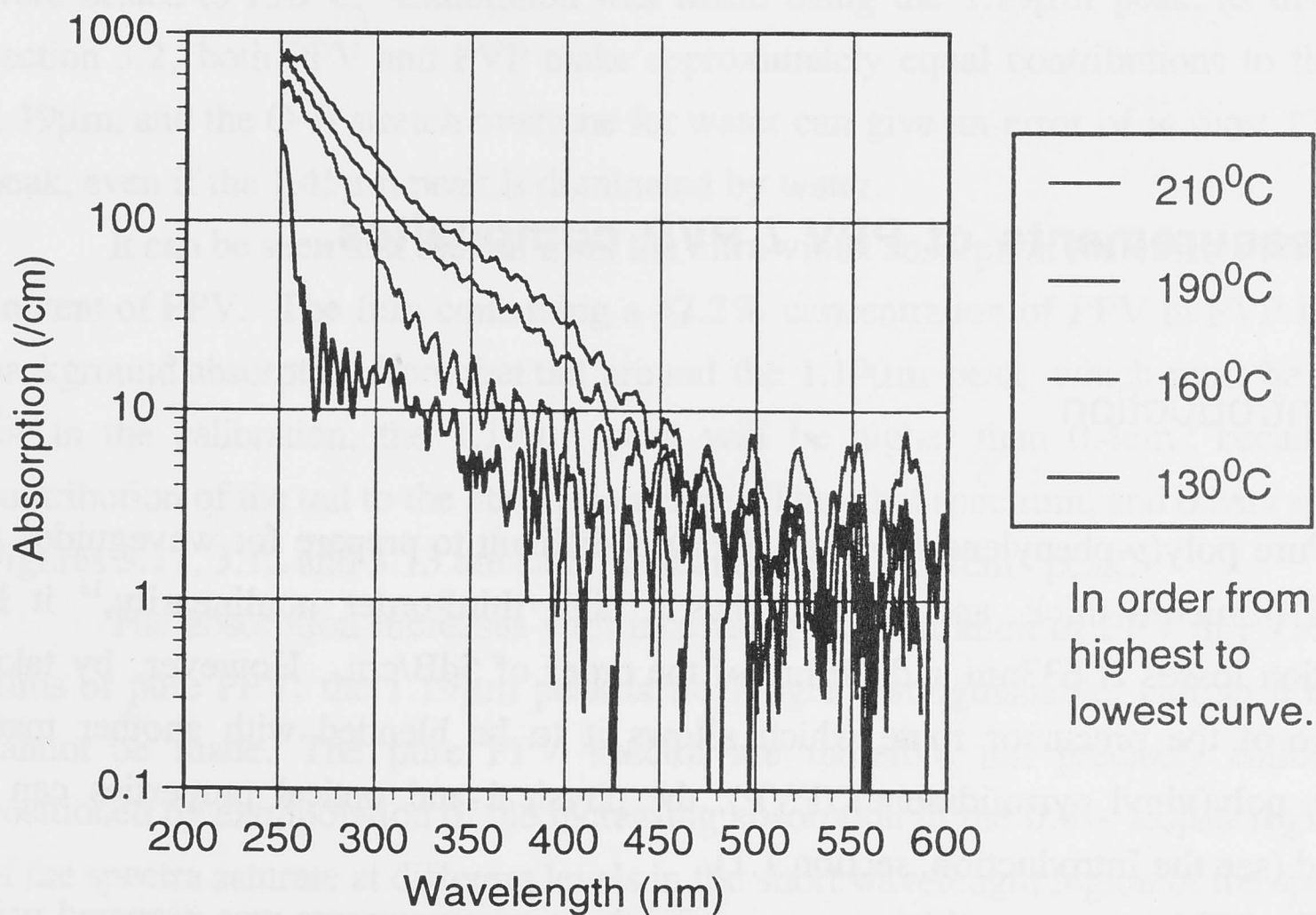


Figure 3.10 Spectrophotometer measurements of the absorption spectra of PVP films dried at different temperatures.

heated to 190° and 210°, above $T_g = 175^\circ\text{C}$. The spectra for the lower temperature slides show noise since the absorption was small and the PDS pump lamp power is low in this region. Figure 3.10 shows the difference between these films as measured by the spectrophotometer, though since the films are so thin (3.1 μm) only the region of stronger absorption at wavelengths shorter than those reached by the photodeflection spectroscopy system is clear.

The large background absorption is perhaps due to some impurity common to this series of samples. All had been kept under the same conditions, out of the light and in a nitrogen rich atmosphere, in the 2 months between preparation and measurement. A repetition of the measurement of slide 1011 from the previous series of measurements showed that it still had a low background absorption after 11 months of being kept in darkness but in air.

Overall, the results from section 3.4.1 indicate the absorption of Sigma-Aldrich PVP with an average molecular weight of 40,000 can have absorption as low as 0.01 cm^{-1} in the 800nm region. Some batches of films of PVP show an increased background absorption, which is most likely related to contamination. The absorption in the tail from the ultra-violet absorption edge is sensitive to the drying temperature used for the films, increasing with temperature above around 175°. However, in general, PVP should have sufficiently low absorption to be an excellent low loss waveguide material and host for PPV.

3.5 Measurements of PPV / PVP composites.

3.5.1 Introduction

Pure poly(*p*-phenylenevinylene) (PPV) is difficult to prepare for waveguides the order of 1 micron thick, and whilst it has a high third-order nonlinearity,¹⁶ it has propagation losses at 633nm and 810nm of the order of 5dB/cm. However, by taking advantage of the precursor route which allows it to be blended with another matrix polymer, poly(vinyl pyrrolidinone) (PVP), the physical and optical properties can be improved (see the Introduction, section 1.1).

The PPV precursor which was used for these measurements was prepared using 20:80 ratio of water:methanol during the polymerisation and tetrabutylammonium

hydroxide as the base, as shown in section 3.3 (precursor D). The PVP used was from Sigma-Aldrich, with average molecular weight 40,000 (section 3.4). In this section, photodeflection spectroscopy measurements of the absorption spectra of PPV/PVP composite materials are presented, and compared with the total waveguide losses for those materials. It was found that the waveguide losses are dominated by factors other than material absorption.

Three series of composite films were prepared, each having a series of different concentrations of PPV in PVP. The first series of films were heated under vacuum in a vacuum oven which was brought up to 130°C over 2 hours, and then kept at 130°C for 3 hours, to allow for conversion of the PPV and drying. The second series was heated to 150°C over the same time span, and the third to 200°C.

All of the photodeflection spectroscopy measurements reported here were made using carbon tetrachloride as the deflection medium.

3.5.2 Photodeflection Spectroscopy Results

Figure 3.11 shows the absorption spectra of the series of PPV / PVP films which were heated to 130°C. Calibration was made using the 1.19 μm peak; as discussed in section 3.2, both PPV and PVP make approximately equal contributions to the peak at 1.19 μm , and the O-H stretch overtone for water can give an error of at most 13% to that peak, even if the 1.45 μm peak is dominated by water.

It can be seen that the tail from the ultra-violet absorption increases with increasing content of PPV. The film containing a 47.2% concentration of PPV in PVP has a large background absorption from that tail around the 1.19 μm peak, which must be accounted for in the calibration: the 1.19 μm peak will be higher than 0.4 cm^{-1} because of the contribution of the tail to the absorption there. Thus that spectrum, and others similarly in Figures 3.11, 3.12 and 3.13 are calibrated at above the 0.4 cm^{-1} peak.

The absorption increases with increasing concentration of PPV in PVP. For the films of pure PPV, the 1.19 μm peak is no longer distinguishable, and so a calibration cannot be made. The pure PPV spectra are therefore not precisely calibrated, but positioned by extrapolation of the increasing absorption in the 0.6 - 1.0 μm region. Some of the spectra saturate at different levels in the short wavelength region of the spectrum, as a result of the films having different thicknesses (see section 2.2.5). The absorption

spectra for the series of films heated to 150°C and 200°C are shown in Figure 3.12 and Figure 3.13 respectively.

A general feature of all these data is the presence of an absorption minimum around 1100nm. In samples dried at the lower temperatures the losses in this region are only $\approx 0.1 \text{ cm}^{-1}$ for PPV contents of up to 10%. This is a promising result, if films dominated by absorption losses alone could be prepared, especially since separate measurements of the optical nonlinearity of PPV/PVP composites indicate that at doping levels of 5-40% PPV, these composites have favourable nonlinear optical properties (best at around 20%).¹⁸

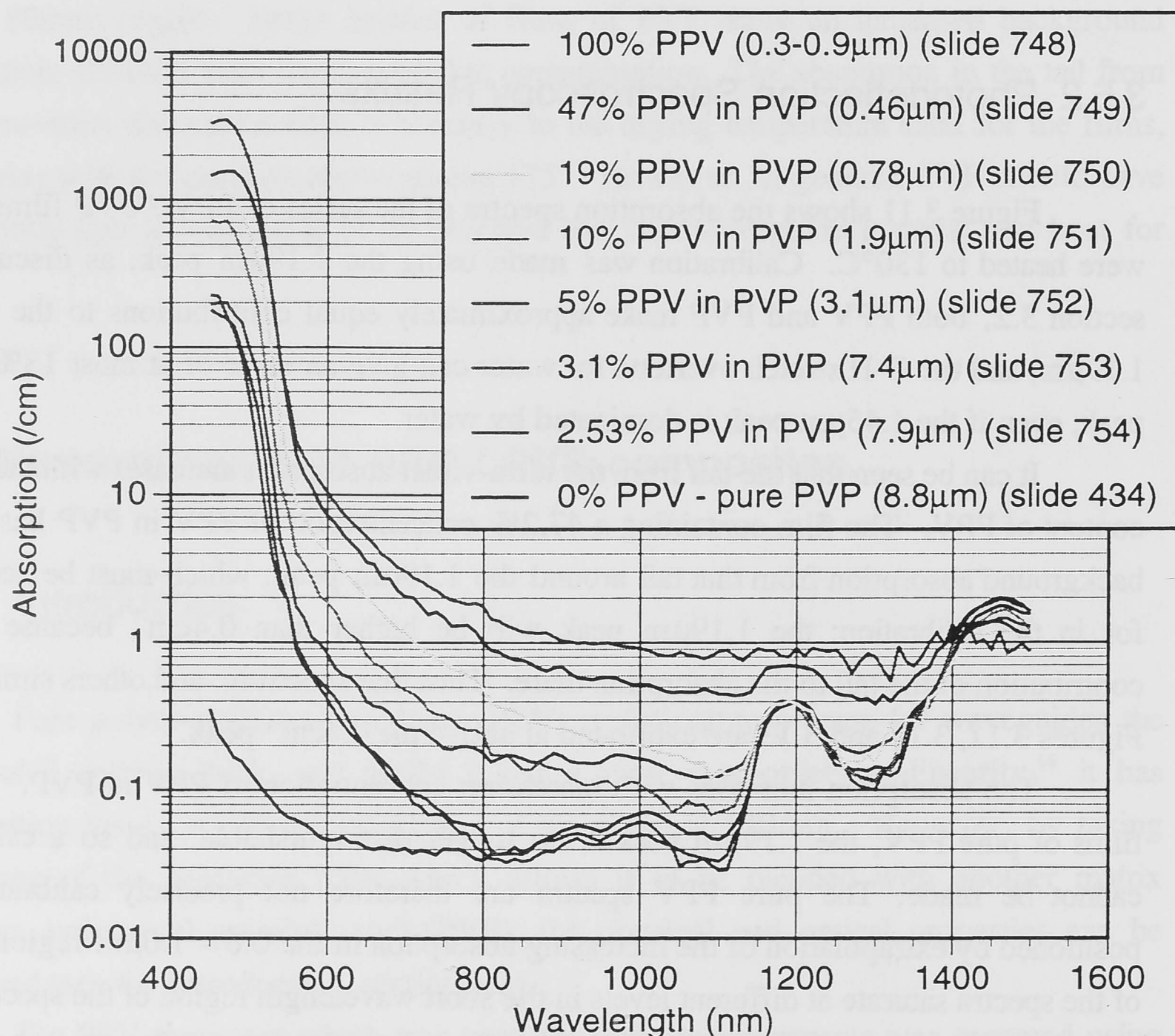


Figure 3.11 PPV in PVP series heated to 130 degrees. The legend is in the same order as the lines appear on the graph.

3.5.3 Comparison with Total Loss Measurements

The total waveguiding losses in the above films were measured by coupling light at 633 and 810nm into them, and measuring the decay in the intensity of the light beam for waveguide with distance from the coupling point. The preparation for this method was discussed in section 2.9. The data used here for the total losses were measured by Dr. A. Tappert at the Laser Physics Centre of the A.N.U. These measurements are given in Table 3.3-Table 4.5. On the other hand, the absorption spectra of the films were measured by

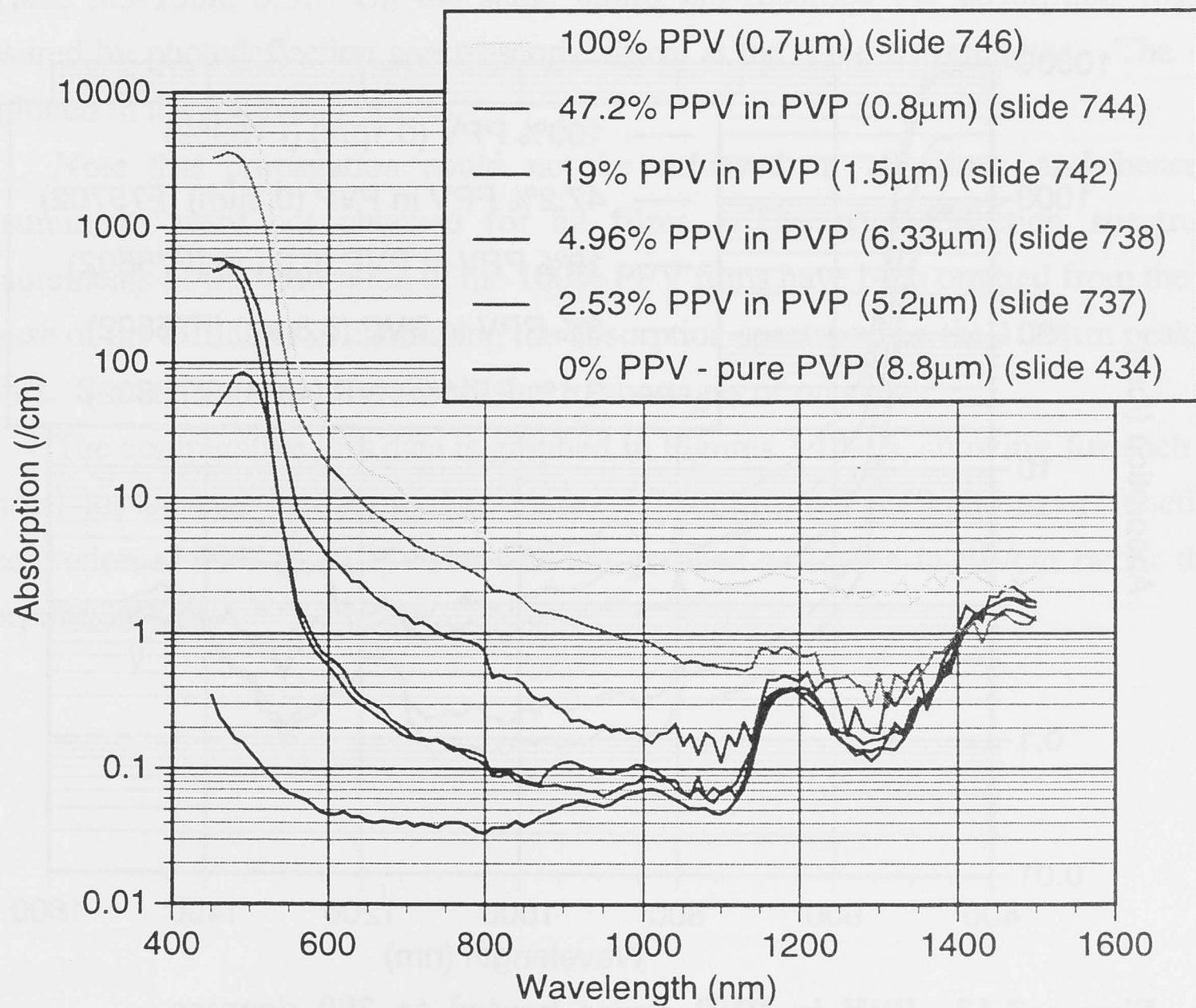


Figure 3.12 PPV in PVP series heated to 150 degrees.

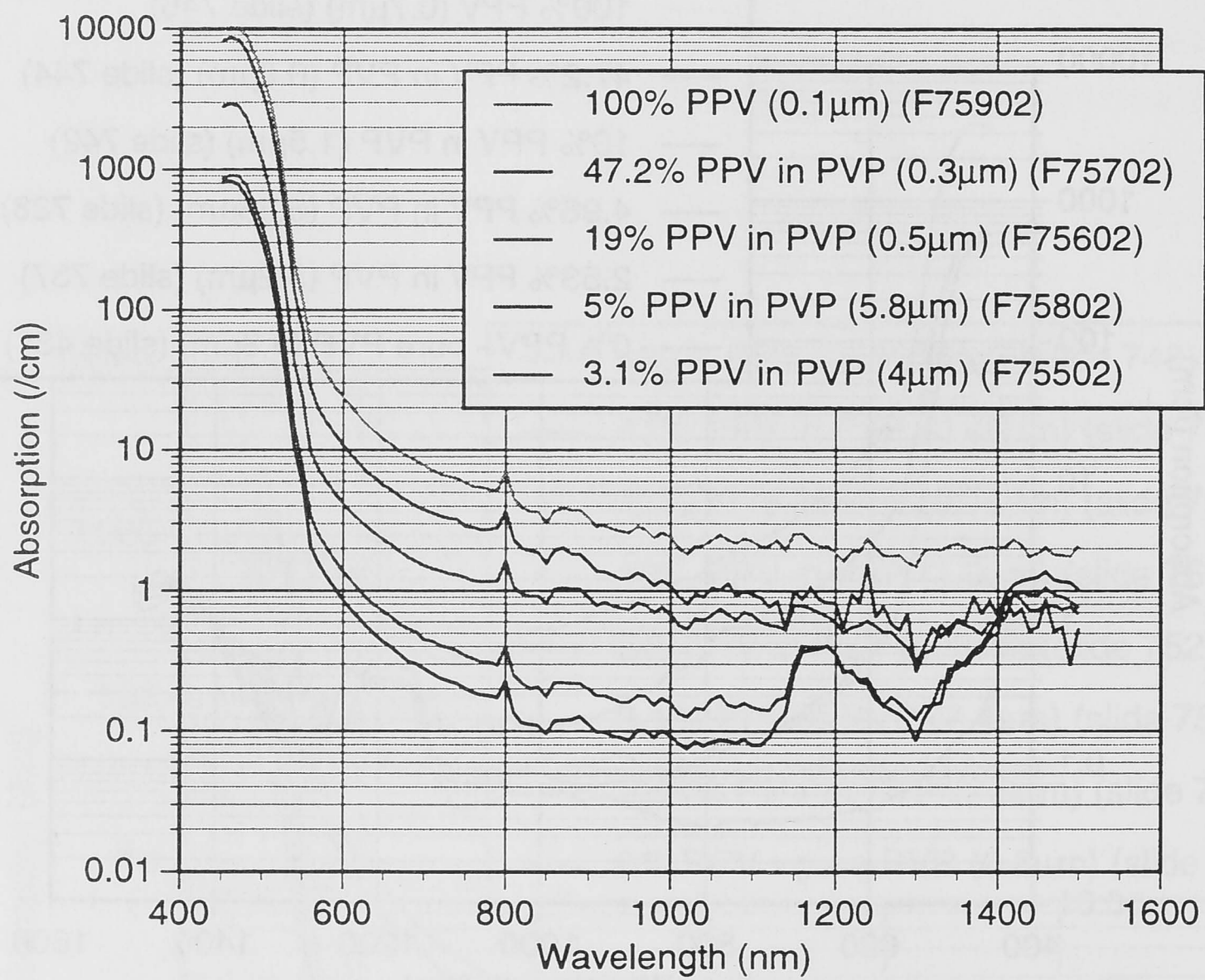


Figure 3.13 PPV in PVP series heated to 200 degrees.

3.5.3 Comparison with Total Loss Measurements

The total waveguiding losses in the above films were measured by coupling light at 633 and 810nm into them, and measuring the decay in the scattering of the light from the waveguide with distance from the in-coupling point. The preparation for this method was discussed in section 2.9. The data used here for the total losses were measured by Dr. A. Samoc of the Laser Physics Centre at the A.N.U. These measurements are given in Table 3.3-Table 3.5. On the same tables are recorded the absorption losses as measured by photodeflection spectroscopy above at the same wavelengths. The results are plotted in the following graphs.

Note that propagation could not be achieved in all films; and hence loss measurements were not obtained for all films. The photodeflection spectroscopy measurements of the absorption of the 100% PPV films have been omitted from the tables because of the difficulty in calibrating the absorption spectra when the 1.19 μ m peak is not distinct. Some data are not available due to shortages of precursor.

The comparative loss data is graphed in Figures 3.14-16, showing for each series the total losses and the absorption losses at 633nm and 810nm, as a function of concentration of PPV in PVP. The data are graphed as losses in dB/cm rather than as absorption in cm^{-1} .

PPV in PVP Conc. (%)	Total loss 633nm (dB/cm)	Absorption loss 633nm (dB/cm)	Total loss 810nm (dB/cm)	Absorption loss 810nm (dB/cm)
0		.44		.37
2.53		2.8		.35
3.1	2.3,2.2	2.4	2.7	.39
4.96	9	5.8	3.6	1.6
10	28.7,30.3	11	6.3	1.8
19		27		3.9
47		48		8.9

Table 3.3 Loss data for films heated to 130 degrees.

PPV in PVP Conc. (%)	Total loss 633nm (dB/cm)	Absorption loss 633nm (dB/cm)	Total loss 810nm (dB/cm)	Absorption loss 810nm (dB/cm)
2.53	5.4,6.4	4.1	3.2,4.9	.94
4.96	18.9,19.1	3.4	8.1,8.6	.90
10	44.5,45		10	
19		24	18.5,21,27,27.5	4.7
47.2		110		21

Table 3.4 Loss data for films heated to 150 degrees.

PPV in PVP Conc. (%)	Total loss 633nm (dB/cm)	Absorption loss 633nm (dB/cm)	Total loss 810nm (dB/cm)	Absorption loss 810nm (dB/cm)
3.1	3.4	5.5	1.3	1.4
4.96		8.8		2.5
19		28	46	11
47		70		23

Table 3.5 Loss data for films heated to 200 degrees.

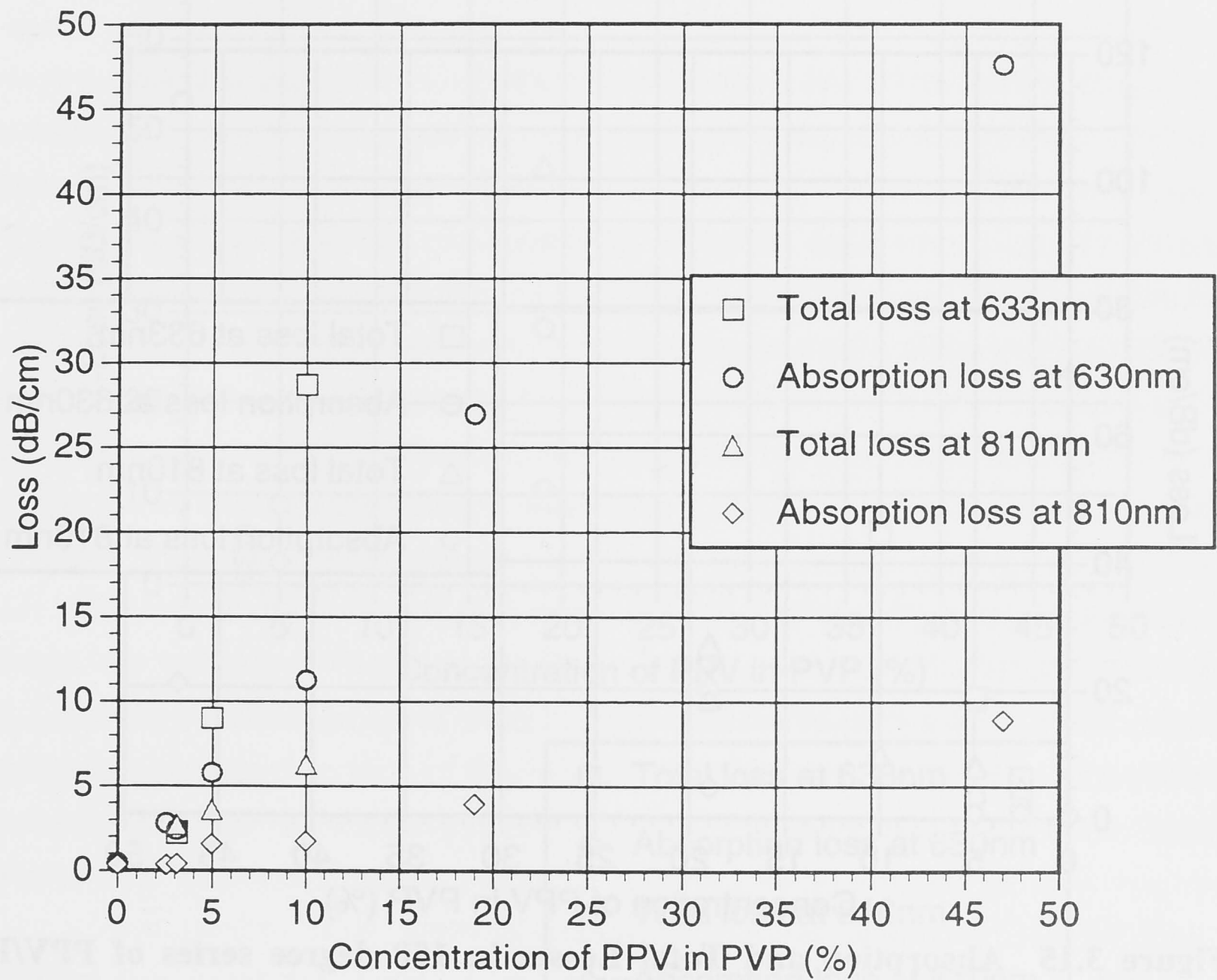


Figure 3.14 Absorption and Total Losses in 130 degree series of PPV/PVP films.

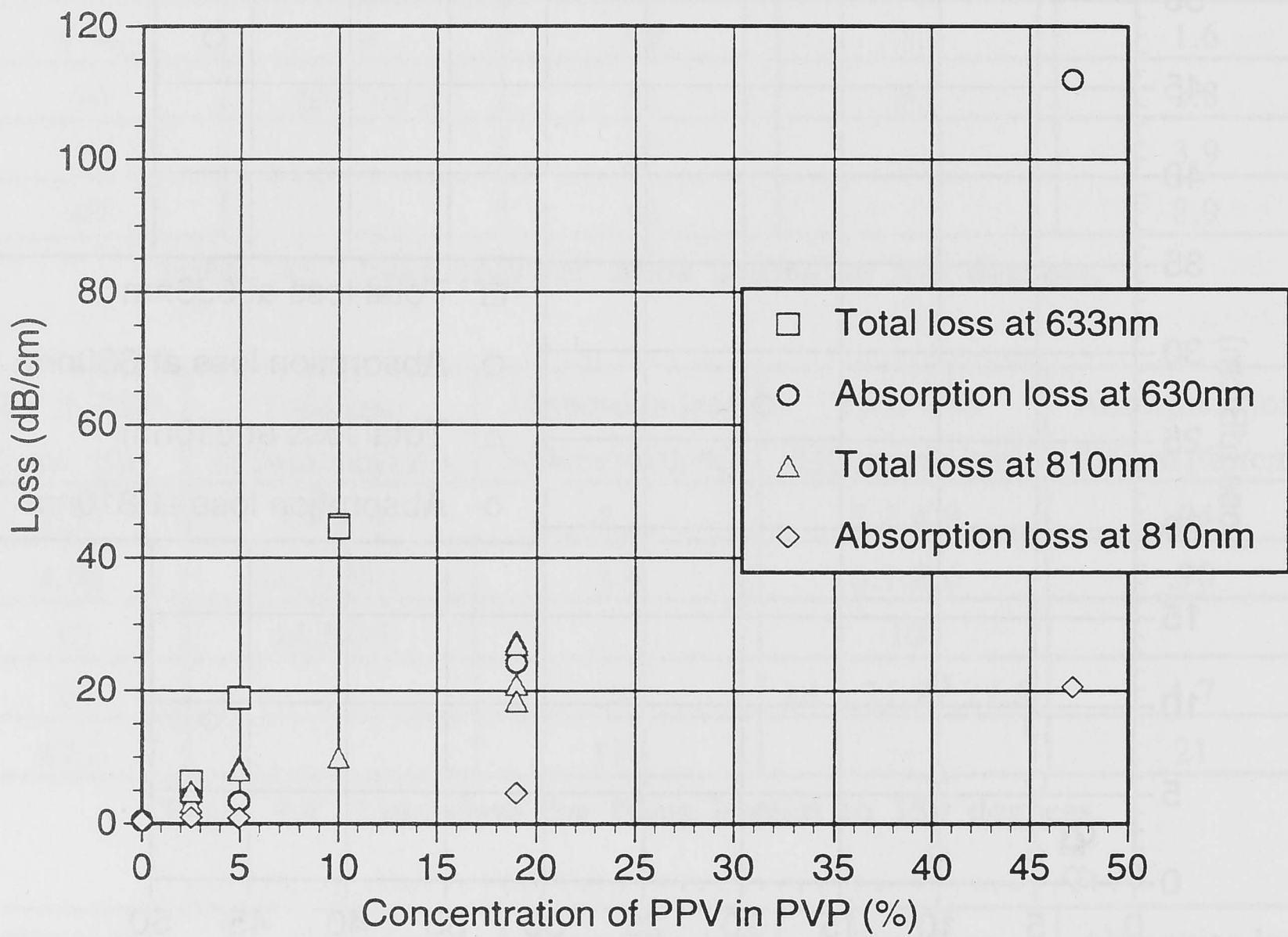
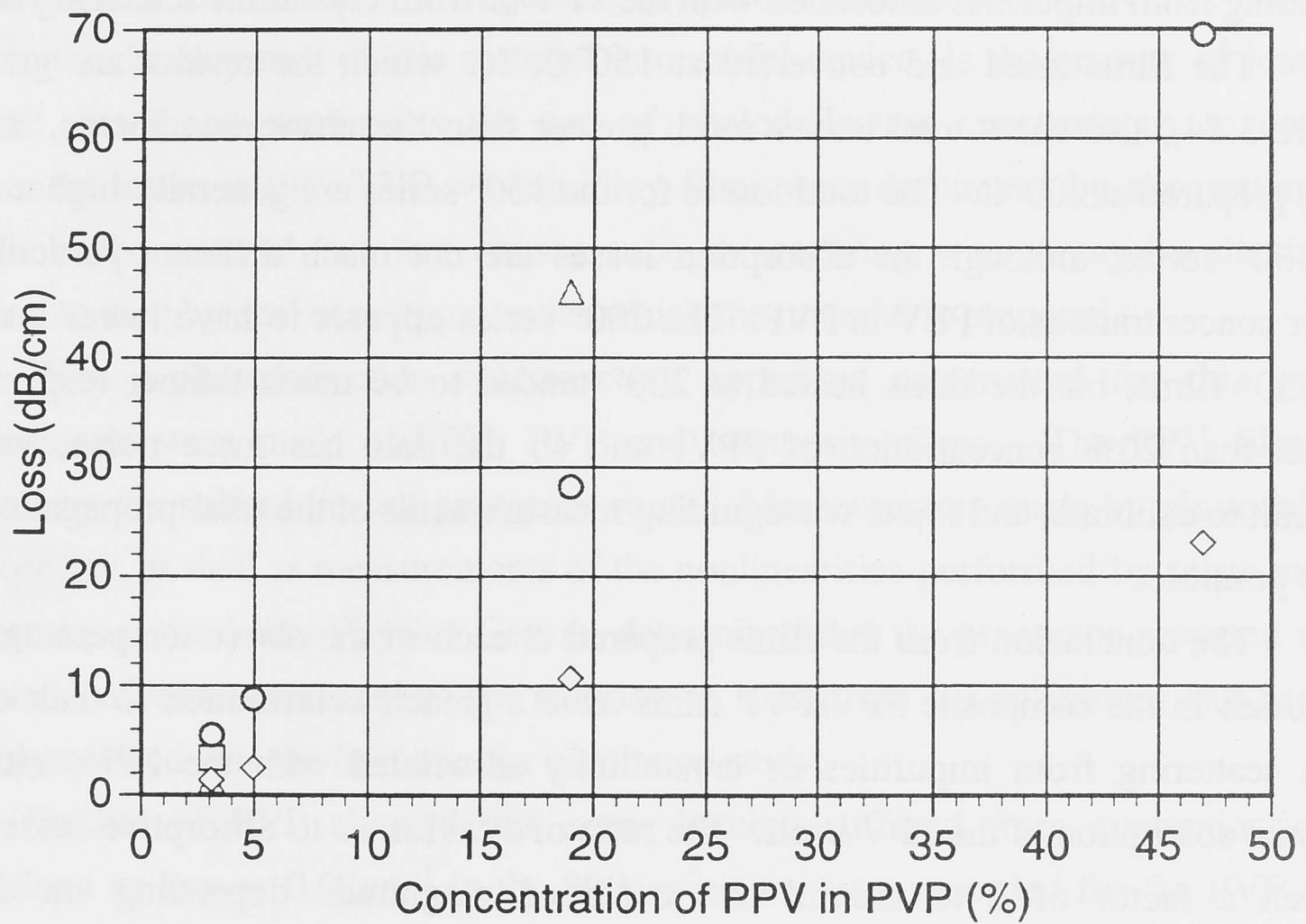


Figure 3.15 Absorption and Total Losses in 150 degree series of PPV/PVP films.



- Total loss at 633nm
- Absorption loss at 630nm
- △ Total loss at 810nm
- ◇ Absorption loss at 810nm

Figure 3.16 Absorption and Total Losses in 200 degree series of PPV/PVP films.

Figure 3.13, which shows the absorption and total losses for the series of PPV/PVP films heated to 130°C, shows that both at 633nm and at 810nm, the absorption losses are much lower than the total losses found in propagation in the waveguide - by a factor of approximately 2. Thus the losses in the waveguides are dominated by factors other than absorption. However, the total losses nevertheless increase with the concentration of PPV in PVP, which implies that they are caused by scattering from impurities associated with the PPV or from crystalline scattering centres.

The films dried and converted at 150°C, for which the results are graphed in Figure 3.14, also show total losses much greater than the absorption losses, as do the films prepared at 200°C. The total losses for the 150° series are generally higher than for the 130° series, although the absorption losses are not much different particularly for lower concentrations of PPV in PVP. The 200° series appears to have lower losses than the 150° films, but the films heated to 200° tended to be much thinner (especially for greater than 20% concentration of PPV) and so the data has more noise, was more difficult to calibrate, and fewer waveguiding measurements of the total propagation losses were possible.

The conclusion from the films prepared at each of the above temperatures is that the losses in the composite PPV/PVP films have a greater contribution to their total loss from scattering from impurities or crystallinity associated with the PPV, rather than material absorption of the PPV itself. The ratio of total losses to absorptive losses ranges between a factor of 2 to around one order of magnitude depending on the PPV concentration. As a result, factors which influence scattering losses within PPV-PVP composites will be the subject of further study with the aim of improving the quality of these materials for waveguide applications. Factors within the precursor preparation process such as the creation of insoluble impurities have subsequently been identified which may lead to these large scattering losses.

4. Conclusion

Poly(*p*-phenylenevinylene) has been the subject of much interest since its high third order nonlinearity makes it a potential candidate for nonlinear optical switching devices. It is being studied as a composite with a host matrix of poly(vinyl pyrrolidinone), for the better waveguiding properties that the latter provides. A limiting factor in the development of this material into useful devices is the amount of loss in the material: this thesis documents the use of photodeflection spectroscopy to determine whether the losses in PPV/PVP waveguiding films were dominated by absorption losses intrinsic to the material, or other causes such as scattering which may be alleviated by attention to the physical conditions under which the material is prepared.

With a photodeflection spectroscopy apparatus constructed for this purpose, measurements were made of PPV, PVP and composite films. The PPV films were prepared by the sulfonium salt precursor route. Measurements made by photodeflection spectroscopy, as well as measurements of the nonlinearities performed by other members of the group at the Laser Physics Centre, determined that the precursor prepared using a 20:80 ratio of water:methanol as the solution in which the *bis*-sulfonium salt monomer was polymerised was the best one for continued study.

Studies of PVP showed that some batches suffered from contamination, but absorptions as low as 0.01cm^{-1} in the 800nm region were recorded for the PVP chosen for use in the composites. It was found that heating the films above about 175°C resulted in an increase in the absorption in the 400-600nm region by up to an order of magnitude, though that increased absorption is still at least 2 orders of magnitude lower than the absorption of PPV in that region.

Measurements of the absorption characteristics of composite PPV/PVP films of different concentrations, having been converted and dried at different temperatures, showed that the absorption losses in the films were much lower than the total losses for 633nm and 810nm light propagating in the waveguiding films. The total losses nevertheless depend on the concentration of PPV in the composite, and so appear to be due to scattering from impurities associated with the preparation of PPV or from crystalline centres formed during the conversion process; the latter has indeed been the focus of a number of recent papers.⁹⁴

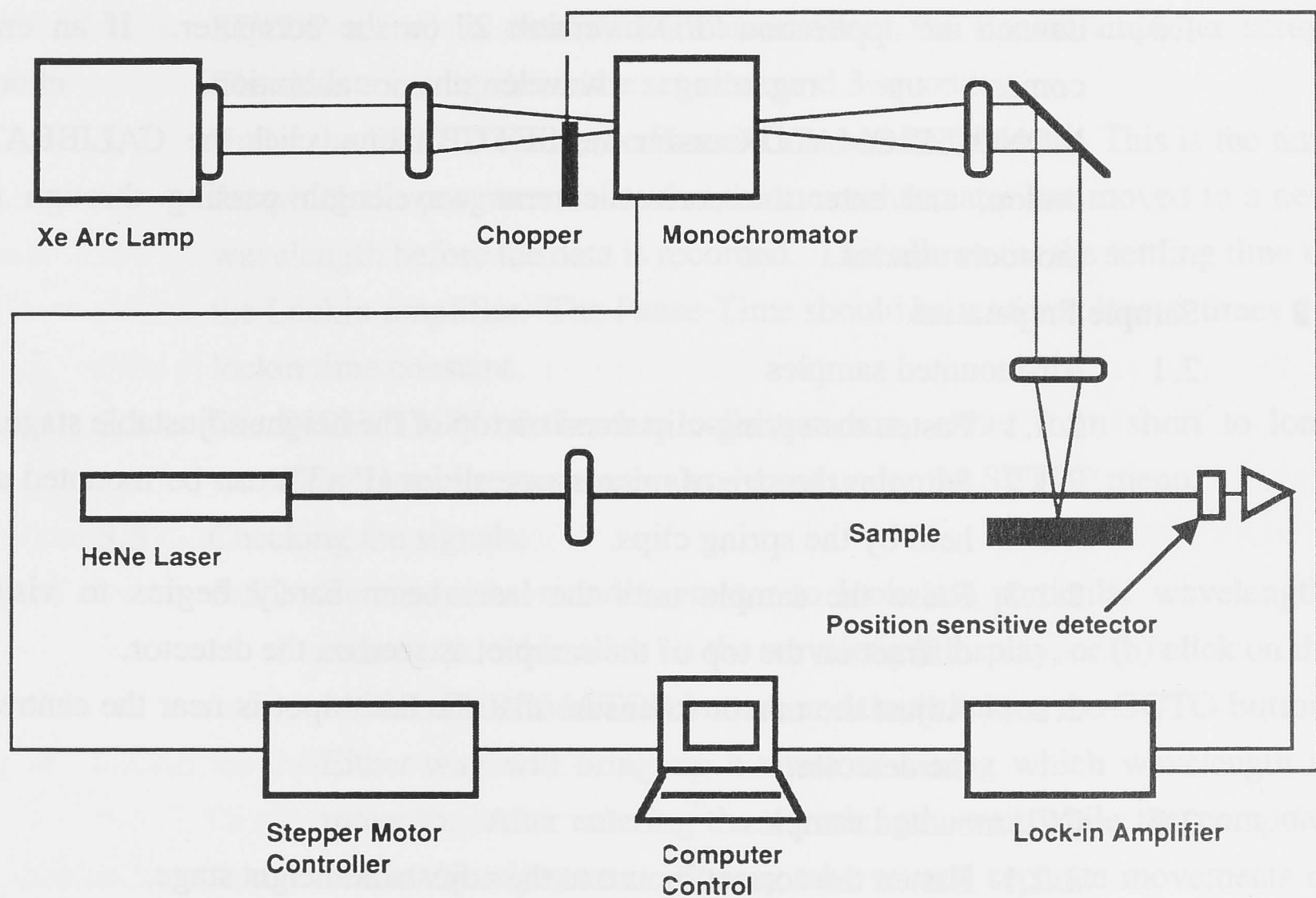
A useful direction for further work with the photodeflection spectroscopy system would be the extension of its wavelength range to include longer wavelengths, enabling films to be calibrated with the stronger overtones which are found there. This would be

particularly useful for measurements of films of pure PPV, for which the base absorption was at least as high as the 1.19 and 1.45 μm overtones, and which thus usually had to be calibrated by extrapolation from the films of lower concentrations of PPV.

Finding that the losses in the composite PPV/PVP films are dominated by causes other than absorption shows that the direction for further investigation of loss reduction in these films will be in attention to the PPV preparation process, and means that loss reductions may be achieved to make this a material suitable for practical nonlinear optical waveguide device purposes.

Appendix A.

Operating and Maintenance Guide for the Photodeflection Spectroscopy apparatus



Schematic Diagram of Photodeflection Spectroscopy System.

1 System Preparation

- 1.1 The system requires power for the following items: Xenon arc lamp, chopper, stepper motor, laser, detector (with battery recharger), Krohn-Hite band-pass filter, CRO, lockin amplifier, computer. A schematic diagram of the system is shown above (the Krohn-Hite and CRO can be inserted between the detector and the lockin amplifier).
- 1.2 Turn on power supply to chopper. This should be running at 30 Hz.
- 1.3 With the chopper on, turn on power supply to Xenon arc lamp, and ignite it. The power level should be adjusted to 300W. The lamp should not be operated far from the 300W level for any extended period.

- 1.4 Turn on power supply to stepper motor control box. Ideally this should never be turned off, so that wavelength calibration cannot accidentally be lost.
- 1.5 Turn on the laser.
- 1.6 Turn on CRO, Lockin-amplifier, and computer.
- 1.7 Turn on the detector.
- 1.8 Launch the application "PDS version 2" on the computer. If an error comes up regarding wavelength calibration, choose MONOCHROMATOR under the SETUP menu, click the CALIBRATE button, and enter the correct current wavelength passing through the monochromator.

2 Sample Preparation

2.1 Air-mounted samples

- 2.1.1 Fasten the spring-clip stand on top of the height-adjustable stage.
- 2.1.2 Samples the size of microscope slides (1"x3") can be mounted and held by the spring clips.
- 2.1.3 Raise the sample until the laser beam barely begins to visibly diffract on the top of the sample, as seen on the detector.
- 2.1.4 Adjust the mirror to ensure that the laser spot is near the centre of the detector.

2.2 CCl₄ mounted samples

- 2.2.1 Fasten the correct mount to the adjustable-height stage.
- 2.2.2 Place the cut sample in the CCl₄ sample-mounting container, secure it in place, and fill with CCl₄, taking care with respect to fumes and spillages (see safety data sheets). Shake or move the mounted sample to release any trapped air-bubbles beneath the sample.
- 2.2.3 Place the container in the platform. The mounting clamps ensure that the angles of the windows prevent interfering reflections at the detector.
- 2.2.4 Adjust the mirror, if necessary, to ensure that the laser spot is near the centre of the detector.
- 2.2.5 Raise the sample stage until diffraction of the laser beam from the top surface of the sample can be seen on the detector, and then drop back slightly.

3 Adjustments

- 3.1 Under the SETUP menu on the computer, the Start Wavelength, Stop Wavelength and Wavelength step size can be selected and changed. They can also be changed by double-clicking on the corresponding displays on the screen (you must double-click, and not just select the display. A dialogue box will appear asking for the change).
- 3.2 Press the LOCKIN button on the screen (or select LOCKIN under the SETUP menu) to obtain information about the Lockin-amplifier setup. The time constant should be set at around 3 seconds.
- 3.3 Under the SETUP menu, the Pause-Time can be adjusted. This is the time for which the program waits after the monochromator has moved to a new wavelength before the data is recorded. This allows for the settling time of the Lockin-amplifier. The Pause-Time should be set for at least 8 times the lockin time constant.
- 3.4 The DIRECTION of the data collection run, either from short to long wavelength or in reverse, can also be set under the SETUP menu.
- 3.5 Checking the signals:
 - 3.5.1 To move the monochromator to look at a particular wavelength, either (a) double click on the wavelength display, or (b) click on the MONOCHROMATOR button, and then click on the GOTO button. Either way will bring up a window asking which wavelength to move to. After entering the wavelength, wait while the computer makes the adjustment. It may take several separate movements of the stepper motors.
 - 3.5.2 To adjust the gain of the lockin, click the "Λ" button or the "V" button to raise or lower the gain, or the LEVEL button for the gain to adjust itself into a suitable range. This may take a few seconds.

4 Collecting Data

- 4.1 Press the START button.
- 4.2 The collection is now automatic, including gain adjustments on the lockin - amplifier.
- 4.3 The program can be interrupted by pressing the PAUSE button. Changes can then be made to any of the display or setup features (the display may not appear fully changed until another data point is collected.) The program can be then made to continue by clicking START, or abandoned altogether by clicking RESET.

- 4.4 While the computer is waiting for the lockin to settle between collecting data points, a "Pause" window is shown on the screen. There is a button on that window which can be clicked to cut short the pause and collect the current data-point immediately, and another button to extend the pause in case the detector or lockin is disturbed.
- 4.5 If the lockin registers an error during the pause before collecting a data point, such as a noise spike, that particular point of data is rejected and the system is paused again to allow the lockin to re-settle and make another reading.
- 4.6 Once the data collection is finished, a reminder will appear to save the data. The data can be saved to disk by selecting SAVE under the FILE menu. Data can be saved in either ASCII format (useful for transfer to other graphics programs) or BINARY format (when disk space is low).
- 4.7 ASCII files are given the extension .PDA; binary files the extension .PDS.

5 Calibration

- 5.1 If there is a data file made by collecting the data from a "black absorber," use the method outlined in 5.3 below; the following point outlines how to create such a file.
- 5.2 Calibrating a run of data with a "black absorber" data file
 - 5.2.1 Under the NORMALISE menu, several files are named. If you wish to calibrate with one of those files, choose it.
 - 5.2.2 If you wish to calibrate with a different file, select "Calibrate for Lamp Power by File" under the NORMALISE menu, and then enter the name of the file by which to calibrate.¹
 - 5.2.3 The calibration is then done automatically. It amounts to dividing the data collected by the particular sample by the data collected on a black absorber, so that the differenced in the illuminating power from the Xenon lamp through the optical system at different wavelengths can be accounted for.
 - 5.2.4 Calibrated data can then also be saved to disk (choose SAVE).
 - 5.2.5 To display both calibrated and uncalibrated data at once, see the instructions under "Display"
- 5.3 Creating a "black absorber" data file

¹ The file "CarbonD4.PDS" is the latest version for use at the time of printing.

- 5.3.1 Use as a sample a microscope slide (or PES slide) covered with soot. Black carbon pellets are suitable for use under carbon tetrachloride.
- 5.3.2 Follow the standard collection procedure outlined above, but taking care that the signal is not so strong as to overload the lockin input. The signal strength can be lowered by lowering the sample stage with respect to the laser, or by slightly reducing the lamp power.
- 5.3.3 Save the data file as usual. It can then be used to calibrate data as above.

6 Display

- 6.1 The graphs can be shown in either logarithmic or linear plots (under STYLE on the GRAPH menu).
- 6.2 The data points can be either all shown on the graph, or suppressed (choose either POINTS AND LINES or LINE GRAPH under STYLE on the GRAPH menu).
- 6.3 The Wavelength range of the graph can be adjusted under the RANGE option.
- 6.4 Loading graphs: Choose LOAD under the file menu. Files with a .PDS extension are automatically assumed to be binary files, and files with a .PDA extension are assumed to be ASCII files.
- 6.5 Overplotting graphs: To show several graphs at once, choose OVERPLOT to plot another graph over the top of previous graphs shown. Up to five graphs can be shown at once.
- 6.6 New data is always collected into the last opened channel. Thus if one graph is shown on the screen, it is written over (on the display) by a new data collection run. If two graphs are shown on the screen, the second graph is overwritten by any new collection of data.
- 6.7 To go back to a single graph on the screen, select CLEAR and REPLOT under the GRAPH menu.
- 6.8 Graphs can be multiplied by constant factors under the NORMALISE menu.
- 6.9 Raw data which is loaded for display can be calibrated after loading under the NORMALISE menu in the way described for calibration above.
- 6.10 Graphs can be printed by selecting PRINT under the graph menu. The computer may be set up to print graphs to disk, or directly to a printer.

Bibliography

- ¹ J Yoshida and M. Naganuma, "Recent Research Trends and Issues in Photonic Switching Devices", *NTT Review*, **7** no.5 24-29 (1995)
- ² J.T. Yardley, "Design and Characterization of Organic Waveguides for Passive and Active Optical Devices" in *Organic Thin Films for Waveguiding Nonlinear Optics*, Amsterdam: Gordon & Breach Publishers, 1996, p.607.
- ³ See eg. T. Kaino, M. Asobe, S. Tomaru, T. Kurihara, and T. Kanamori, "Ultrafast Nonlinear Optical Switches", *NTT Review*, **7** no.5 47-54 (1995)
- ⁴ See eg. R. DeSalvo, D.J. Hagan, M. Shiek-Bahae, G.I. Stegeman, H. Vanherzeele, and E.W. Van Stryland, "Self-focussing and defocusing by cascaded second order effects in KTP", *Opt. Lett.* **17** 28-30 (1992); C. Bosshard, "Cascading of second-order nonlinearities in polar materials", *Advanced Materials* **8** 584-97 (1996); and G.I. Stegeman, D.J. Hagan, and L. Torner, " $\chi^{(2)}$ cascading phenomena and their applications to all-optical signal processing, mode-locking, pulse compression and solitons", *Optical and Quantum Electronics* **38** 1691-1740 (1996)
- ⁵ R. DeSalvo, M. Sheik-Bahae, A.A. Said, D.J. Hagan, E.W. Van Stryland, "Z-scan measurements of the anisotropy of nonlinear refraction and absorption in crystals", *Optics Letters* **18** 194-6 (1993)
- ⁶ See eg. J.S. Aitchison, A.H. Kean, C.N. Ironside, A. Villeneuve, and G.I. Stegeman, "Ultrafast all-optical switching in $\text{Al}_{0.18}\text{Ga}_{0.82}\text{As}$ directional coupler in 1.55 μm spectral region", *Electron. Lett.* **27** 1709-10 (1991), cited in a review by C.N. Ironside, "Ultrafast all-optical switching", *Contemporary Physics* **34** 1-18 (1993).
- ⁷ R.J. Crook, N.P.K. Cotter, J.R. Sambles, R. Rangel-Rojo, G. Spruce and B.S. Wherrett, "Electronic nonlinear optical behaviour of a grating coupled polymer 4BCMU waveguide", *Optics Communications* **113** 344-52 (1994).
- ⁸ C.N. Ironside, J.S. Aitchison, and J.M. Arnold, "An all optical switch employing the cascaded second-order nonlinear effect", *IEEE J. Quantum. Electron.* **29** 2650-4 (1993).
- ⁹ See eg. M.N. Islam, "Ultrafast fibre switching devices and systems", *Cambridge Studies in Modern Optics* 12 (Cambridge: Cambridge University Press, 1992).
- ¹⁰ R. McLeod, K. Wagner, and S. Blair, "(3+1) dimensional optical soliton dragging logic", *Phys. Rev. A.* **52** 3254-78 (1995).

- ¹¹ M.N. Islam, C.E. Socolich, and D.A.B. Miller, "Low-energy ultrafast fiber soliton logic gates", *Optics Letters* **15** 909-11 (1990).
- ¹² B. Luther-Davies and Yang Xiaoping, "Waveguides and Y junctions formed in bulk media by using dark spatial solitons", *Opt. Lett.* **17** 496-8 (1992).
- ¹³ Yardley pp.611-2.
- ¹⁴ C. Bubeck, "Relations between structure and third-order nonlinearities of molecules and polymers", in *Organic Thin Films for Waveguiding Nonlinear Optics*, Amsterdam: Gordon & Breach Publishers, 1996, p.145.
- ¹⁵ Ibid. pp. 146-59. Poly(*p*-phenylenevinylene) is discussed in D.D.C. Bradley and T. Mori, *Jpn. J. Appl. Phys.* **28** 174 (1989), and D. McBranch, M. Sinclair, A.J. Heeger, A.O. Patil, S. Shi, S. Askari, and F. Wudl, *Synth. Met.* **19** E85 (1989)
- ¹⁶ A. Samoc, M. Samoc, M. Woodruff, and B. Luther-Davies, "Tuning the properties of poly(*p*-phenylenevinylene) for use in all-optical switching", *Optics Letters* **20** 1241-3 (1995)
- ¹⁷ P.N. Prasad, D.J. Williams, "Introduction to Nonlinear Optical Effects in Molecules & Polymers", John Wiley & Sons Inc., 1991, pp.235-8
- ¹⁸ A. Samoc, M. Samoc and B. Luther-Davies, "Linear and nonlinear optical properties of poly(*p*-phenylenevinylene) - poly(vinyl pyrrolidinone) (PPV-PVP) composites", in M.G. Kuzyk (ed.) "Nonlinear Optical Properties of Organic Materials X", *Proceedings of SPIE* vol. 3147, 166-77 (1997)
- ¹⁹ K.S. Wong, S.G. Han and Z.V. Vardeny, "Femtosecond degenerate four wave mixing studies of third order electronic nonlinearities in conjugated polymers", *Synth. Metals.* **41-43** 3209-12 (1991)
- ²⁰ G.I. Stegeman in "Contemporary Nonlinear Optics", Academic Press, 1992 p.22
- ²¹ V. Mizrahi, K.W. DeLong, G.I. Stegeman, M.A. Saifi, and M.J. Andrejco, "Two-photon absorption as a limitation to all-optical switching", *Opt. Lett.* **14** 1140-2 (1989)
- ²² B.P. Singh, P.N. Prasad, and F.E. Karasz, *Polymer* **29** 1940 (1988)
- ²³ Y. Pang, M. Samoc, and P.N. Prasad, *J. Chem. Phys.* **94** 5282 (1991)

- ²⁴ V. Philippart, M. Dumont, J.M. Nunzi, "Femtosecond Kerr Ellipsometry in Polydiacetylene Solutions: two-photon effects", *Appl. Phys. A.* **56** 29-34 (1993)
- ²⁵ J. Wang, M. Sheik-Bahae, A.A. Said, "Time-resolved Z-scan measurements of optical nonlinearities", *J. Opt. Soc. Am. B.* **11** 1009-17 (1994)
- ²⁶ See Yardley p. 663-4
- ²⁷ Such as the Shimadzu UV-3101PC UV-visible-NIR spectrophotometer used in experiments described in this thesis.
- ²⁸ A.C. Boccara, D. Fournier, and J. Badoz, "Thermo-optical spectroscopy: Detection by the 'mirage effect'", *Appl. Phys. Lett.* **36** 130-2 (1980)
- ²⁹ M. Thakur, R.C. Frye, and B.I. Greene, "Nonresonant absorption coefficient of single-crystal films of polydiacetylene measured by photothermal deflection spectroscopy", *Appl. Phys. Lett.* **36** 1187-8 (1990)
- ³⁰ A. Skumanich and J.C. Scott, "Photothermal deflection spectroscopy: a sensitive absorption technique for organic thin films", *Mol. Cryst. Liq. Cryst.*, **183** 365-70 (1990)
- ³¹ A. Skumanich and C.R. Moylan, "The vibrational overtone spectrum of a thin polymer film", *Chem. Phys. Lett.* **174** 139-44 (1990)
- ³² C.H. Seager, M. Sinclair, D. McBranch, A.J. Heeger and G.L. Baker, "Photothermal deflection spectroscopy of conjugated polymers", *Synthetic Metals* **49-50** 91-7 (1992)
- ³³ S.K. So, M.H. Chan, and L.M. Leung, "Photothermal deflection spectroscopy of polymer thin films", *Appl. Phys. A* **61** 159-61 (1995)
- ³⁴ A. Hordvik and H. Schlossberg, "Photoacoustic technique for determining optical absorption coefficients in solids", *Appl. Opt.* **16** 101-7 (1977)
- ³⁵ A. Rosencwaig, "Photoacoustics and photoacoustic spectroscopy." John Wiley & Sons, 1980.
- ³⁶ J.C. Murphy and L.C. Aamodt, "Photothermal spectroscopy using optical beam probing: Mirage effect", *J. Appl. Phys.* **51** 4580-8 (1980)
- ³⁷ C. Halvorson and A.J. Heeger, "Two-photon absorption and ultrafast optical computing", *Synthetic Metals* **71** 1649-52 (1995)

- ³⁸ W.B. Jackson, N.M. Amer, A.C. Boccara, and D. Fournier, "Photothermal deflection spectroscopy and detection," *Applied Optics* **20** 1333-44 (1981)
- ³⁹ Jackson et al refer to D. Fournier and A.C. Boccara, in *Scanned Image Microscopy*, ed. E.A. Ash (London: Academic, 1980)
- ⁴⁰ J.C. Murphy and L.C. Aamodt, "Photothermal spectroscopy using optical beam probing: Mirage effect", *J. Appl. Phys.* **51** 4580-8 (1980)
- ⁴¹ G. Rousset, F. Charbonnier and F. Lepoutre, "Influence of radiative and convective transfers in a photothermal experiment", *J. Appl. Phys.* **56** 2093-6 (1984)
- ⁴² S. Surnez and D. Ivanov, "Influence of the dc laser heating on the optical beam deflection", *Revue de Physique Appliquée* **25** 457-62 (1990)
- ⁴³ A.L. Glazov and K.L. Muratkov, "Photodeflection and interferometric methods of detecting the signal in photothermal microscopy and spectroscopy", *Sov. Tech. Phys. Lett.* **16** 718-20 (1990)
- ⁴⁴ A.L. Glazov and K.L. Muratkov, "Photodeflection signal formation in thermal wave spectroscopy and microscopy of solids within the framework of wave optics - 'Mirage' effect geometry", *Optics Communications* **84** 283-9 (1991)
- ⁴⁵ M. Woelker, B.K. Bein, J. Pelzl and H.G. Walther, "Contributions to the technique and interpretation of the photothermal beam deflection experiment", *J. Appl. Phys.* **70** 603-10 (1991)
- ⁴⁶ D. Fournier, A.C. Boccara, N.M. Amer, and R. Gerlach, "Sensitive in situ trace-gas detection by photothermal deflection spectroscopy", *Appl. Phys. Lett.* **37** 519-21 (1980)
- ⁴⁷ M.A. Shannon, A.A. Rostami, and R.E. Russo, "Photothermal deflection measurements for monitoring heat transfer during modulated laser heating of solids", *J. Appl. Phys.* **71** 53-62 (1992)
- ⁴⁸ R.C. Frye, J.J. Kumler, and C.C. Wong, "Investigation of surface passivation of amorphous silicon using photothermal deflection spectroscopy", *Appl. Phys. Lett.* **50** 101-3 (1987)
- ⁴⁹ P. Grunow and R. Schieck, "Optoelectronic characterization by photothermal deflection: Silicon solar cells", *J. Appl. Phys.* **77** 2773-81 (1995)

- ⁵⁰ A. Skumanich, "Optical absorption spectra of carbon 60 thin films from 0.4 to 6.2eV", Chem. Phys. Lett. **182** 486-90 (1991)
- ⁵¹ A.C. Boccara, D. Fournier, W. Jackson, and N.M. Amer, "Sensitive photothermal deflection technique for measuring absorption in optically thin media", Optics Letters **5** 377-9 (1980)
- ⁵² L. Chen and S.Y. Zhang, "Photothermal detection for light-scattering material by laser interferometry", Appl. Phys. Lett. **50** 1340-2 (1987)
- ⁵³ F. Charbonnier and D. Fournier, "Compact design for photothermal deflection (mirage): Spectroscopy and imaging", Rev. Sci. Instrum. **57** 1126-8 (1986)
- ⁵⁴ C.J. Manning, R.A. Palmer, J.L. Chao, and R. Charbonnier "Photothermal beam deflection using the reverse mirage geometry: Theory and experiment", J. Appl. Phys. **71** 2433-40 (1992)
- ⁵⁵ S. Horita, E. Miyagoshi, M. Ishimaru, and T. Hata, "Improvement of sensitivity of photothermal deflection spectroscopy by a double pass method", Rev. Sci. Instrum. **63** 1909-13 (1992)
- ⁵⁶ M.N. Özisik, "Heat Transfer, A Basic Approach", McGraw-Hill Book Company (USA) 1985, chapter 5.
- ⁵⁷ *ibid.*, pp190-1
- ⁵⁸ Data for the thermal conductivity, density and specific heat of air found in R.C. Weast (ed.), *CRC Handbook of Chemistry and Physics*, 70th edition (Florida: CRC Press, 1989-90), p.F-10, citing Rev. Mod. Phys. **52** p.533 (1980). The value for dn/dT is calculated from data in E.W. Washburn (ed.) *International Critical Tables of Numerical Data, Physics, Chemistry and Technology*, (National Research Council) (New York: McGraw Hill, 1930), vol. 7 p.4, and is consistent with the value used by Murphy and Aamodt (ref. 30).
- ⁵⁹ CRC Handbook of Chemistry and Physics, 70th Edition, p.F-64. Data for dn/dT from H. Milan, *Interpretation and Processing of Vibrational Spectra*, (John Wiley, 1978) p.182
- ⁶⁰ CRC Handbook of Chemistry and Physics, 70th Edition, p.F-64.
- ⁶¹ GoodFellow, Cambridge Science Park, England
- ⁶² Oriel model number 6259

- ⁶³ Melles Griot model number 05-LHP-991 10mW minimum 632.8nm Helium Neon laser.
- ⁶⁴ CRC Handbook for Chemistry and Physics, 70th edition, p.E-382.
- ⁶⁵ C.H. Seager and C.E. Land, "Optical absorption in ion-implanted lead lanthanum zirconate titanate ceramics", Appl. Phys. Lett. **45** 395-7 (1984)
- ⁶⁶ P. Grunow and M. Kunst, "Optoelectronic characterization by photothermal deflection: Single-crystalline semiconductors", J. Appl. Phys. **77** 2767-72 (1995)
- ⁶⁷ I. Edwards, "Using Photodetectors for Position Sensing", Sensors December 1988.
- ⁶⁸ Stanford Research Systems model SR850 DSP Lock-In Amplifier.
- ⁶⁹ PCL-838 Stepping Motor Control Card, Advantech Co., Ltd. 1992.
- ⁷⁰ The concentrations used were 0.0009% (could not obtain 410nm peak), 0.008%, 0.024, 0.08%, 0.25%, 0.8%, 10%, 21%.
- ⁷¹ G. Köpping-Grem, G. Leising, M. Schimetta, F. Stelzer, A. Huber, "Quantum efficiencies of poly(*para*-phenylenevinylene)s", Synthetic Metals **76** 53-6 (1996)
- ⁷² D.R. Gagnon, J.D. Capistran, and F.E. Karasz, "Synthesis, doping, and electrical conductivity of high molecular weight poly(*p*-phenylene vinylene)", Polymer **28** 567 (1987)
- ⁷³ R.W. Lenz, C-C Han, J. Stenger-Smith and F.E. Karasz, "Preparation of poly(phenylene vinylene) from cycloalkylene sulfonium salt monomers and polymers", J. Polym. Sci., Part A, Polym. Chem. Ed. **26** 3241 (1987)
- ⁷⁴ S. Tokito, T. Momii, H. Murata, T. Tsutsui and S. Saito, "Polyarylenevinylene films prepared from precursor polymers soluble in organic solvents", Polymer **31** 1137 (1990)
- ⁷⁵ P.L. Burn, D.D.C. Bradley, R.H. Friend, D.A. Halliday, A.B. Holmes, R.W. Jackson, and A. Kraft, "Precursor route chemistry and electronic properties of poly(*p*-phenylene vinylene), poly[(2,5-dimethyl-*p*-phenylene)vinylene] and poly[(2,5-dimethoxy-*p*-phenylene)vinylene]", J. Chem. Soc., Perkin Trans **1** 3225 (1992)
- ⁷⁶ D.A. Halliday, P.L. Burn, D.D.C. Bradley, R.H. Friend, O.M. Gelsen, A.B. Holmes, A. Kraft, J.H.F. Martens and K. Pichler, "Large changes in optical response

through chemical pre-ordering of poly(*p*-phenylenevinylene)", *Advanced Materials* **5** 40 (1993)

⁷⁷ The films were spun using a Headway Research Inc. Spin Coater

⁷⁸ A. Samoc, M. Samoc, M. Woodruff and B. Luther-Davies, "Poly(*p*-phenylenevinylene) - an attractive material for photonics applications", in D.L. Wise et al. (eds) *Photonic Polymer Systems* World Scientific Publishing Co. Pty. Ltd. in print.

⁷⁹ A good resume of coupling techniques can be found in R.G. Hunsperger, "Integrated Optics: Theory and Technology" (2nd edition) Springer-Verlag (1984)

⁸⁰ M.L. Dakss, L. Kuhn, P.F. Heidrich, and B.A. Scott, "Grating coupler for efficient excitation of optical guided waves in thin films", *Appl. Phys. Lett.* **16** 523-5 (1970)

⁸¹ R. Moshrezadeh, X. Mai, C.T. Seaton, and G.I. Stegeman, "Efficient grating couplers for polymer waveguides", *Applied Optics* **26** 2501 (1987)

⁸² LiCONiX 200 series Helium Cadmium laser, Model 4210N, lasing at 441.6nm with a maximum output power of 15mW.

⁸³ Metricon Corp. Prism Coupler, model 2010.

⁸⁴ G. Köpping-Grem, G. Leising, M. Schimetta, F. Stelzer, A. Huber, "Quantum efficiencies of poly(*para*-phenylenevinylene)s", *Synthetic Metals* **76** 53-6 (1996)

⁸⁵ T. Kaino, "Absorption Losses of Low Loss Plastic Optical Fibres", *Jap. J. Appl. Phys.* **24** 1661-5 (1985)

⁸⁶ A. Skumanich, M. Jurich and J.D. Swalen, "Absorption and scattering in nonlinear optical polymeric systems", *Appl. Phys. Lett.* **62** 446-8 (1993)

⁸⁷ The internal codes used for these precursors and films are: A=precursor 7A, B=7B, C=8, D=11, E=6B. The slides are A1=636, B1=637, C1=DD0801, D1=748, E1=609.

⁸⁸ Slides A1, B1, D1 and E1 were prepared by Dr. A. Samoc.

⁸⁹ Measurements of the optical nonlinearity of the films were made by other members of the Laser Physics Group, in particular M. Samoc and B. Luther-Davies.

⁹⁰ Y.Y. Tan and G. Challa, *Polymer* **17** 739 (1976), as referenced in Kirk-Othmer (ed), "Encyclopedia of Chemical Technology", 3rd edition, volume 23, p971 (1983). Tan and

Challa measure the variation of the glass transition temperature with water content; 175°C is the glass transition temperature for anhydrous PVP.

⁹¹ Cole Parmer Instrument Co., Chicago, Illinois.

⁹² This film was subsequently damaged and not used in the measurements which follow.

⁹³ The internal codes for these films are D61,D62,D63,D64,D65 respectively.

⁹⁴ X.B. Zhang, G. Van Tendeloo, J. Van Landuyt, D. Van Dijck, J. Briers, Ying Bao, and H.J. Geise, "An electron microscopic study of highly oriented undoped and FeCl₃-doped poly(*p*-phenylenevinylene)", *Macromolecules* **29** 1554-61 (1996); T.A. Ezquerra, E. Lopez-Cabarcos, F.J. Balta-Calleja, J.D. Stenger-Smith, and R.W. Lenz, "Real time X-ray scattering study during the thermal conversion of a precursor polymer to poly(*p*-phenylenevinylene)", *Polymer* **32** 781-5 (1991); Y.B. Moon, S.D.D.V. Rughooputh, A.J. Heeger, A.O Patil and F. Wudl, "X-ray scattering study of the conversion of poly(*p*-phenylenevinylene) precursor to the conjugated polymer", *Synthetic Metals* **29** E79-E84 (1989).